UNIVERSITÀ DEGLI STUDI DELL' INSUBRIA

FACOLTÀ DI SCIENZE MATEMATICHE, FISICHE E NATURALI

CORSO DI LAUREA MAGISTRALE IN MATEMATICA

DIPARTIMENTO DI MATEMATICA E FISICA

Mathematical models and numerical methods for the mechanics of cardiac tissue

Relatore Interno

Chiar.mo Prof. Giorgio Mantica

Laureando

Davide Baroli

Matricola 711728

Relatore Esterno

Chiar.mo Prof. Alfio Quarteroni

Research supervisor

Dott. Ric. Ricardo Ruiz-Baier

ANNO ACCADEMICO 2010-2011

-To my family-

Abstract

In this thesis we investigate an incompressible nonlinear elastostatic problem in total Lagrangian deformation-pressure formulation and we develop a discontinuous Galerkin method with a suitable interior penalty stabilization. The novelty of this thesis lies in the convergence study of DG formulation for nonlinear incompressible materials.
The study of nonlinear elasticity problem find a large number of applications in structural analysis, biomechanics and engineering design. In particular, our interest is motivated by the study of anisotropic soft living materials such as the cardiac tissue, which present the ability of actively deform without need of external loads. The finite elestostatics problem requires the resolution of nontrivial quasilinear elliptic partial differential equations accounting for the balance of forces and related constitutive laws. The momentum equation is coupled with a nonlinear volumetric equation, because we are taking in account an incompressible underlying material and we are using a Lagrangian formulation. In contrast, the usual divergence free condition is employed in fluid mechanics, linear elasticity and other systems formulated in the current configuration. We solve a class of nonlinear elastic problems, employing a common iterative approach, namely Newton method, which requires a consistence linearization of the original weak formulation. Moreover, we prove for a generic step, that the linearized problem is welposed by demonstrating (at least for sufficiently small deformations) solvability and stability in the sense of the classical Babuska-Brezzi theory for saddle-point problem.
By far the most used strategy for the spatial discretization of elasticity problem are finite elements, because of their flexibility and computational robustness. For large deformation elasticity problems many effects need to be taken into account and slightly different methods may feature substantial differences depending on the choice of finite element spaces, hexaedra or tetrahedra, conforming or nonconforming and formulations leading to symmetric or nonsymmetric linear systems, ad so on. In addition it is well know that the main numerical difficulty in carrying out the low-order conforming finite element approximations of elasticity problems, subject to the volume preserving constraint, is the undesirable so-called volume locking phenomenon, which consists in a decreasing of the displacements in a non-physical fashion. Herein, we formulate a discontinuous Galerkin (DG) method, in its interior penalty variant to weakly impose the interelement continuity. The inclusion of penalty terms in the energy functional is a common strategy to reduce the spurious numerical instabilities generated by discontinuous formulations. The advantage of using a DG method lies in the ability of handling complex domains, anisotropic and nonconforming meshes, PDEs with discontinuous coefficients, $p-$ and $hp-$ adaptive refinement, featuring better accuracy than

standard finite elements for a given number of degree of freedoms.

Summary

The introduction presented in Chapter 1 is intended to motivate our investigation of modeling mechanical behavior of cardiac tissue into the framework of continuum mechanics. In this chapter, we give also a brief exposition of the morphological structure of cardiac tissue and the electro-physiological behavior at microscale in order to acquaint the reader with the active and passive living behavior of myocardial wall.
In Chapter 2, we introduce the basic notion of continuum mechanics, we discuss some of recent results in modeling the passive cardiac behavior due to external excitation and load, and in the active modeling due to internal force, mainly due to contraction of myocardial fibers. The last section of this chapter deal with the description of the active strain formulation, based on multiplicative decomposition. In this model, the coupling between the cardiac mechanics and the cardiac electrophysiology is carried out via the active strain function γ_f, that is included as a parameter in the nonlinear finite elastic PDE. The model proposed is compared with the classical active stress formulation, based on an additive decomposition. In particular, this new formulation is able to capture the variation of detail at microscale level on the fiber contraction.
In Chapter 3, we analyze the physical model from the mathematical point of view. The hyperelastic equation that describes the motion of cardiac tissue and at the same time the contraction of length of sarcomere at microscale during cardiac cycle is a nonlinear PDE coupled with the nonlinear constraint that represents the preserving of volume. Using the Hamilton-Lagrange principle and Gataux's derivate tool, we linearize the problem with respect to a generic configuration and we study its well-posedness.
Chapter 4 is dedicated to the main novelty of this thesis, introducing the formulation of a family of discontinuous Galerkin method by the lifting operator to approximate the nonlinear elastic incompressible problem with mixed boundary conditions. Moreover we have proved the optimal convergence of the method and its locking-free property.
In Chapter 5 we gather numerical tests in 2D to validate the optimal convergence of the numerical scheme. In order to validate the robustness and the locking free property we proposed significant tests with discontinuous active parameters, entailing a varying electrophysiological input, but keeping a continuous description parametrization of the fibers direction. In these tests we evidence the volumetric locking phenomenon that occurs using standard finite elements and and moreover we observe that is not necessary to employ the incremental loading technique in the framework of Newton algorithm to achieve convergence, as usually required when using standard finite elements. We close the chapter with some simulations of the active contraction of a cube using both continuous and discontinuous

pressure approximations (and discontinuous for displacements). In this case we observe once again the robustness of the proposed method.
Finally, in Chapter 6 we present a critical analysis and relevant conclusions of the present work, and we discuss some future perspectives.

This work of thesis has developed at the chair of modelling and scientific computing (**CMCS**) in the Mathematics Institute of Computational Science and Engineering (**MATHICSE**) of École Polytechnique Fédérale de Lausanne, during an experience of six months' stage.

Università degli Studi dell'Insubria di Como,
École Polytechnique Fédérale de Lausanne,

Como e Losanna, marzo 2012.

Contents

List of Figures

Chapter 1

Introduction

> The heart is the beginning of life; the sun of the microcosm, even as the sun in his turn might well be *designated the heart of the world.*
>
> *- William Harvey, 1578-1675*

The cardiac tissue is a biological living tissue. It exhibits a nonlinear, essentially incompressible elastic response and undergoes large deformations.

In the modelling of mechanical behavior, both its passive response at the macroscopic level due to elastin and collagen, and its active response at the microscopic level due to contraction of muscle fibers have to be taken into account. The passive mechanical response has been extensively investigated through uniaxial and biaxial tests; however, very few data is available on the active response due to the presence of muscle fibers, even though the physiological mechanism regulating the contraction of muscle fibers is well understood. The excitation-contraction coupling in cardiac muscular fibers is a complex nonlinear mechanism involving many variables such as membrane potential, ionic conductance, intracellular calcium concentration, membrane strain and stress, and changes in the rest length of muscle fibers due to the interaction of actin and myosin. The geometrical data, material parameters and boundary conditions are complex and, at least in vivo, they are affected by a severe uncertainty [2].

1.1 Qualitative description of cardiac tissue

In this section we describe the morphology of the cardiac tissue and we put into evidence the motivation to present its description within a mechanical framework.

1.1.1 Anatomy and tissue structure of the heart

The human heart consists of four chambers, namely the right and left atria, which receive blood from the body, and the left and right ventricles, which pump blood around the body. There is still an ongoing debate concerning the structure of the heart and the anisotropic cardiac micro-structure. One approach describes the heart as a single muscle coiled in a helical pattern, whereas the other approach considers the heart to be a continuum composed

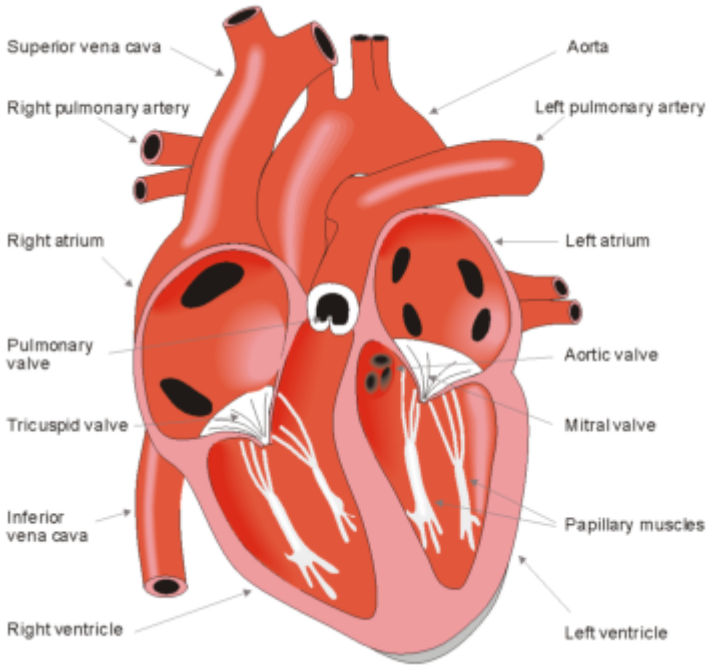

Figure 1.1: Anatomy of heart and associated vessels. Reproduced from [83].

of laminar sheets, an approach we are adopting in this thesis. Let us point out the difference between cardiac muscle and other skeletal muscles in several important respects. First, the cardiac action potential is not initiated by neural activity but specialized cardiac muscle tissue in the heart itself initiates the action potential, which then spreads directly from muscle cell to muscle cell. Neural influences have only a modulatory effect on the heart rate. Second, the duration of the cardiac action potential is quite long. As a matter of fact, the full force of cardiac contraction results from a single action potential. The force of contraction is not the same for every beat of the heart and can be modulated by the cardiac nerves. Finally, all cells in the heart contract together as a unit in a coordinated fashion with every beat.

The left ventricle has the largest volume of the four chambers and serves the particular purpose of distributing blood with a higher pressure that the right ventricle. As a consequence of the need to support higher pressure, the wall thickness of the left ventricle is larger than that of the right ventricle. The wall thickness and curvature of the left ventricle vary spatially; it is thickest at the base and at the equator, and thinnest at its apex. The wall thickness and curvature also vary temporally through the cardiac cycle. The left ventricular wall can be regarded as a continuum of myocardial fibers, with a smooth transmural variation of the fiber orientations. The cavity of the left ventricle (LV) resembles a truncated ellipsoid in which both inflow and outflow tracts are adjacent. It is modeled reasonably well as a thick-walled ellipsoid of revolution that is truncated at the base.

The heart wall consists of three distinct layers (Fig. 1.2) [73]: an inner layer (the endocardium), a middle layer (the myocardium) and an outer layer (the epicardium). We focus our attention on the behavior of the myocardium of the left ventricle. The ventricular myocardium is a functional tissue of the heart wall with a complex structure. The left ventricle wall is composite of sheet of parallel myocytes (see Fig. 1.3), which are the predominant

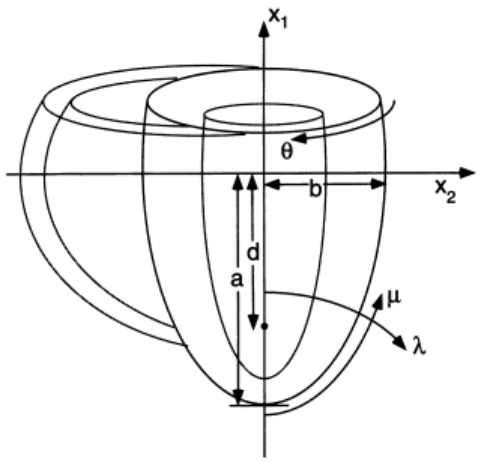

Figure 1.2: Truncated ellipsoidal representation of ventricular geometry. The major and minor radii of the outer surface of LV are denoted by a and b, the focal length (d), and coordinates for a prolate spheroidal representation (λ, μ, θ). Taken from [67].

fiber types, occupying about 70% of the volume. The remaining 30% consists of various interstitial components, whereas only 2-5% of the interstitial volume is occupied by collagen (see Fig. 1.4) arranged in a spatial network that forms lateral connections between adjacent muscle fibers, with attachments near the $z-$line of the sarcomere.

The layered organization of myocytes is characterized by right-handed orthonormal set of basis vectors and an associated orthogonal curvilinear system of coordinates. The local fixed set of unit basis vectors consists of the fiber axis $\mathbf{f}_0$, which coincides with the muscle fiber orientation, the sheet axis $\mathbf{s}_0$, defined to be in the plane of the layer perpendicular to the fiber direction and the sheet-normal axis $\mathbf{n}_0$, defined to be orthogonal to the other two. The morphologic structure of ventricular myocardium permits us to describe it as a continuum with a hierarchical architecture consisting of discrete interconnected sheets of aligned muscle. The architecture of transmural variation of myocardium tissue structure is responsible for the resistance of the heart to bending and twisting during the cardiac cycle.

Let us describe the microscopic level of myocardium in order to motivate and understand how the active behavior at this level influences the macroscopic contraction of cardiac muscle. At the cellular level [48], the myocardium consists of two cell types cardiac myocytes and fibroblast, plus an abundant extracellular matrix, that consists of proteins (e.g. collagen, elastin etc). Although not capable of dividing, the cardiac myocyte is biologically active; indeed, it is capable of synthesizing new proteins and thereby altering its size and structure in response to changes in its environment. In particular, myocytes may replace the bulk of their protein molecules every week or two [1], which is accomplished via a balance between synthesis and degradation. Cardiac myocytes are typically 10 to 20 μm in diameter and 80 to 125 μm in length; they contain mainly myofibrils (1 to 2 μm in diameter) within their cytoplasm. Each myofibril consists of a string of tiny contractile units (2.2 μm long) called sarcomeres, and it is the end-to-end organization of these units that gives cardiac muscle its striated appearance. Each sarcomere, in turn, consists of overlapping thin actin (5 nm in diameter) and thick myosin (10 to 12 nm in diameter) filaments, an end view of which reveals a hexagonal stacking arrangement. The myosin has many transversely arms that

are about 13 nm long and connect to the actin. The contraction is initiated by the release of Ca^{2+}, which is inside the sarcoplasmic reticulum (Fig. 1.5), and results in a smooth ratcheting action (15 mm/sec) as the cross-bridges release, move forward, and re-attach, thus shortening the sarcomere. Normally, this cross-bridge cycling is reversible, thus permitting contraction and relaxation of muscle at macroscale.

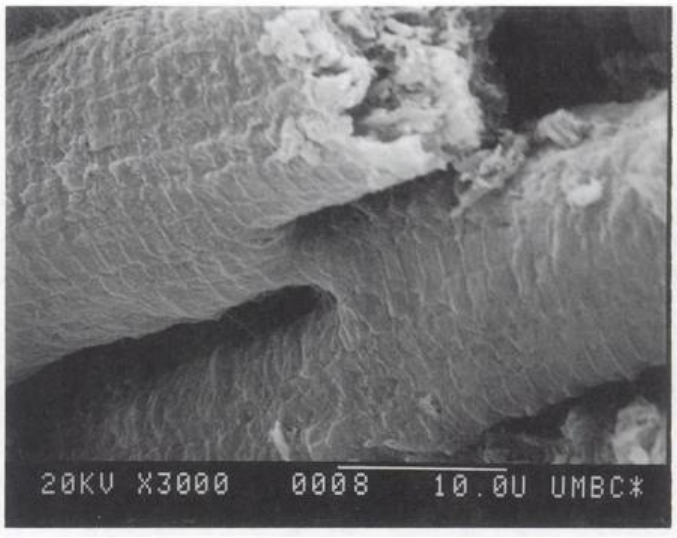

Figure 1.3: Scanning electron micro-graph showing a side-a-side connection between two cardiac muscle fibers. Reproduced from [48].

1.1.2 Mechanical behavior of passive myocardium

In the literature, the deformations of myocardial tissue are assumed a priori volume-preserving. The heart muscle is made mainly of connective tissue, cardiac cells and extracellular matrix filled with fluid, that consist essentially of water. Nevertheless the cardiac tissue is actually compressible, as shown by [101], since it is perfused with blood. During a contraction cycle the small vessels which supply oxygen to the cell are squeezed and the blood is left out, so that the total volume change amounts a 20-40%. From the mathematical point of view the advantage of the incompressibility assumption is simplification of the nonlinear equation, used to describe the mechanical behavior of hyperelastic material, because of the geometric simplification of zero volume change. Moreover, it is possible to obtain analytic closed-form solutions for a large class of interesting problems. The disadvantage of using the incompressibility constraint is numerical difficulties that appear in using finite element analysis. The discussion on whether the myocardium should be modeled as incompressible or nearly incompressible is still an open question,since in vitro experiments are not yet available. The myocardium tissue appears to be viscoelastic, this aspect of its behavior is not important from the point of view of mechanical modelling on the time scale of the cardiac cycle, which is short compared with the relaxation time of the viscoelastic response. We treat the tissue behavior as hyperelastic. It is therefore important to model the passive response of the left ventricular myocardium as (non)-homogeneous, thick-walled, incompressible (nearly incompressible), orthotropic nonlinearly elastic material.

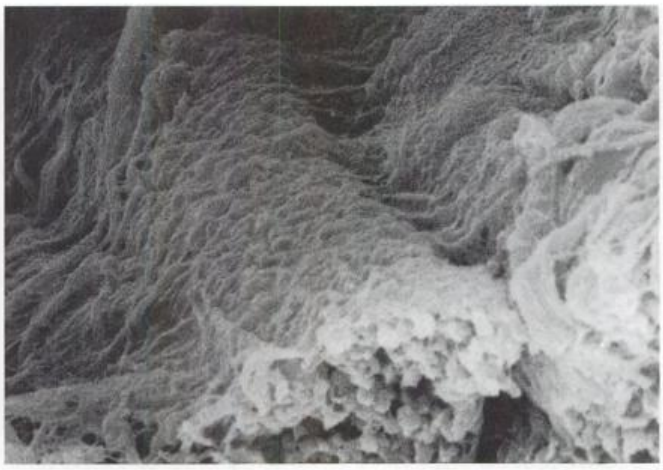

Figure 1.4: Scanning electron micro-graph of collagen micro-structure within heart, taken from [48].

1.2 Electromechanical modeling of cardiac tissue

A set of different interconnected physical processes are driven by electrical and mechanical activities in the cardiac tissue. More specifically, the muscles contraction controlled by electrical activity via excitation-contraction coupling (ECC) [57], while changes in tissue length affect electrophysiological properties via mechano-electrical feedback (MEF) [71]. The first quantitative mathematical model of wave propagation in biological tissues dates back more than 50 years [45] and has been the basis on which realistic ionic and phenomenological models of cardiac tissue have been elaborated [32, 77, 70]. Ionic models are well able to reproduce the depolarization and re-polarization phases of the action potential, restitution properties, and dynamic changes in ionic concentration; however, such a modeling is effective at small length and time scales, while many important problems, such as the question of re-entrant electrical sources occur only in large spatial regions of cardiac tissue.

The electromechanical model describes the propagation of activation waves in the excitable cardiac tissue. The effect of electrical activity on cardiac mechanics is a key issue in any electromechanical model. Usually, this effect is modelled by assuming that, when cardiac muscle fibers are stimulated, they generate contractile forces which, at the macro scale of the tissue, are described by an active stress tensor constitutively related to the tissue's electro-physiological activity. The overall stress in the tissue is then recovered by adding to the active stress a passive stress, depending on the mechanical properties of the myocardium. While the muscle fiber distribution influences the active response of the tissue, the spatial variation in collagen distribution is related to material constitutive parameters and determines the highly nonlinear, anisotropic passive response of the cardiac tissue.

The active strain model is based on a novel point of view presented in the notion of active contraction as opposed to that of active stress. We assume that, at the macroscopic scale, the activation of the cardiac muscle is described by the contraction of its fibers, that is, by a change of fibers' ground state; thus, at any given instant, the stress state in the activated tissue is due to the difference between its actual configuration and the ground state. The active deformation is in turn related to the electro-physiological activity of the tissue; as suggested

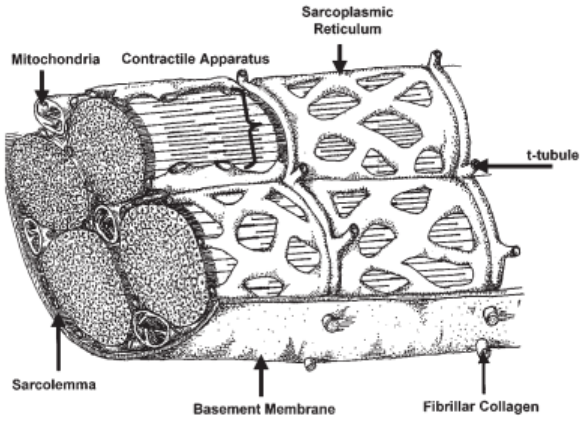

Figure 1.5: Longitudinal cross section of an individual cardiac myocyte. The basement membrane, which is composed of collagen, glycoproteins, and proteoglycans, provides an interface for myocyte adhesion, as well as continuity with the extracellular matrix. The basement membrane serves as an anchoring site for the collagen fibrils. Taken from [98].

by many experiments, calcium concentration is the main factor driving the variation in the length of muscular fibers. Finite elasticity subsumes these assumptions with the idea underlying the Kroner-Lee decomposition of the deformation gradient, originally introduced to distinguish between elastic and viscoplastic strains [56, 59], much later proposed for growth modeling [87, 96], and recently refined with a noteworthy improvement in dynamics, in [23].

The contraction of cardiac tissue affects the process of wave propagation in two ways. It induces changes in the medium in which the propagation occurs, the sarcoplasmic reticulum, and alters the electro-physiological activity of the heart. Some light has been shed on the underlying (sub-)cellular mechanisms of cardiac MEF; these include stretch activation of sarcommal ion channels and electro-physiological effects of mechanical modulation of cellular Ca^{2+} handling [55]. Recent studies have combined a description of the electrical activity of the cardiac tissue and a modeling of the mechanical processes that occur during heart beats and attempted to model MEF in cardiac tissues. In [74], an electromechanical model of two-dimensional elastic, isotropic, and excitable tissues is proposed but no mechano-electrical feedback is included in the modeling. In [80], the same model is reviewed and a macroscopic modeling of the stretch-activated ion currents is included; the model corresponds to an external current that depends linearly both on the local volume changes in the tissue and on the tissue voltage. The cellular mechanism of stretch-activation of ion channels, a relevant role is played by the deformation of the cell from a reference state.

The phenomenon of MEF has been studied in the clinical community for well over a century and may have both pro-rhythmic and arrhythmogenic consequences [54] . It has been shown that mechanical deformations alter the electrical properties of myocytes and play an important role in ventricular arrhythmias [30, 93]. On a larger scale, both the contraction of the heart itself and variations in circulatory parameters can alter the length and the tension in cardiac tissue and may affect cardiac electrophysiology via mechano-electrical transduction. At the same time, mechano-electrical transduction is an integrative regulatory system in the heart. Mechanical energy can be translated into electrical or chemical energy by the distortion of the molecular conformation. Membrane stretch opens the channels to admit

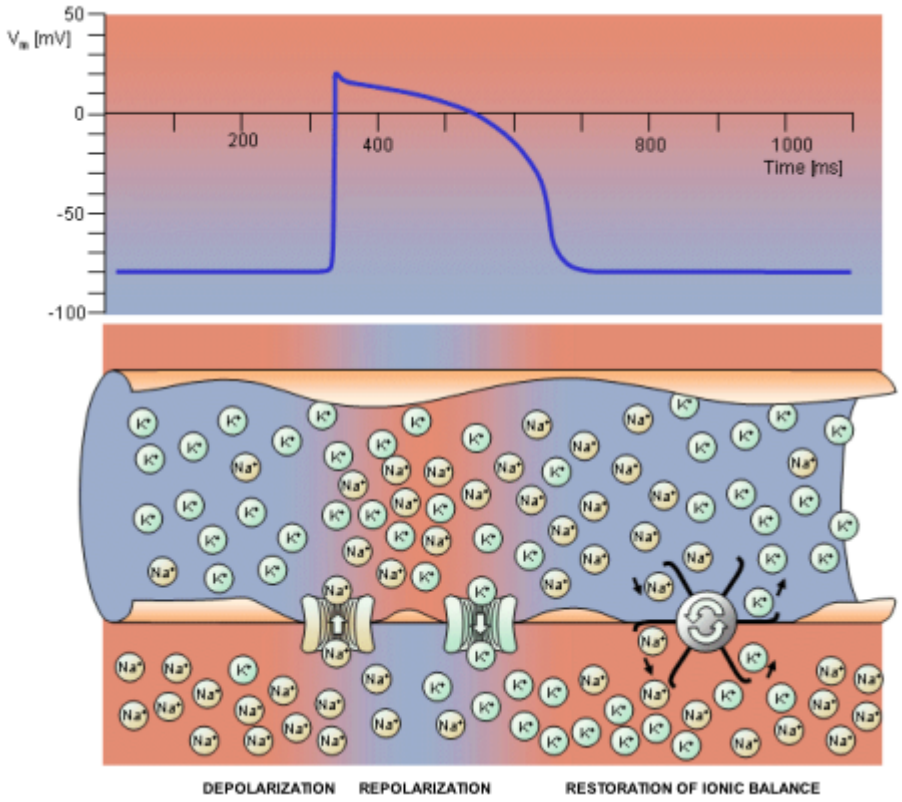

Figure 1.6: Electrophysiology of the cardiac muscle cell. Reproduce from [83].

charge-carrying ions which influence the membrane potential.

The myocardium is contractile and, in addition to extracellular or extraneously applied forces, active contraction provides an intracellular generator of stress and strain, and thus a possible transducing mechanism. Pressure/volume changes and stretch can alter diastolic depolarization, action potential duration and refractory periods as well as produce after-depolarizations.

1.2.1 Mechanics of Cardiac Muscle

In the heart muscle cell, or myocyte, electric activation takes place by means of the same mechanism as in the nerve cell - that is, from the inflow of sodium ions across the cell membrane. The amplitude of the action potential is also similar, being about 100 mV for both nerve and muscle. The duration of the cardiac muscle impulse is, however, two orders of magnitude longer than that in either nerve cell or skeletal muscle. A plateau phase follows cardiac depolarization, and thereafter repolarization takes place. As in the nerve cell, repolarization is a consequence of the outflow of potassium ions. Associated with the electric activation of cardiac muscle cell is its mechanical contraction, which occurs a little later.

An important distinction between cardiac muscle tissue and skeletal muscle is that in cardiac muscle, activation can propagate from one cell to another in any direction. As a result, the activation wavefronts are of rather complex shape. The only exception is the

boundary between the atria and ventricles, which the activation wave normally cannot cross except along a special conduction system, since a non-conducting barrier of fibrous tissue is present.

The propagation of electrical waves resulting from the excitability of individual cardiac cells and the electrical coupling of cardiac cells via gap junctions, that is, at the basis of the electrophysiological processes is well described by phenomenological models such as the reaction-diffusion type models.

Intracellular Ca^{2+} dynamics play a major role in the process of excitation- contraction coupling, and also produce a feedback effect on the shape and duration of the action potential. Calcium dynamics drive calcium influx from the extracellular medium through Ca^{2+} channels into the cell membrane and from internal stores. The surface membrane channels are of different types; voltage-dependent Ca^{2+} channels are the most important in cardiac cells and open in response to depolarization of the cell membrane (see Fig. 1.6).

Chapter 2

Physical description of the electromechanical coupling of cardiac tissue

The mathematical framework for describing the mechanical behavior of cardiac tissue is continuum nonlinear solid elastic mechanics. The heart muscle is hyperelastic, anisotropic, incompressible (nearly incompressible) and (non) homogeneous tissue. As state of art, the passive response is modeled using either isotropic models [48, 101], transversely isotropic, or fully orthotropic descriptions [21, 26, 44]. The active response has non-standard behavior and has been modeled in e.g. [39, 41, 53, 74, 72] using the additive decomposition of the standard passive stress and the active one. We investigate an alternative model, the active strain proposed in [2, 18, 76]. The basic feature of this model is the inclusion of the micro-level information on the fiber contraction in the kinematics without the intermediate transcription of their role in terms of stress. For sake of completeness we present the coupling with the electric behavior, even though we will focus our attention on active solid mechanics.

2.1 Basic notion of continuum nonlinear mechanics

We introduce in this section the basic notion of nonlinear continuum mechanics [11, 16] that we apply to soft biological tissue: reference and current deformation, tensor of gradient of deformation, strain and stress tensor of Cauchy and first Piola-Kirchhoff, theory of hyperelasticity. We focus on convexity of strain-energy that characterizes the hyperelastic materials and its relation with stability.

2.1.1 Kinematics relationship

Let $\mathbf{X}$ and $\mathbf{x}$, respectively denote the position vector of a material (Lagrangian) point in some reference configuration, denoted $B_0 \subset \mathbb{R}^3$, and the (deformed) current configuration, denoted $B_t \subset \mathbb{R}^3$, which vary with time t. The motion (or time-dependent deformation) from B_0 to B_t is known when $\mathbf{x}$ is specified as a function of $\mathbf{X}$ and t, and we write this in

the form

$$\mathbf{x} = \chi(\mathbf{X}, t), \tag{2.1}$$

where χ is the function describing the motion. For each t, χ is invertible and satisfies appropriate regularity conditions: continuous differentiable in all variables, at least up to second derivate. These mathematical assumptions correspond to a specific physical requirements. This ensures a degree of smoothness of the trajectories of material points that will allow us to define quantities such as the velocity and acceleration. The invertibility of motion implies that the two following conditions are met: impenetrability of the body, and voids cannot be created in the body. The second condition implied that the Jacobian J of the transformation (2.1) is non-zero at all times $t \geq 0$ and all points in the body. Here, J is

$$J = \det(\frac{\partial \chi(\mathbf{X}, t)}{\partial \mathbf{X}}).$$

In particular, if the reference configuration was at any time $t^\star$ an actual configuration of the body, then at this time, $\mathbf{x} = \mathbf{X}$ and the consistence condition is $J(t^\star) = 1$. However, as just stated, J can never vanish, so that if J is positive on time, it must be positive at all times. In particular, a deformation with the constraint $J = 1$ at every particle in every configuration and time t is called volume-preserving. The field variables such as the density, ρ, can either be written as a function of $\mathbf{X}$ and t (the referential or Lagrangian description) or as a function of $\mathbf{x}$ and t (the spatial or Eulerian description),

$$\rho = \bar{\rho}(\mathbf{X}, t) = \hat{\rho}(\mathbf{x}, t)$$

$$\hat{\rho}(\mathbf{x}, t) = \hat{\rho}(\chi(\mathbf{X}, t), t) = \bar{\rho}(\mathbf{X}, t) \tag{2.2a}$$

$$\bar{\rho}(\mathbf{X}, t) = \hat{\rho}(\chi^{-1}(\mathbf{x}, t), t) = \hat{\rho}(\mathbf{x}, t). \tag{2.2b}$$

We note that the Eulerian $\hat{\rho}(\mathbf{x}, t)$ description is independent of the information about the position of individual material particles. We use the conventional notation capital letter/low case letter when we use referential/current variable to describe entities (e.g. gradient) that involve spatial derivate.

$$\nabla\ f = \frac{\partial f(\mathbf{X}, t)}{\partial \mathbf{X}} \quad \text{grad}\ f = \frac{\partial f(\mathbf{x}, t)}{\partial \mathbf{x}}.$$

In this framework, the displacement $\mathbf{u}$ of a particle P at time t is defined by,

$$\mathbf{u} = \mathbf{x} - \mathbf{X}.$$

The Eulerian form of displacement obtained using (2.2a),

$$\hat{\mathbf{u}}(\mathbf{x}, t) = \mathbf{x} - \chi^{-1}(\mathbf{x}, t)$$

Alternatively, using (2.2b) we obtain the Lagrangian description,

$$\bar{\mathbf{u}}(\mathbf{X}, t) = \chi(\mathbf{X}, t) - \mathbf{X}$$

Let us introduce the definition of gradient of the deformation. Let $\mathbf{x}$ be the position of a material point L in B_0 and $\mathbf{y}$ be the position of another particle M in the neighborhood $\mathcal{N}$ of L. We assume $\text{diam}\,(\mathcal{N}) < \epsilon$. The rectangular components of dx_i can be written as

$$dx_i = \frac{\partial \chi_i(\mathbf{x}, t)}{\partial X_A} dX_A$$

The components $\frac{\partial \chi_i(\mathbf{x},t)}{\partial X_A}$, where $i, A = 1, 2, 3$, transform under a change of basis, the components of a second order tensor. We denote this tensor as $\mathbf{F}$, so that, the deformation gradient tensor is :

$$\mathbf{F} = \frac{\partial \chi(\mathbf{X}, t)}{\partial \mathbf{X}}, \quad \mathbf{F}_{iA} = \frac{\partial \chi_i(\mathbf{X}, t)}{\partial X_A}$$

and its inverse is

$$\mathbf{F}^{-1} = \frac{\partial \chi^{-1}(\mathbf{x}, t)}{\partial \mathbf{x}}, \quad \mathbf{F}^{-1}_{Ai} = \frac{\partial \chi^{-1}_A(\mathbf{x}, t)}{\partial x_A}$$

Using this notation, it follows $d\mathbf{x} = \mathbf{F}d\mathbf{X}$ or by components $d\mathbf{x}_i = \mathbf{F}_{iA}d\mathbf{X}_A$. From this last expression, we note that $\mathbf{F}$ determines how infinitesimal vectors in the reference configuration are deformed (stretched and rotated) during the motion. For this reason, $\mathbf{F}$ is called the deformation gradient tensor. The local invertibility of the deformation requires that $\mathbf{F}$ be non-singular. If $\mathbf{F}$ depend on $\mathbf{X}$, the deformation is called inhomogeneous deformation, otherwise it is called homogeneous. Using the notation introduced above, we see that the $\mathbf{F}$ and $\mathbf{F}^{-1}$ are related to the gradient of the displacement vector through

$$\mathbf{F} = \nabla \mathbf{u} + \mathbf{I}, \quad \mathbf{F}^{-1} = \mathbf{I} - \operatorname{grad} \mathbf{u}.$$

Note the following relationships between the material gradient and material divergence, and the spatial gradient and spatial divergence of the smooth scalar Ψ, vector $\boldsymbol{u}$ and tensor field $\mathbf{A}$ hold:

$$\begin{aligned} \operatorname{grad} \Psi &= \mathbf{F}^{-1} \nabla \Psi \\ \operatorname{grad} \boldsymbol{u} &= \nabla \boldsymbol{u} \mathbf{F}^{-1} \\ \operatorname{div} \mathbf{A} &= \nabla \cdot \mathbf{A}\mathbf{F}^{-T}. \end{aligned}$$

The tensorial relationship between transformation of an infinitesimal material element from the reference configuration to the current one is determinate by the gradient of the deformation. This transformation can be extent to transformation of infinitesimal area and volume as [66, 86]:

$$d\mathbf{a} = J\mathbf{F}^{-T} d\mathbf{A} \text{ (Nanson's formula)}, \quad dv = JdV. \tag{2.3}$$

Now we consider some specific characteristics of the gradient of deformation, in particular the stretch and strain undergone by this material element. The strain of infinitesimal material element can be defined in different ways.

2.1.2 Material strain tensor: Cauchy-Green and Green-Lagrange

We compute the change in length between two close points $\mathbf{X}$ and $\mathbf{Y}$, located in the reference configuration B_0 endowed by a metric, occurring during a deformation. To be clear the meaning of " close", we give a geometry in the reference configuration:

$$\begin{aligned} \mathbf{Y} = \mathbf{Y} + (\mathbf{X} - \mathbf{X}) = \mathbf{X} + |\mathbf{Y} - \mathbf{X}| \frac{\mathbf{Y} - \mathbf{X}}{\mathbf{Y} - \mathbf{X}} = \mathbf{X} + d\mathbf{X} \\ d\mathbf{X} = dS\mathbf{a}_0 \\ dS = |\mathbf{Y} - \mathbf{X}|\mathbf{a}_0 = \frac{\mathbf{Y} - \mathbf{X}}{|\mathbf{Y} - \mathbf{X}|}. \end{aligned}$$

We denote the material length of the material line element $d\mathbf{X} = \mathbf{Y} - \mathbf{X}$ by dS. It is the distance between two point $\mathbf{X}$ and $\mathbf{Y}$, with $dS/|\mathbf{X}| << 1$ ($|\mathbf{X}| \neq 0$). The unit vector $\mathbf{a}_0$ at the reference position $\mathbf{X}$ describes the direction of the material line element (in context of soft tissue, it may imagined by fiber). In addition using the definition above we find $d\mathbf{X} \cdot d\mathbf{X} = dS\mathbf{a}_0 \cdot dS\mathbf{a}_0 = dS^2$. We apply a deformation map χ to two neighboring point $\mathbf{X}, \mathbf{Y}$: $x = \chi(\mathbf{X}, t)$, $y = \chi(\mathbf{Y}, t)$ are located in the current configuration B_t. We compute their distance. Using Taylor's expansion we can express y in term of vector of reference configuration and deformation gradient:

$$\mathbf{y} = \chi(\mathbf{Y}, t) = \chi(\mathbf{X} + dS\mathbf{a}_0, t) = \chi(\mathbf{X}, t) + dS\mathbf{F}(\mathbf{X}, t)\mathbf{a}_0 + o(\mathbf{Y} - \mathbf{X})$$

Using the geometry of reference configuration, we write the previous identity as:

$$\mathbf{y} - \mathbf{x} = dS\mathbf{F}(\mathbf{X}, t)\mathbf{a}_0 + o(\mathbf{Y} - \mathbf{X}) = \mathbf{F}(\mathbf{X}, t)(\mathbf{Y} - \mathbf{X}) + o(\mathbf{Y} - \mathbf{X})$$

We note that the term $\mathbf{F}(\mathbf{Y} - \mathbf{X})$ linearly approximates the relative deformation $\mathbf{y} - \mathbf{x}$. Next, we define the stretch vector $\lambda_{\mathbf{a}_0}$ in the direction of the unit vector $\mathbf{a}_0$ at $\mathbf{X} \in B_0$ as $\lambda_{\mathbf{a}_0} = \mathbf{F}(\mathbf{X}, t)\mathbf{a}_0$. The stretch is the length $\lambda = |\lambda_{\mathbf{a}_0}|$. Using previous relationship, we obtain the identity: $|\mathbf{y} - \mathbf{x}| = \lambda dS$. Therefore we can deduce that a material line element $d\mathbf{X}$ at $\mathbf{X}$ with length dS at time $t = 0$ becomes the length λdS at time t. The stretch is a measure of how much the unit vector $\mathbf{a}_0$ has stretched. In particular, the line element is extended, unstretched or compressed if $\lambda > 1$,$\lambda = 0$, $\lambda < 1$ respectively. Using the definition of the stretch we calculate its square:

$$\lambda^2 = \mathbf{a}_0 \cdot \mathbf{F}^T\mathbf{F}\mathbf{a}_0 = \mathbf{a}_0 \cdot \mathbf{C}\mathbf{a}_0$$

where $\mathbf{C}$ is so-called right Cauchy-Green tensor and it is an important strain measure in material coordinate. Note $\mathbf{C} = \mathbf{F}^T\mathbf{F}$ is symmetric and positive definite at all point of reference configuration and its determinant is J^2. Its inverse $\mathbf{B} = \mathbf{F}^{-1}\mathbf{F}^{-T}$ is so-called Piola deformation tensor. The elements of right Cauchy-Green tensor locate at the diagonal and off-diagonal have a physical significance: $\mathbf{C}_{ii}$ is the square of the stretch of a material element which was aligned with the direction $\mathbf{e}_i$ in reference configuration, while the non-zero element of off-diagonal $\mathbf{C}_{ij}$ means that the angle between the two infinitesimal material elements of reference configuration with unit vectors $\mathbf{e}_i$ and $\mathbf{e}_j$ change respect the angle between infinitesimal element of current configuration with same unit vectors. In formulas:

$$\cos\alpha = \frac{C_{ij}}{\sqrt{C_{ii}C_{jj}}},$$

if $\alpha = 90^\circ$ then $C_{ij} = 0$, if $\alpha < 90^\circ$ then $C_{ij} > 0$, and if $\alpha \in (90^\circ, 270^\circ)$ then $C_{ij} < 0$.

As a further strain measure we define the change in the square length $(\lambda dS)^2 - dS^2$

$$\frac{1}{2}[(\lambda dS)^2 - dS^2] = \frac{1}{2}[(dS\mathbf{a}_0) \cdot \mathbf{F}^T\mathbf{F}(dS\mathbf{a}_0) - dS^2] = d\mathbf{X} \cdot \mathbf{E}d\mathbf{X}$$
$$\mathbf{E} = \frac{1}{2}(\mathbf{F}^T\mathbf{F} - \mathbf{I}).$$

The identity $\mathbf{E}$ is so-called Green-Lagrange strain tensor. We have introduce $\mathbf{C}, \mathbf{E}$ as material strain tensor, using the same argument we can define correspondent spatial strain tensor : $\mathbf{b} = \mathbf{F}\mathbf{F}^T$ and $\mathbf{e} = \frac{1}{2}(\mathbf{I} - \mathbf{F}^{-\mathbf{T}}\mathbf{F}^{-\mathbf{1}})$ called left Cauchy-Green tensor and Euler-Almansi strain tensor, respectively. Moreover, we can write the Euler-Almansi strain tensor with respect to the gradient of the displacement $\mathbf{e} = \frac{1}{2}(\operatorname{grad}\boldsymbol{u} + \operatorname{grad}\boldsymbol{u}^T - \operatorname{grad}\boldsymbol{u}^T\operatorname{grad}\boldsymbol{u})$.

Pull-back and push-forward operations

In this section, we introduce two operation push-forward and its inverse pull-back that are two transformation from reference and current configuration and vice-versa. We use these operation in the description of the mechanism of decomposition of deformation and construction of active strain-energy. In literature [66] these operation are indicated as $\chi_*(\cdot)$ and $\chi_*(\cdot)^{-1}$. In particular, a push-forward is an operation which transform a vector or tensor-value quantity based on the reference configuration to the current configuration. For example, we can compute the push-forward of Euler-Almansi strain tensor and we obtain Green-Lagrange strain tensor:

$$\begin{aligned}\mathbf{e} &= \frac{1}{2}(\mathbf{I} - \mathbf{F}^{-T}\mathbf{F}^{-1}) = \mathbf{F}^{-T}[\frac{1}{2}\mathbf{F}^{-T}(\mathbf{I} - \mathbf{F}^{-T}\mathbf{F}^{-1})\mathbf{F}]\mathbf{F}^{-1} \\ &= \mathbf{F}^{-T}[\frac{1}{2}\mathbf{F}^{-T}(\mathbf{F}^T\mathbf{F} - \mathbf{I})]\mathbf{F}^{-1} = \mathbf{F}^{-T}\mathbf{E}\mathbf{F}^{-1} \\ &= \chi_*(\mathbf{E})\end{aligned}$$

A pull-back is an inverse operation, which transform a vector or tensor-value quantity based on the current configuration to the reference configuration. We illustrate some propriety of gradient of deformation and strain tensor using the decomposition technique.

2.1.3 Invariants

The invariant of strain tensor $\mathbf{C}$ (or $\mathbf{B}$) plays an important role in the definition of function that characterized the material proprieties of soft tissue. The principal invariants of $\mathbf{C}$ are defined by

$$I_1 = \operatorname{tr}\mathbf{C}, \quad I_2 = \frac{1}{2}[(\operatorname{tr}\mathbf{C})^2 - \operatorname{tr}(\mathbf{C}^2)], \quad I_3 = \det\mathbf{C}$$

for incompressible material we have the relationship $I_3 = J^2 = 1$. These invariant are isotropic. If the material ha s a preferred direction in the reference configuration, denoted by the unit vector $\mathbf{a}_0$, this introduces anisotropy, transverse isotropy, and with it come two additional transversely isotropic invariants defined by

$$I_4 = \mathbf{a}_0 \cdot (\mathbf{C}\mathbf{a}_0), \quad I_5 = \mathbf{a}_0 \cdot (\mathbf{C}^2\mathbf{a}_0).$$

Note that these are unaffected by reversal of direction of $\mathbf{a}_0$. If there are two preferred directions, the second denoted by $\mathbf{b}_0$, then this introduce the invariant associated with it

$$I_5 = \mathbf{b}_0 \cdot (\mathbf{C}\mathbf{b}_0), \quad I_6 = \mathbf{b}_0 \cdot (\mathbf{C}^2\mathbf{b}_0).$$

Additionally a coupling invariant, denoted by I_8, which we define here by

$$I_8 = \mathbf{a}_0 \cdot (\mathbf{C}\mathbf{b}_0) = \mathbf{b}_0 \cdot (\mathbf{C}\mathbf{a}_0)$$

Note that this changes sign if either $\mathbf{a}_0$ and $\mathbf{b}_0$ is reversed and is note strictly invariant in this sense but it is more convenient to use this than the I_8^2 or $I_8\mathbf{a}_0\mathbf{b}_0$. In particular, if the two preferred directions are orthogonal , [68] the magnitude of I_8 depends on $I_1, \ldots, I_7$

$$I_8 = I_2 + I_4I_6 + I_5 + I_7 - I_1(I_4 + I_6).$$

2.1.4 Measures of stress

In this subsection, we introduce a crucial notion of continuum mechanics: stress tensor, which is responsible for deformation of materials. In particular, we consider a deformable body during finite deformation(motion). It is convenient to express the tensor in term of coordinate of reference or intermediate configuration, because usually the current configuration is unknown. We provide two type of stress measure:Cauchy and Piola-Kirchhoff. The first tensor works on the current configuration and it play an important role in elastic theory, while the second tensor acts on the reference configuration and it is an important measure of force in the framework of hyperelastic theory apply to biological tissue. Firstly, we introduce the Cauchy tensor by the following theorem.

Theorem 2.1.1 (Theorem of Cauchy (existence of stress tensor))**.**
Let's $\mathbf{t}(\mathbf{x}, t, \mathbf{n})$ *stress vector, that is continuous respect to* $\mathbf{x}$*,* $\rho(\mathbf{x}, t)\mathbf{b}(\mathbf{x}, t)$ *and* $\rho(\mathbf{x}, t)\mathbf{a}(\mathbf{x}, t)$ *are bounded. Then the principle of conservation of motion quantity imply that a stress tensor exists* $\sigma(\mathbf{x}, t)$ *such that*

$$\mathbf{t}(\mathbf{x}, t, \mathbf{n}) = \sigma(\mathbf{x}, t)\mathbf{n}, \quad \mathbf{t}_i(\mathbf{x}, t, \mathbf{n}) = \sigma_{ij}(\mathbf{x}, t)\mathbf{n}_j.$$

Applying the principle of conservation of motion and quantity, the Divergence and Cauchy theorems, we may deduce the Cauchy equation of motion:

$$\nabla \cdot \sigma(\mathbf{x}, t) + \rho(\mathbf{x}, t)\mathbf{b}(\mathbf{x}, t) = \rho(\mathbf{x}, t)\mathbf{a}(\mathbf{x}, t), \quad \sigma_{ij,j} + \rho b_i = \rho a_i.$$

Moreover, the conservation of kinetic energy imply the symmetry of Cauchy stress. For the absence of knowledge of current configuration, we want to measure the stress tensor that act on reference configuration (undeformed). The start point to define this kind of tensor, is the representation of contact force acting on the surface of current configuration by a stress tensor artificially applied to the correspondent surface of the reference configuration. Let $\mathbf{t}(\mathbf{x}, t, \mathbf{n})$ be the stress Cauchy vector at $\mathbf{x} \in B_t$ acting on the element of deformed surface's element $\mathbf{n}ds$. The first stress vector of Piola-Kirchhoff $\mathbf{T}(\mathbf{X}, t, \mathbf{N}(\mathbf{X}))$ applies at $\mathbf{X} \in B_0$ on surface's element of reference configuration $\mathbf{N}dS$ associated to $\mathbf{n}ds$ is defined by

$$\mathbf{T}(\mathbf{X}, t, \mathbf{N}(\mathbf{X}))dS = \mathbf{t}(\chi(\mathbf{X}, t), t, \mathbf{n}(\mathbf{x}, t))ds \tag{2.4}$$

Note that dS and ds are both positive scalar then the equation (2.4) implies $\mathbf{T}$ and $\mathbf{t}$ have the same direction. The stress vector $\mathbf{T}$ represent the current magnitude. It act on current configuration and it is a function of $\mathbf{X}$ and of normal vector $\mathbf{N}$ on dS that is a infinitesimal surface of reference configuration. The relation (2.4) gives the elementary force acting on the current configuration. Applying the Cauchy's theorem in the equation (2.4) and Nanson's formula (2.3), we obtain:

$$\begin{aligned}\mathbf{T}(\mathbf{X}, t, \mathbf{N})dS &= \mathbf{t}(\chi(\mathbf{X}, t), t, \mathbf{n})ds = \sigma(\chi(\mathbf{X}, t), t)\mathbf{n}ds \\ &= J(\mathbf{X}, t)\sigma(\chi(\mathbf{X}, t), t)\mathbf{F}^{-T}\mathbf{N}dS,\end{aligned}$$

with $ds > 0$, we may deduce

$$\mathbf{T}(\mathbf{X}, t, \mathbf{N}) = \mathbf{P}(\mathbf{X}, t)\mathbf{N} \tag{2.5}$$

where

$$\mathbf{P}(\mathbf{X}, t) = \mathbf{J}(\mathbf{X}, t)\sigma(\chi(\mathbf{X}, t), t)\mathbf{F}^{-T} \tag{2.6}$$

is so-called first Piola-Kirchhoff stress tensor. The equation (2.5) is equivalent to the Cauchy's theorem. Using the symmetry of Cauchy stress tensor and (2.6) we obtain

$$\mathbf{P}\mathbf{F}^T = \mathbf{F}\mathbf{P}^T.$$

2.1.5 Hyperelastic materials

In continuum mechanics Cauchy's equation on motion cannot be solved until we know how the stress depends on the motion, likewise in particle mechanics we cannot solve the Newton's second law until we know how the force depends on the position and velocity of the particle. A material is called *elastic* when we we can write the first Piola-Kirchhoff stress $\mathbf{P}$ as a function $\hat{\mathbf{P}}$ of points $\mathbf{X} \in B_0$ and the tensorial variable , namely the deformation gradient $\mathbf{F}$ such that the stress associate with a configuration χ is

$$\mathbf{P}(\mathbf{X}) = \hat{\mathbf{P}}(\mathbf{X}, \mathbf{F}(\mathbf{X}))$$

Specification of a $\hat{\mathbf{P}}$ for an elastic material is called a stress-strain law, and $\hat{\mathbf{P}} : \bar{B}_0 \times \mathbb{M}^n_+ \to \mathbb{M}^n$ is called a constitutive function or response function of the material, where $\mathbb{M}^n$ is tensor $n \times n$ and $\mathbb{M}^n_+$ is its subset such that the determinant is positive. The *hyperelastic* materials is a useful class of elastic materials for which there is a stored energy density $W : \bar{B}_0 \times \mathbb{M}^n_+ \to \mathbb{R}$ depending on the points $\mathbf{X} \in B_0$ and gradient deformation. Its response function $\hat{\mathbf{P}}$ can be fully reconstructed from $\mathbf{W}$ by means of the relation

$$\hat{\mathbf{P}}(\mathbf{X}, \mathbf{F}) = \frac{\partial W}{\partial \mathbf{F}} \quad \forall (X, \mathbf{F}) \in B_0 \times \mathbb{M}^n_+$$

where $\frac{\partial W}{\partial \mathbf{F}}$ denotes the Gateaux derivative of W with respect the variable $\mathbf{F}$. In other words, at each $X \in B_0$ $\frac{\partial W}{\partial \mathbf{F}}(\mathbf{X}, \mathbf{F})$ is the unique tensor in $\mathbb{M}^n$ that satisfies

$$W(\mathbf{X}, \mathbf{F} + \mathbf{H}) = W(W(\mathbf{x}, \mathbf{F}) + \frac{\partial W}{\partial \mathbf{F}}(\mathbf{x}, \mathbf{F}) : \mathbf{H} + o(|\mathbf{H}|),$$

for all $\mathbf{F} \in \mathbb{M}^n_+$ and $\mathbf{H} \in \mathbb{M}^3$ and $|\mathbf{H}| = (\mathrm{tr}\,(\mathbf{H}^T\mathbf{H}))^{1/2}$.

We remark that the stored energy function of a given hyperelastic material is only defined up to the addition of an arbitrary function of $\mathbf{X} \in B_0$. In the following theorem and its corollary, we give the classical equivalence's results between a boundary value problem and variational problem for hyperelastic material.

Theorem 2.1.2. *Let there be given a hyperelastic material subjected to conservative applied forces and conservative applied surface forces. Then the boundary value problem is: Find the position $\boldsymbol{u}$ such that*

$$\begin{cases} -\mathrm{div}(\frac{\partial W}{\partial \mathbf{F}}(\mathbf{x}, \nabla \boldsymbol{u}(\mathbf{x}))) = \hat{f}(\mathbf{x}, \boldsymbol{u}(\mathbf{x})) & \mathbf{x} \in B_0 \\ \frac{\partial W}{\partial \mathbf{F}}(\mathbf{x}, \nabla \boldsymbol{u}(\mathbf{x}))\mathbf{n} = \hat{f}(x, \nabla \boldsymbol{u}(\mathbf{x})) & \mathbf{x} \in \partial_N B_0 \\ \boldsymbol{u}(\mathbf{x}) = \boldsymbol{u}_0(\mathbf{x}) & \mathbf{x} \in \partial_D B_0, \end{cases} \tag{2.7}$$

are formally equivalent to the equations

$$I'(\boldsymbol{u})\mathbf{v} = 0,$$

for all smooth maps $\mathbf{v} : \bar{B}_0 \to \mathbb{R}^n$ that vanish on $\partial_D B_0$, where the functional I is defined for smooth enough mapping $\psi : \bar{B}_0 \to \mathbb{R}^n$ by

$$I(\psi) = \int_{B_0} W(\mathbf{x}, \nabla \psi(\mathbf{x})) - \hat{f}(\mathbf{x}, \psi(\mathbf{x}))\mathbf{v}(\mathbf{x}) - \hat{q}(\mathbf{x}, \nabla \psi(\mathbf{x}))\mathbf{v}(\mathbf{x}) \tag{2.8}$$

The functional $\hat{W}(\phi)$ associated to store energy is called strain energy and the functional I is called the total energy. In order to be in the usual framework where both the functions and their variations lie in same vector space, we assume that there exists a mapping from B_0 into $\mathbb{R}^n$ that coincides with the given function $\boldsymbol{u}_0 \in \partial_D B_0$. Denoting such a mapping with the same letter $\boldsymbol{u}_0$, consider the functional I_0 defined for an arbitrary mapping $\mathbf{w}$ by

$$I_0(\mathbf{w}) = I(\mathbf{w} + \boldsymbol{u}_0).$$

Since the functions $\boldsymbol{u} - \mathbf{w}$ and $\mathbf{v}$ belong to the same vector space, we can conclude that the functional I_0 is stationary at the point $(\boldsymbol{u} - \boldsymbol{u}_0)$, since

$$I_0'(\boldsymbol{u} - \boldsymbol{u}_0) = 0 \text{ if and only if } I_0'(\boldsymbol{u} - \boldsymbol{u}_0)\mathbf{v} = I'(\boldsymbol{u})\mathbf{v} = 0 \text{ for all } \mathbf{v} \text{ vanishing on } \partial_D B_0.$$

So, the total energy I is stationary at the deformation $\boldsymbol{u}$ with respect to variations vanishing on $\partial_D B_0$. The observation that a minimum of the total energy is a particular stationary point of the functional I_0 leads to the following crucial corollary:

Corollary 2.1.3. *Let the assumption and notation be as in Theorem 2.1.2. Then any smooth enough mapping $\boldsymbol{u}$ that satisfies*

$$\begin{aligned} \boldsymbol{u} \in V &= \left\{\psi : \bar{B}_0 \to \mathbb{R}^n : \psi = \boldsymbol{u}_0 \text{ on } \partial_D B_0\right\} \\ I(\boldsymbol{u}) &= \inf_{\mathbf{w} \in V} I(\mathbf{w}) \\ I(\mathbf{w}) &= \int_{B_0} W(\mathbf{x}, \nabla \mathbf{w}(\mathbf{x}))dx - \hat{\mathbf{f}}(\mathbf{x}, \mathbf{w}(\mathbf{x}))\mathbf{v}(\mathbf{x}) - \hat{\mathbf{g}}(\mathbf{x}, \nabla \mathbf{w}(\mathbf{x}))\mathbf{v}(\mathbf{x}), \end{aligned}$$

solves the boundary value problem (2.7).

In the language of the calculus of variations, this boundary value problem forms the Euler-Lagrange equations associated with the total energy I, in the sense that any smooth enough minimizer $\boldsymbol{u}$ of the total energy I over the set of admissible solutions V i.e. any $\boldsymbol{u} \in V$ that satisfies $I(\boldsymbol{u}) = \inf_{\mathbf{v} \in V} I(\mathbf{v})$, is a solution of this boundary value problem. We observe that the orientation-preserving condition $\det \nabla \boldsymbol{u} > 0$ that a genuine deformation should satisfy in B_0 is easily taken care of, since the set

$$\left\{\mathbf{w} \in \mathcal{C}^1(\bar{B}_0, \mathbb{R}^n) : \det(\nabla \boldsymbol{u} + \mathbf{w}) > 0 \text{ in } \bar{B}_0 \, \mathbf{w} = 0 \text{ on } \partial_D B_0\right\}$$

is an open subset of $\left\{\mathbf{w} \in \mathcal{C}^1(\bar{B}_0, \mathbb{R}^n) : \mathbf{w} = 0 \text{ on } \partial_D B_0\right\}$. Now we examine further proprieties of the stored energy function that will all play a crucial role in the existence theory. We will say that a stored energy function satisfies the axiom of material frame-indifference if the response function for the Cauchy stress is itself frame-indifferent. The following result, which gives two necessary and sufficient conditions for this property to holds.

Theorem 2.1.4. *The stored energy function $W : \bar{B}_0 \times \mathbb{M}^n_+ \to \mathbb{R}$ of a hyperelastic material is frame-indifferent if and only if at all points $\mathbf{x} \in \bar{B}_0$:*

$$W(\mathbf{x}, \mathbf{Q}\mathbf{F}) = W(\mathbf{x}, \mathbf{F}) \quad \forall \mathbf{F} \in \mathbb{M}^n_+, \mathbf{Q} \in \mathbb{O}^n_+ \tag{2.9}$$

or equivalently , is and only if there exists a function $\tilde{W} : \bar{B}_0 \times SO^n \to \mathbb{R}$ such that

$$W(\mathbf{x}, \mathbf{F}) = \tilde{W}(\mathbf{x}, \mathbf{F}^T\mathbf{F}) \quad \forall \mathbf{F} \in \mathbb{M}^n_+$$

For a proof see [16]. We shall see later that the requirement that $W(\mathbf{QF}) = W(\mathbf{F})$ for all $\mathbf{F} \in \mathbb{M}^n_+, Q \in \mathbb{O}^n_+$ precludes the convexity of the mapping $\mathbf{F} \to W(\mathbf{F})$. The holding of (2.9) is an objective property of W (see e.g. [79]). The following theorem permit us to define the response function for the second Piola-Kirchhoff stress.

Theorem 2.1.5. *Given a hyperelastic material whose stored energy function W is frame-indifferent, let the function $\tilde{W} : \bar{B}_0 \times SO^n \to \mathbb{R}$ be defined at each point $\mathbf{x} \in \bar{B}_0$ by:*

$$\tilde{W}(\mathbf{x}, \mathbf{C}) = W(\mathbf{x}, \mathbf{C}^{1/2}) \quad \forall\, \mathbf{C} \in SO^n$$

and assume without loss of generality that the derivative $\frac{\partial \tilde{W}}{\partial \mathbf{C}}(\mathbf{x}, \mathbf{C})$ is a symmetric tensor. Then the response function for the second Piola-Kirchhoff stress is given by:

$$\mathbf{S}(\mathbf{x}, \mathbf{F}) = \mathbf{S}(\mathbf{x}, \mathbf{C}) = 2\frac{\partial \tilde{W}}{\partial \mathbf{C}}(\mathbf{x}, \mathbf{C}), \mathbf{C} = \mathbf{F}^T\mathbf{F} \quad \forall\, \mathbf{F} \in \mathbb{M}^3_+$$

Conversely, an elastic material whose response $\mathbf{S}$ is of the form

$$\mathbf{S}(\mathbf{x}, \mathbf{F}) = 2\frac{\partial \tilde{W}}{\partial \mathbf{C}}(\mathbf{x}, \mathbf{F}^T\mathbf{F}) \quad \forall\, \mathbf{F} \in \mathbb{M}^n_+ \; \tilde{W} : \bar{B}_0 \times SO^n \to \mathbb{R}$$

is hyperelastic with a stored energy function given by

$$W(\mathbf{x}, \mathbf{F}) = \tilde{W}(\mathbf{x}, \mathbf{F}^T\mathbf{F}) \quad \forall\, \mathbf{F} \in \mathbb{M}^n_+$$

For proof see [16]. Another property of store energy is isotropic pointwise. The following sufficient and necessary condition is a criterion to identify this property.

Theorem 2.1.6. *The stored energy function $W : \bar{B}_0 \times \mathbb{M}^n_+ \to \mathbb{R}$ of a hyperelastic material is isotropic at $\mathbf{x}$ if and only if*

$$W(\mathbf{x}, \mathbf{F}) = W(\mathbf{x}, \mathbf{FQ}) \quad \forall \mathbf{F} \in \mathbb{M}^3_+, \, Q \in \mathbb{O}^3_+$$

Taking account these two properties at same time we obtain the following result.

Theorem 2.1.7. *The stored energy function of an hyperelastic material is frame-indifferent and isotropic pointwise if and only if there exists a function*

$$\dot{W} : \{(I_1(A), I_2(A), I_3(A)) : A \in SO^n\} \to \mathbb{R},$$

such that:

$$W(\mathbf{x}, \mathbf{F}) = \dot{W}(\mathbf{x}, (I_1(\mathbf{F}^T\mathbf{F}), I_2(\mathbf{F}^T\mathbf{F}), I_3(\mathbf{F}^T\mathbf{F}))) \quad \mathbf{F} \in \mathbb{M}^n_+$$

A consequence of this result is that given a stored function in terms of the principal invariant of $\mathbf{C} = \mathbf{F}^T\mathbf{F}$, we can associate a response function in the following way:

$$\frac{1}{2}\hat{\mathbf{P}}(\mathbf{x}, \mathbf{F}) = \frac{\partial \dot{W}}{\partial I_1(\mathbf{C})}\mathbf{F} + \frac{\partial \dot{W}}{\partial I_2(\mathbf{C})}(I_1(\mathbf{C})I - \mathbf{F}\mathbf{F}^T) + \frac{\partial \dot{W}}{\partial I_3(\mathbf{C})}I_3(\mathbf{C})\mathbf{F}^{-T}$$

An example of material frame-indifference, isotropic and homogeneous hyperelastic is St Venant-Kirchhoff's material, whose store energy function is:

$$W(\mathbf{E}) = \frac{\lambda}{2}(tr(\mathbf{E}))^2 + \mu \mathrm{tr}\, \mathbf{E}^2$$

where $\mathbf{E} = \frac{1}{2}(\mathbf{F}^T\mathbf{F} - I)$ and λ, μ are Lamé constants of the material.

We describe the behavior of the store energy function for large strain, which mathematically reflect the idea that "infinite stress should accompany extreme strains" both in the form of the behavior as $\det \mathbf{F} \to 0^+$:

$$W(\mathbf{F}) \to +\infty \quad \text{as} \det \mathbf{F} \to 0^+.$$

In case of hyperelastic materials, it corresponds to the requirement that the stored energy function W approaches $+\infty$ if any of the eigenvalues $\lambda_i(\mathbf{C})$ of the matrix $\mathbf{C}$ approaches 0 or $+\infty$. Keeping two eigenvalues $\lambda_{i+1}(\mathbf{C})$ and $\lambda_{i+2}(\mathbf{C})$ in a compact interval of $(0, +\infty)$ we have the following equivalence

$$\begin{aligned}
\lambda_i(\mathbf{C}) &\to 0^+ && \text{if and only if } \det \mathbf{F} \to 0^+ \\
\lambda_i(\mathbf{C}) &\to +\infty && \text{if and only if } \|\mathbf{F}\| \to +\infty \\
\lambda_i(\mathbf{C}) &\to +\infty && \text{if and only if } \|\mathrm{Cof}\, \mathbf{F}\| \to +\infty \\
\lambda_i(\mathbf{C}) &\to +\infty && \text{if and only if } \det \mathbf{F} \to +\infty.
\end{aligned}$$

We are thus led to the following assumptions governing the behavior for large strains of the stored energy function at each point $\mathbf{x} \in \bar{B}_0$

$$\begin{aligned}
W(\mathbf{x}, \mathbf{F}) &\to +\infty && \text{as} \det \mathbf{F} \to 0^+ \\
W(\mathbf{x}, \mathbf{F}) &\to +\infty && \text{as} \{\|\mathbf{F}\| + \|\mathrm{Cof}\, \mathbf{F}\| + \|\det \mathbf{F}\|\} \to +\infty \quad \mathbf{F} \in \mathbb{M}^n_+
\end{aligned}$$

This first assumption is called the behavior as $\det \mathbf{F} \to 0^+$. A sharper version of the second assumption takes the form of the following coercivity inequality, which is a tool in the existence theorems of Ball :

$$\begin{aligned}
\alpha > 0, p > 0, q > 0, r > 0 \\
W(\mathbf{x}, \mathbf{F}) \geq \alpha \{\|\mathbf{F}\|^p + \|\mathrm{Cof}\, \mathbf{F}\|^q + (\det \mathbf{F})^r\} - \beta \\
\forall\, (\mathbf{x}, \mathbf{F}) \in \bar{B}_0 \times \mathbb{M}^3_+
\end{aligned}$$

where $p \geq 2, q \geq \frac{p}{p-1}, r > 1$.

2.1.6 Existence of solutions for hyperelastic materials

From a mathematical prospective the fundamental issue is to guarantee the existence of (unique) solutions for a given constitutive model. Local existence and uniqueness theorems in nonlinear elastostatics and elastodynamics are based on *ellipticity*. The ellipticity condition states that an energy function $W(\mathbf{F})$ leads to an elliptic system if and only if the well known Legendre-Hadamard condition holds,

$$\frac{\partial^2 W}{\partial \mathbf{F} \partial \mathbf{F}}(\mathbf{F}) \geq 0$$

for all $\mathbf{F}(\mathbf{X}) \in GL^+(3, \mathbb{R}), \mathbf{X} \in \mathbb{R}^3$. If the inequality holds we say that W is strongly elliptic or uniform rank-1 convex. Originally, the global existence theory for elastic problems was based on *convexity* of the free energy function. A scalar function is said to be convex if, for all $\mathbf{x}_1, \mathbf{x}_2 \in \mathbb{R}^3$, holds

$$\phi(\lambda \mathbf{x}_1 + (1 - \lambda)\mathbf{x}_2) \leq \lambda \phi(\mathbf{x}_1) + (1 + \lambda)\phi(\mathbf{x}_2) \lambda \in (0, 1)$$

However, from a physical point of view that condition may be to strong. This leads to the important concept of *quasiconvexity*, introduced by Morrey [69]. On a fixed domain Ω a function W is quasiconvex if

$$\int_\Omega W(\mathbf{F} + \operatorname{grad} \mathbf{u})dx \geq \int_\Omega W(\mathbf{F})dx \qquad \forall \mathbf{F} \in GL^+(3,\mathbb{R}), \mathbf{u} \in \mathcal{C}_0^\infty.$$

Morrey showed that (under suitable growth conditions) quasiconvexity is a necessary and sufficient condition for a functional to be weakly lower semi-continuous, i.e., $W(\mathbf{F}) \geq \alpha$. Thus, quasiconvexity is closely related to the existence of minimizers of an energy function. Finally, following [66], the implication chain, under indicated, relates all introduced concepts

$$\text{convexity } \Rightarrow \text{polyconvexity } \Rightarrow \text{quasiconvexity } \Rightarrow \text{rank}-1 \text{ convexity (ellipticity).}$$

2.1.7 Concepts of convexity and polyconvexity

In this subsection we point out on the relation between convexity and existence theory. There are two tool to study the existence of solution of variational problem: The implicit function theorem and the minimization of a cost functional. The last one requires the notion of polyconvexity function.

A subset of a vector space is convex if, whenever it contains two points u and v, it contains the close segment $[u, v]$. A closed convex hull $\overline{co(U)}$ of U is the smallest closed convex subset of V that contain U. In elasticity we identify two particular convex hulls:

$$co\mathbb{M}^3_+ = \mathbb{M}^3_+ \tag{2.10a}$$
$$co\left\{(\mathbf{F}, \operatorname{Cof}\mathbf{F}, \det\mathbf{F}) \in \mathbb{M}^3 \times \mathbb{M}^3 \times \mathbb{R}\right\} = \mathbb{M}^3 \times \mathbb{M}^3 \times \mathbb{R}^+$$

From (2.10a), we deduce that $\mathbb{M}^3$ is not convex. Now we point out the some relations between the convexity of sets and the minima of functions.

Theorem 2.1.8. *Let $J : U \to \mathbb{R}$ be a function defined on a convex subset U of normed vector space. If a point $u \in U$ is a local minimum of the function $J : U \to \mathbb{R}$ and if the function J is differentiable at u then*

$$J'(u)(v - u) \geq 0 \quad \forall\, v \in U$$

A function $J : U \to \mathbb{R}$ defined on a convex subset U of a vector space V is convex on U if

$$u, v \in U,\ \theta \in [0, 1] \to J(\theta u + (1 - \theta)v) \leq \theta J(u) + (1 - \theta)J(v)$$

and strictly convex on U if

$$u, v \in U,\ u \neq v, \theta \in (0, 1) \to J(\theta u + (1 - \theta)v) < \theta J(u) + (1 - \theta)J(v)$$

For example the function $F \to \|\mathbf{F}\| = \operatorname{tr}(\mathbf{F}^T\mathbf{F})^{1/2}$ is strictly convex function. The following result point out the relation between the convexity of functions and minima of functions.

Theorem 2.1.9. *Let $J : U \to \mathbb{R}$ be a convex function defined on a convex subset U of a normed vector space. Then any local minimum of J on U is a minimum. If J is strictly*

convex, it has at most one minimum on U, and it is a strict minimum. Let J be differentiable at a point $u \in U$ then u is a minimum of J on U if and only if

$$J'(u)(v-u) \geq 0 \quad \forall\, v \in U$$

If the set U is open, a point u is a minimum of J on U if and only if $J'(u) = 0$.

Convexity of the stored energy function with respect to its argument $\mathbf{F}$ point-wisely would reader the mathematical analysis of associated minimization problem straightforward. The simple convex function may be a good candidate for constructing stored energy functions. Nevertheless such seemingly innocuous examples must be ruled out, on the ground that they contradict the most immediate physical experience, as we now show.

Theorem 2.1.10. *Let $\mathbf{x} \in \bar{B}_0$ be such that the function*

$$W(\mathbf{x}, \cdot) : \mathbf{F} \in \mathbb{M}^3_+ \to W(\mathbf{x}, \mathbf{F}) \in \mathbb{R}$$

is convex. Then this property is incompatible with the behavior for large strains of the stored energy function and the axiom of material frame-indifference implies that hold these inequality:

$$\tau_1 + \tau_2 \geq 0, \tau_2 + \tau_3 \geq 0, \tau_3 + \tau_1 \geq 0 \quad \tau_i = \lambda_i(\sigma)$$

John Ball [8] has made the crucial observation that if the convexity of the stored energy function must be ruled out, it can be replaced by the weaker requirement that the function $W^\star$ defined by $W^\star(\mathbf{x}, \mathbf{F}, \operatorname{Cof}\mathbf{F}, \det\mathbf{F}) = W(\mathbf{x}, \mathbf{F})$ for all $\mathbf{F} \in \mathbb{M}^3_+$ be convex on $\{(\mathbf{F}, \operatorname{Cof}\mathbf{F}, \det\mathbf{F}) \in \mathbb{M}^3 \times \mathbb{M}^3 \times \mathbb{R}\}$. Contrary to convexity requirement and indeed, it is satisfied by realistic models. The definition proposed by J. Ball is essentially the following one. A stored energy function $W : \bar{B}_0 \times \mathbb{M}^3_+$ is polyconvex if for each $\mathbf{x} \in \bar{B}_0$, there exists a convex function

$$\mathbb{W}(x, \cdot) : \mathbb{M}^3 \times \mathbb{M}^3 \times \mathbb{R}^+ \to \mathbb{R}$$

such that

$$W(\mathbf{x}, \mathbf{F}) = \mathbb{W}(\mathbf{x}, \mathbf{F}, \operatorname{Cof}\mathbf{F}, \det\mathbf{F})$$

For example, the functions $\mathbf{F} \to \|\operatorname{Cof}\mathbf{F}\|^2$ and $\mathbf{F} \to \det\mathbf{F}$ are both polyconvex but are not convex. Combining these examples we obtain a stored energy function of the form:

$$W(\mathbf{F}) = a\|\mathbf{F}\|^2 + b\|Cof\mathbf{F}\|^2 + \Gamma(\det\mathbf{F})$$

where $a > 0, b > 0$ and $\Gamma : \mathbb{R}^+ \to \mathbb{R}$ is a convex function, is polyconvex. An important class of stored energy function is Ogden's stored function:

$$W(\mathbf{F}) = \sum_{i=1}^{M} a_i(\nu_1^{\gamma_i} + \nu_2^{\gamma_i} + \nu_3^{\gamma_i}) + \sum_{i=1}^{M} b_j((\nu_2\nu_3)^{\delta_l} + (\nu_3\nu_1)^{\delta_l} + (\nu_1\nu_2)^{\delta_l})$$

where $\nu_i(\mathbf{F})$ are the singular value of $\mathbf{F}$, $a_i > 0$ and $\gamma_i \geq 1$, $1 \leq i \leq M$, $b_j > 0$, $\delta_l \geq 1$, $1 \leq j \leq N$. Then the stored function is polyconvex and it satisfies the coercivity inequality.

The result expressed by theorems 2.3.1 and 2.3.2 permit us to claim that the variational equation (2.8), associated with the equation of nonlinear three-dimensional elasticity (2.7), are the Euler equations associated to the minimization problem

$$I(\phi) = \min_{\psi \in \mathcal{M}} I(\psi),$$

where $\mathcal{M}$ is an appropriate set of all admissible deformations $\psi : B_0 \to \mathbb{R}^n$. John Ball's theory provides an existence theorem for this minimization problem when th function W is polyconvex.

Theorem 2.1.11. *(John Ball) Let B_0 be a domain in $\mathbb{R}^n$ and let W be a polyconvex function that satisfies the following proprieties.*

The function $W(\cdot, \mathbf{F}, \mathbf{H}, \delta) : B_0 \to \mathbb{R}$ is measurable for all $(\mathbf{F}, \mathbf{H}, \delta) \in \mathbf{M}^3 \times \mathbf{M}^3 \times (0, \infty)$; There exist numbers $p \geq 2, q \geq \frac{p}{p-1}, r > 1, \alpha > 0$ and $\beta \in \mathbb{R}$ such that hold coercivity inequality

$$W(\mathbf{x}, \mathbf{F}) \geq \alpha \left\{ \|\mathbf{F}\|^p + \|\mathrm{Cof}\, \mathbf{F}\|^q + (\det F)^r \right\} + \beta$$

for almost all $\mathbf{x} \in B_0$ and for all $\mathbf{F} \in \mathbb{M}^n_+$. For almost all $\mathbf{x} \in B_0$, $W(\mathbf{x}, \mathbf{F}) \to +\infty$ if $\mathbf{f} \in \mathbf{M}^n_+$ is such that $\det \mathbf{F} \to 0$. Let $\partial_N B_0$ be a relatively open subset of ∂B_0, let $\partial_D B_0 = \partial B_0 \backslash \partial_N B_0$, and let there be given fields $\hat{\mathbf{f}} \in L^{6/5}(B_0; \mathbb{R}^n)$ and $\hat{\mathbf{g}} \in L^{4/3}(B_0; \mathbb{R}^n)$. Define the functional

$$I(\mathbf{w}) = \int_{B_0} W(\mathbf{x}, \nabla \mathbf{w}(\mathbf{x}))dx - \hat{\mathbf{f}}(\mathbf{x}, \mathbf{w}(\mathbf{x}))\mathbf{v}(\mathbf{x}) - \hat{\mathbf{g}}(\mathbf{x}, \nabla \mathbf{w}(\mathbf{x}))\mathbf{v}(\mathbf{x})$$

and the set

$$\begin{aligned} \mathcal{M} = \{\, \mathbf{w} \in W^{1,p}(B_0, \mathbb{R}^3) :& \mathrm{Cof}\,(\nabla \mathbf{w}) \in L^q(B_0; \mathbf{M}^3), \det(\nabla \mathbf{w}) \in L^r(B_0), \\ & \det(\nabla \mathbf{w}) > 0 \, \textit{a.e.} \text{ in } B_0, \mathbf{w} = \mathbf{id} \, \textit{on} \, \partial_D B_0 \,\} \end{aligned}$$

Finally, assume that area $\partial_D B_0 > 0$ and that $\inf_{\mathbf{w} \in \mathcal{M}} I(\mathbf{w})$. Then there exists $\mathbf{w} \in \mathcal{M}$ such that

$$I(\mathbf{u}) = inf_{\mathbf{w} \in \mathcal{M}} J(\mathbf{w})$$

The existence theory can also provide using the tool of implicit function. The theory of existence based on implicit theorem asserts that the equations of nonlinear three-dimensional elasticity have solution if the solutions to the associated equations of linearized three-dimensional elasticity are smooth enough, and the applied forces are small enough.

Theorem 2.1.12. *The nonlinear boundary value problem has a solution $\mathbf{u} \in W^{2,p}(B_0; \mathbf{R}^n)$ if B_0 is a domain with a boundary if class $\mathcal{C}^2$ and for some $p > 3$, $\hat{\mathbf{f}} \in L^p(B_0, \mathbb{R}^n)$ and $\|\hat{\mathbf{f}}\|_{L^p(B_0, \mathbb{R}^n)}$ is small enough.*

See [17] for a proof.

2.1.8 Material stability: Strong ellipticity and strict monotonicity

In this section, we describe the condition for stability of material: the strictly monotone of constitutive function and its weak form, the strong ellipticity. The constitutive function is strictly monotone is strictly monotone if

$$(\hat{\mathbf{P}}(\mathbf{F} + \alpha \mathbf{H}) - \hat{\mathbf{P}}(\mathbf{F})) : \mathbf{H} > 0 \, \forall \mathbf{F} \in \mathbb{M}^3_+, \mathbf{H} \neq 0, \alpha \in (\, 0, 1 \,],$$

such that $\det(\mathbf{F} + \alpha \mathbf{H}) > 0$.

In the case of hyperelastic materials, this definition is equivalent to impose the strict convexity of strain energy function. However, it is too restrictive condition. A well established weaker characterization is the strong ellipticity. In particular if we choice the increment $\mathbf{H}$ of rank-one the strain-energy is rank-one. From the Marsden's chain, we deduce that the polyconvexity is a necessary condition for stability of material.

We say that the constitutive function $\hat{\mathbf{P}}$ is strongly elliptic at a deformation $\mathbf{F}_0$ if the elasticity tensor $\frac{\partial \hat{\mathbf{P}}}{\partial \mathbf{F}}$ satisfies

$$\mathbf{H} : [\frac{\partial \hat{\mathbf{P}}}{\partial \mathbf{F}}] : \mathbf{H} > 0 \quad \forall \mathbf{H} = \mathbf{a} \otimes \mathbf{b}, |\mathbf{a}|, |\mathbf{b}| = 1$$

By components:

$$\frac{\partial \mathbf{P}_{i,j}(\mathbf{F}_0)}{\partial F_{kl}} a_i a_k b_j b_l > 0$$

This condition is closely related to Legendre-Hadamard necessary condition for stability in boundary-value problems. We mention here also the statical interpretation of the strong ellipticity condition.

For appropriate choice of $\mathbf{a}$ and $\mathbf{b}$, that to extend a body in a given direction, a component of force must be applied in that direction or to shear a body in a given direction, a sharing force must be applied in that direction.

We can also relate the strong ellipticity to order preserving, in the following sense: an increase in a component of strain is accompanied by an increasing in the corresponding component of first Piola-Kirchhoff stress. For incompressible hyperelastic materials, the definition of strong ellipticity reads as follows. The function $\hat{\mathbf{P}}$ is strongly elliptic at a deformation $\mathbf{F}_0$ with $\det(\mathbf{F}_0) = 1$ if W satisfies

$$\mathbf{H} : [\frac{\partial}{\partial \mathbf{F}}(\mathbf{F}\frac{\partial W}{\partial \mathbf{C}}(\mathbf{F}^T\mathbf{F}))] : \mathbf{H} > 0 \text{ at } \mathbf{F} = \mathbf{F}_0 \tag{2.11a}$$

$$\forall \mathbf{H} = \mathbf{a} \otimes \mathbf{b}, |\mathbf{a}|, |\mathbf{b}| = 1 \text{ such that } \mathbf{F}_0^{-T} : \mathbf{H} = 0 \tag{2.11b}$$

The restriction (2.11b) says that (2.11a) is required to hold only at rank-1 tensors $\mathbf{H}$ that are tangent to the constraint manifold defined by $\det(\mathbf{F}) = 1$. We can rewrite the LHS of the condition in more compact form:

$$\mathbf{H} : [\frac{\partial}{\partial \mathbf{F}}(\mathbf{F}\frac{\partial W}{\partial \mathbf{C}}(\mathbf{F}^T\mathbf{F}))] : \mathbf{H} = W_{,i}\alpha_u + 2W_{,ij}\beta_i\beta_j$$

where

$$\alpha_i = \frac{\partial I_i}{\partial \mathbf{C}} : \mathbf{H}^T\mathbf{H} + \mathbf{F}^T\mathbf{H} : \frac{\partial^2 I_i}{\partial \mathbf{C}^2} : (\mathbf{F}^T\mathbf{H} + \mathbf{H}^T\mathbf{F}),$$

$$\beta_j = \frac{\partial I_j}{\partial \mathbf{C}} : \mathbf{F}^T\mathbf{H}.$$

Walton et al. [99] provide a sufficient condition for transversely isotropic materials:

Theorem 2.1.13. *Let $W : \mathbb{R}^3 \to \mathbb{R}$ be twice continuously differentiable and let the stored-energy function $\hat{W} : \mathbb{M}^3_+ \to \mathbb{R}$ satisfy*

$$\hat{W}(\mathbf{C}) = W(I_1(\mathbf{C}), I_2(\mathbf{C}), I_3(\mathbf{C})).$$

If W satisfies

$$W_{,j} > 0 \quad j = 1, 2, 3$$

$$[W_{,ij}] \textit{positive definite}$$

at $(I_1(\mathbf{C}_0), I_2(\mathbf{C}_0), I_3(\mathbf{C}_0))$ for some deformation $\mathbf{F}_0$, then $\hat{W}$ satisfies the strong ellipticity condition.

Some constitutive relations

We have seen the requirement that the stored-energy function may satisfy such that the boundary value problem have solutions. The are different type of stored-energy correspondent to different hyperelastic cardiac tissue (isotropic, transversely isotropic, anisotropic): Neo-Hookean, Mooney-Rivlin, that have derived by Ogden material. The compressible Neo-Hookean stored-energy function, depend only on the invariant I_1, can be expressed as:

$$W = \frac{\mu_1}{2}(I_1 - 3) - \mu ln(J) + \frac{\lambda}{2}(lnJ)^2$$

where $\mu_1 > 0$ is shear modulus. The incompressible Neo-Hookean material is:

$$W = \frac{\mu_1}{2}(I_1 - 3)$$

The compressible Mooney-Rivlin stored-energy function, depend on the invariant I_1 and I_2:

$$W = \frac{\mu_1}{2}(I_1) - \frac{\mu_2}{2}(I_2)$$

The incompressible Mooney-Rivlin is:

$$W = \frac{\mu_1}{2}(I_1 - 3) - \frac{\mu_2}{2}(I_2 - 3)$$

Anisotropic compressible stored-energy function from [51]:

$$W = \sum_{r=1}^{s} \frac{\mu_r}{4} \left\{ \frac{1}{\alpha_r}(\exp[\alpha_r(\tilde{I}_r - 1)] - 1) + \frac{1}{\beta_r}(\exp[\beta_r(\tilde{J}_r - 1)] - 1) + \frac{1}{\gamma_r}(\tilde{I}_3^{-\gamma_r} - 1)] \right\}$$

where $\tilde{I}_r = \sum_i w_i^{(r)} \mathrm{tr}\,(\mathbf{C}\mathbf{L}_i)$ and $\tilde{J}_r = \sum_i w_i^{(r)} \mathrm{tr}\,(\mathrm{Cof}\,(\mathbf{C})\mathbf{L}_i)$. We denote by $\mathbf{L}_i$ the structural tensor describe the orthotropic symmetry group. For transversely isotropic material holds the relation between $w_i^{(r)}$ and $n = 2$: $w_2^r = w_3^r = \frac{1}{2}(1 - w_1^r)$. For incompressible materials, the stored-energy function take the form:

$$W = \frac{1}{4} \sum_{r=1}^{s} \mu_r \left\{ \frac{1}{\alpha_r}(\exp[\alpha_r(\tilde{I}_r - 1)] - 1) + \frac{1}{\beta_r}(\exp[\beta_r(\tilde{K}_r - 1)] - 1) \right\}$$

where $\tilde{\mathbf{K}}_r = tr(\mathbf{C}^{-1} \sum_{i=1}^{3} w_i^{(r)} \mathbf{L}_i)$. The Fung-type model [34, 35, 36] has been widely used in soft tissue modeling and it has inspired potential in which the exponential was replaced by other monotonically increasing function. It is stored-energy function has the form:

$$W = c\frac{1}{2}(\exp(Q) - 1),$$

where Q represents a quadratic form with respect to the components of Green-Lagrange strain tensor $\mathbf{E}$ as

$$Q = \sum_{i,j=1}^{3} a_{ij}\mathbf{E}_{ii}\mathbf{E}_{jj} + 2\sum_{i\neq j=1}^{3} G_{ij}E_{ij}^2$$

where a_{ij} and G_{ij} denote material dimensionless constant . However, the simple fitting of the parameter of a Fung-typer potential to experimental stress-strain curves may lead to non-convexity, with undesirable effects on the reliability of the algorithms used in finite element simulations. Indeed, the stiffness matrices in Finite Element routines are typically based on the elasticity tensor $\mathbb{A}$, which is the second derivative of W with respect to $\mathbf{E}$, and reliability of the simulations is guaranteed only if the stiffness matrices are positive definite, which happens only when $\mathbb{A}$ is positive definite at every $\mathbf{E}$ i.e., if, W is convex at every $\mathbf{E}$.

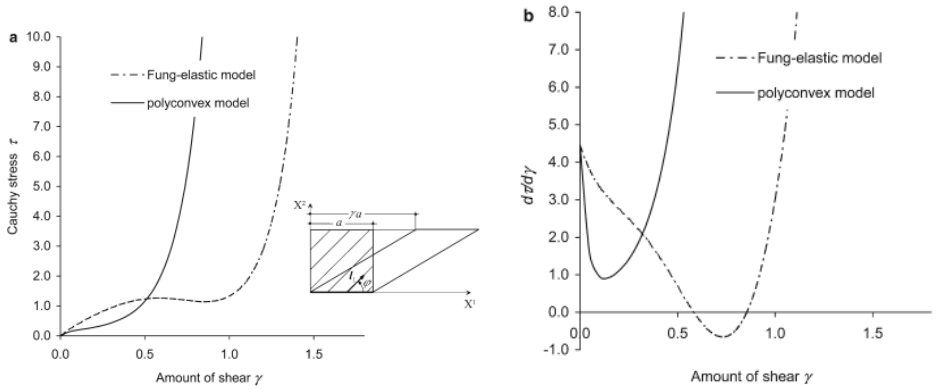

Figure 2.1: The figure represents the comparison between the choice $c = 1, a_{11} = 13.79, a_{22} = a_{33} = 3.78, a_{12} = a_{13} = a_{21} = a_{31} = -6.89, a_{23} = a_{32} = 3.11, G_{12} = G_{13} = 0.582, G_{23} = 0.336$ for Fung model and a polyconvex stored-energy of Itskov [51].

We observe that, with this choice of parameter, the Fung model is non-elliptic, which leads to the drop of the shear stress and the negative slope of the shear curve. This spurious shear stress behavior occurs at moderate amount of shear lying within the range of deformation relevant for most soft biological tissue. In contrast, the polyconvex strain-energy function provides shear stresses monotonically increasing in the whole range of the shear deformations. Sun and Sacks [95] attempted to formulate necessary condition that the coefficients of their two-dimensional Fung-type potential needed to satisfy in order to obtain convexity. The necessity part is based on the requirement of consistency of a non-linear potential with the quadratic potential representing its linearization. Giaquinta et al [29] provide sufficient condition for convexity of Fung-type potentials: if the forth-order tensor $\mathbb{Q}$ associated to the quadratic form Q is positive definite, then W is strictly convex. Finally we present the transversely isotropic material introduced by Humphrey [48]:

$$W = c_1(\sqrt{I_1}-1)^2 + c_2(\sqrt{I_3}-1)^3 + c_3(\sqrt{I_1}-3) + c_4c_1(I_1-3)(\sqrt{I_3}-1) + c_5(I_1-3)^2.$$

2.2 Describing the mechanical behavior of the heart

In this framework, we describe the passive myocardium models of [38, 44] and comparison with other model in current state of art. In cardiac dynamics, the active response plays an

important role during the systole cycle and it interact with the electronic and the physiological activity of heart. It has modeled by the active stress and strain formulation [71, 88], using deformation decomposition and pullback operation.

2.2.1 Model of passive Myocardium

Let us present a review of the most important model for passive myocardium. Several of earlier models were based on linear isotropic elasticity which is inappropriate as illustrated by experiment (the data for biaxial test indicate high nonlinearity and anisotropy). Equally the early nonlinear model do not capture all the features alluded to ([22], in which present a isotropic exponential form based in the invariant I_2). In the state of art, there are a number of transversely isotropic models:[46, 47, 60, 52]. Other transversely isotropic models based on the use of the components of Green-Lagrange strain tensor were developed by [40, 20]. The viscoelasticity feature of myocardium tissue has been taken into account in the model of [50], in which it regards the materials as sponge-like and treats it as a biphasic (fluid-solid) model based on the quasi-viscoelastic constitutive model due to Fung [36]. Several orthotropic models have been proposed in literature. Some of them are inappropriate for modeling myocardial tissue [10] because they do not reflect the morphology of the myocardium. We describe three orthotropic models partly structurally based, relating to the fiber, sheet and normal direction, and partly phenomenological: [90, 49]. Finally we illustrated a structurally based model for passive myocardium of [39, 44]. The strain energy function is transversely isotropic if the material has a single preferred axis along the muscle direction. This assumption was justified by the micro-structural evidence of a regular distribution of endomysal collagen structure around myocytes and long coiled perimysial fibers parallel to them [65]. Humphrey and Yin model is the sum of two exponentials, one in I_1 and one in I_4, specifically the strain-function is:

$$W = c\left\{\exp[b(I_1 - 3)] - 1\right\} + A\left\{\exp[a(\sqrt{I_4} - 1)^2] - 1\right\},$$

and contains four material parameters c, b, A and a. This was the first anisotropic invariant-based model that took account of the fiber structure. Another transversely isotropic model, also based on the invariants I_1 and I_4, was constructed by Humphrey et al. (1990). This has the form:

$$W = c_1(\sqrt{I_4} - 1)^2 + c_2(\sqrt{I_4} - 1)^3 + c_3(I_1 - 3) + c_4(I_1 - 3)(\sqrt{I_4} - 1) + c_5(I_3 - 3)^2$$

where $c_1, \ldots, c_5$ are five material constants obtained from biaxial data (canine left ventricle wall). These model are referred to incompressible material but the there are also compressible transversely isotropic model e.g. Kerckhoffs model:

$$W = a_0[\exp(a_1\hat{I}_1^2 + a_2\hat{I}_2^2) - 1] + a_3[\exp(a_4 E_{ff}^2) - 1] + a_5(I_3 - 1)^2 \tag{2.12}$$

and contains six material parameters $a_0, \ldots, a_5$, where $\hat{I}_1$ and $\hat{I}_2$ are the principal invariants of $\mathbf{E}$ and E_{ff} is the Green-Lagrange strain in the fiber direction. These invariant are related to the principal invariants I_1 and I_2 of $\mathbf{C}$ defined in equation by

$$\hat{I}_1 = \frac{1}{2}(I_1 - 3) \qquad\qquad \hat{I}_2 = \frac{1}{4}(I_2 - 2I_1 + 3).$$

The first term in (2.12) represents the isotropic component related to tissue shape change, the second term relates to the extra stiffness of the material in the myofiber direction and the third term is related to volume changes.

The ventricular myofibers are organized into branching laminae, suggesting that myocardium may be locally orthotropic having the sheet planes [61]. Regional variations in sheet orientation and branching are also significant [60]. Considering the fibrous structure of the myocardium, in [21] it is used the Fung-type exponential strain-energy function:

$$W = \frac{1}{2}C(\exp(Q) - 1),$$

where Q is expressed in terms of strain components E_{ij} referred to a local system of coordinate fiber, sheet and normal coordinates (f, s, n)

$$Q = b_{ff}E_{ff}^2 + b_{ss}E_{ss}^2 + b_{nn}E_{nn}^2 + 2b_{fs}E_{fs}^2 + 2b_{fn}E_{fn}^2 + b_{sn}E_{sn}^2,$$

where b_{ff}, b_{ss} and b_{nn} represent stiffnesses along the fiber, sheet and sheet-normal axes, respectively. b_{ss}/b_{nn} governs anisotropy in the plane normal to the local modulus in the sheet plane, and b_{fn} and b_{sn} represent shear stiffness between adjacent sheets. Another Fung-type model consisting of separate exponential terms for each component E_{ij} was introduced by Schmid et al (2006) to decouple the effect of the material parameters in the single-exponential model of [21] with 12 material parameters, it is given by

$$\begin{aligned} W =& \frac{1}{2}a_{ff}[\exp(b_{ff}E_{ff}^2) - 1] + \frac{1}{2}a_{fn}[\exp(b_{fn}E_{fn}^2) - 1] + \frac{1}{2}[\exp(b_{fs}E_{fs}^2) - 1] \\ & \frac{1}{2}a_{nn}[\exp(b_{nn}E_{nn}^2) - 1] + \frac{1}{2}a_{ns}[\exp(b_{ns}E_{ns}^2) - 1] + \frac{1}{2}[\exp(b_{ss}E_{ss}^2) - 1] \end{aligned}$$

[49] proposed the pole-zero strain-energy, motivated by biaxial tension tests of [94], which has the form

$$\begin{aligned} W = & \frac{k_{ff}E_{ff}^2}{|a_{ff} - |E_{ff}||^{b_{ff}}} + \frac{k_{fn}E_{fn}^2}{|a_{fn} - |E_{fn}||^{b_{fn}}} + \frac{k_{nn}E_{nn}^2}{|a_{nn} - |E_{nn}||^{b_{nn}}} \\ & \frac{k_{fs}E_{fs}^2}{|a_{fs} - |E_{fs}||^{b_{fs}}} + \frac{k_{ss}E_{ss}^2}{|a_{ss} - |E_{ss}||^{b_{ss}}} + \frac{k_{ns}E_{ns}^2}{|a_{ns} - |E_{ns}||^{b_{ns}}}. \end{aligned}$$

As mentioned in [73], it was considered unlikely to be suitable for other modes of deformation. Now we describe the structurally based model proposed by Holzapfel and Ogden [44] is an orthotropic model.

Firstly, we redefine the invariant I_4, I_5 respect with three direction $\mathbf{f}_0, \mathbf{s}_0, \mathbf{n}_0$ and I_8 associated with the pairs of directions :

$$\begin{aligned} I_{4f} &= \mathbf{f}_0 \cdot (\mathbf{C}\mathbf{f}_0) & I_{4s} &= \mathbf{s}_0 \cdot (\mathbf{C}\mathbf{s}_0) & I_{4n} &= \mathbf{n}_0 \cdot (\mathbf{C}\mathbf{n}_0) \\ I_{5f} &= \mathbf{f}_0 \cdot (\mathbf{C}^2\mathbf{f}_0) & I_{5s} &= \mathbf{s}_0 \cdot (\mathbf{C}^2\mathbf{s}_0) & I_{5n} &= \mathbf{n}_0 \cdot (\mathbf{C}^2\mathbf{n}_0) \\ I_{8fs} &= \mathbf{f}_0 \cdot (\mathbf{C}\mathbf{s}_0) & I_{8fn} &= \mathbf{f}_0 \cdot (\mathbf{C}\mathbf{n}_0) & I_{8sn} &= \mathbf{s}_0 \cdot (\mathbf{C}\mathbf{n}_0) \end{aligned} \tag{2.13}$$

Note that hold the I_1 and I_{4f}, I_{4s}, I_{4n} are dependent, in fact:

$$\sum_{i=f,s,n} I_{4i} = \mathbf{C} : (\mathbf{f}_0 \otimes \mathbf{f}_0 + \mathbf{s}_0 \otimes \mathbf{s}_0 + \mathbf{n}_0 \otimes \mathbf{n}_0) = \mathbf{C} : \mathbf{I} = I_1.$$

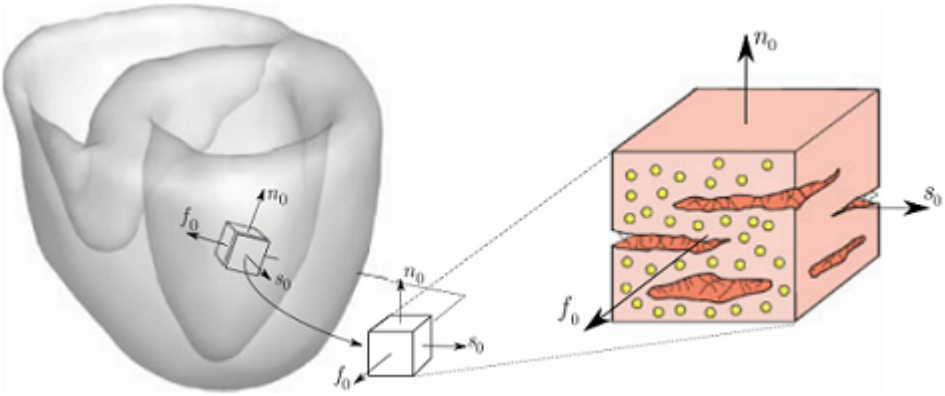

Figure 2.2: Orthotropic architecture of the myocardium. The orthogonal unit vectors $\mathbf{f}_0$ and $\mathbf{s}_0$ are the preferred fiber and sheet direction in the reference configuration. The third direction $\mathbf{n}_0$ is orthogonal to the latter (from [39]).

This implies that in strain-energy function we can omit one of them. The invariants (2.13) are related by the relationship

$$\sum_{i=f,s,n} I_{5i} = I_1^2 - 2I_2$$

Additionally, the invariant (2.13) can be expressed in term of other invariants:

$$I_{5f} = I_{4f}^2 + I_{8fs}^2 + I_{8fn}^2, \quad I_{5s} = I_{4s}^2 + I_{8fs}^2 + I_{8sn}^2, \quad I_{5n} = I_{4n}^2 + I_{8fn}^2 + I_{8sn}^2$$
$$I_{4f}I_{4s}I_{4n} - I_{4f}I_{8sn}^2 - I_{4n}I_{8fs}^2 - I_{4n}I_{8fs}^2 + 2I_{8fs}I_{8fn}I_{8sn} = I_3.$$

From this last equation, that involves the invariant I_3, we can deduce that: if the material is compressible then there are seven parameter independent invariant, otherwise there are only six. From comparison of the number of invariants of this model respect to two non-orthogonal preferred direction model, that have eight (compressible material) and seven (incompressible material) invariants, we can deduce the results: *the orthogonality of Ogden-Holzapfel model reduces the number of invariant by one*. For compressible material the Cauchy tensor is

$$J\sigma = 2\frac{\partial W}{\partial I_1}\mathbf{F}\mathbf{F}^T + 2\frac{\partial W}{\partial I_{4f}}\mathbf{f}\otimes\mathbf{f} + 2\frac{\partial W}{\partial I_{4s}}\mathbf{s}\otimes\mathbf{s} + 2I_3 2\psi_3\mathbf{I}$$

For incompressible material the Cauchy tensor is

$$\sigma = 2\frac{\partial W}{\partial I_1}\mathbf{F}\mathbf{F}^T + 2\frac{\partial W}{\partial I_{4f}}\mathbf{f}\otimes\mathbf{f} + 2\frac{\partial W}{\partial I_{4s}}\mathbf{s}\otimes\mathbf{s} + 2I_3 2\psi_3\mathbf{I} - p\mathbf{I}$$

where the energy-strain function depend on the constitutive law choice (Neo-Hookean, Mooney-Rivlin, etc). In [26], the data indicate the the shear response is stiffest when the fiber direction is extended, least stiff when the normal direction is extended and has intermediate stiffness when the sheet direction is extended. This feature is equivalent to request $\frac{\partial W}{\partial I_{4f}} > \frac{\partial W}{\partial I_{4s}} > 0$. However, the data also show that there are differences between the pairs of directions (fs) and (fn) and between (sf) and (sn) response, while the (sf) and (sn) response are indistinguishable.

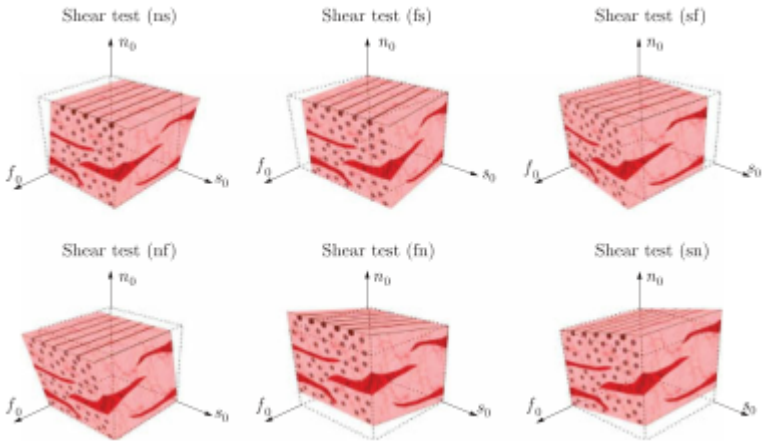

Figure 2.3: Illustration of six shear experiments [26] serving as database for parameter identification. Reproduced from [39].

Taking account of these information we can rewrite the Cauchy stress for compressible material as:

$$\begin{aligned} J\sigma =& 2\frac{\partial W}{\partial I_1}\mathbf{F}\mathbf{F}^T + 2\frac{\partial W}{\partial I_2}(I_1\mathbf{F}\mathbf{F}^T - (\mathbf{F}\mathbf{F}^T)^2) + 2I_3\frac{\partial W}{\partial I_3}\mathbf{I} + 2\frac{\partial W}{\partial I_{4f}}\mathbf{f}\otimes\mathbf{f} + 2\frac{\partial W}{\partial I_{4s}}\mathbf{s}\otimes\mathbf{s} \\ &+ \frac{\partial \hat{W}}{\partial I^2_{8fs}}I_{8fs}(\mathbf{f}\otimes\mathbf{s} + \mathbf{s}\otimes\mathbf{f}) + \frac{\partial \hat{W}}{\partial I^2_{8fn}}I_{8fn}(\mathbf{f}\otimes\mathbf{n} + \mathbf{n}\otimes\mathbf{f}) \end{aligned} \tag{2.14}$$

where $\hat{W}(\ldots, I_{8ij}, \ldots) = W(\ldots, I^2_{8ij}, \ldots)$. In the reference configuration, equation (2.14) reduces to

$$2(\frac{\partial W}{\partial I_1} + 2\frac{\partial W}{\partial I_2} + \frac{\partial W}{\partial I_3})\mathbf{I} + 2\frac{\partial W}{\partial I_{4f}}\mathbf{f}_0\otimes\mathbf{f}_0 + 2\frac{\partial W}{\partial I_{4s}}\mathbf{s}_0\otimes\mathbf{s}_0 = \mathbf{0},$$

assuming the reference configuration is stress-free, and this means:

$$\frac{\partial W}{\partial I_1} + 2\frac{\partial W}{\partial I_2} + \frac{\partial W}{\partial I_3} = 0 \qquad\qquad \frac{\partial W}{\partial I_{4f}} = 0\frac{\partial W}{\partial I_{4s}} = 0. \tag{2.15}$$

Thus, there conditions must be satisfied along with

$$\frac{\partial \hat{W}}{\partial I^2_{8fs}}I_{8fs} = \frac{\partial \hat{W}}{\partial I^2_{8fn}}I_{8fn} = 0,$$

in the reference configuration. For an incompressible material the Cauchy stress becomes:

$$\begin{aligned} \sigma =& 2\frac{\partial W}{\partial I_1}\mathbf{F}\mathbf{F}^T + 2\frac{\partial W}{\partial I_2}(I_1\mathbf{F}\mathbf{F}^T - (\mathbf{F}\mathbf{F}^T)^2) - p\mathbf{I} + 2I_3\frac{\partial W}{\partial I_3}\mathbf{I} + 2\frac{\partial W}{\partial I_{4f}}\mathbf{f}\otimes\mathbf{f} \\ &+2\frac{\partial W}{\partial I_{4s}}\mathbf{s}\otimes\mathbf{s} + \frac{\partial \hat{W}}{\partial I^2_{8fs}}I_{8fs}(\mathbf{f}\otimes\mathbf{s} + \mathbf{s}\otimes\mathbf{f}) + \frac{\partial \hat{W}}{\partial I^2_{8fn}}I_{8fn}(\mathbf{f}\otimes\mathbf{n} + \mathbf{n}\otimes\mathbf{f}) \end{aligned}$$

The conditions that must be satisfied in the reference configuration are as above except for the first equation of (2.15), which is replaced by $2\frac{\partial W}{\partial I_1} + 4\frac{\partial W}{\partial I_2} - p_0 = 0$, where p_0 is the value of p in the reference configuration.

The energy-function depend on the invariants, that take an important role to describe the material. The isotropic term based in invariant I_1 has associated with the underlying non-collagenous and non-muscular matrix. From morphology of myocardium muscle, we know that the muscle fibers are extended and the inter-fiber distances are decreased, while the collagenous network offers little resistance laterally but does contribute to the exponential increasing stress in the muscle fiber direction and the laterally stretching of the collagen fiber contribute to the relatively high compressive stiffness of the myocardium. The stiffness behavior in the muscle direction is take account using the exponential lax in I_{4f}. For the sheet direction, that crosses to the muscle fiber, the stiffening is in part associated with the collagen fibers connecting the muscle fibers. For this reason, in the function W there is an exponential function of the invariant I_{4s}. When the associated directions are under tension, these term contribute to the stored energy. However, when they are under compression, their contribution is minimal because the fiber do not support compression. For this reason, the authors include these terms in the energy function only if $I_{4f} > 1$ or $I_{4s} > 1$.

Holzapfel and Ogden proposed in [44] the following strain-energy function:

$$W = \frac{a}{2b}\exp[b(I_1 - 3)] + \sum_{i=f,s}\frac{a_i}{2b_i}\left\{\exp[b_i(I_{4i} - 1)^2] - 1\right\} + \frac{a_{fs}}{2b_{fs}}[\exp(b_{fs}I_{8fs}^2) - 1], \tag{2.16}$$

where $a, b, a_f, b_f, b_s, a_{fs}$ and b_{fs} are eight positive material constants, the a parameters having dimension of stress, whereas the b parameters are dimensionless. This consists of an isotropic term I_1, the transversely isotropic terms I_{4f} and I_{4s}, and the orthotropic term I_{8fs}. Now substituting this energy function in the expression of the Cauchy stress tensor for incompressible material we obtain:

$$\begin{aligned}\sigma = {} & a\exp[b(I_1 - 3) - 1]\mathbf{F}\mathbf{F}^T - p\mathbf{I} + 2a_f(I_{4f} - 1)\exp[b_f(I_{4f} - 1)^2]\mathbf{f}\otimes\mathbf{f} \\ & 2a_s(I_{4s} - 1)\exp[b_s(I_{4s} - 1)^2]\mathbf{s}\otimes\mathbf{s} + a_{fs}I_{8fs}\exp(b_{fs}I_{8fs}^2)(\mathbf{f}\otimes\mathbf{s} + \mathbf{s}\otimes\mathbf{f}).\end{aligned}$$

The material parameters for the energy function come from experiments ([26] for shear data and [101] for biaxial tension tests).

Let us discuss the convexity of strain-energy function of Ogden-Holzapfel that ensures material stability and physically meaningful and unambiguous mechanical behavior. The form of the strain-energy function has particular advantages because it is the sum of separate functions of different invariants, with no cross-terms between the invariants involved. This enables the convexity status of each term to be assessed separately. We shall consider in succession the three functions $\mathcal{F}(I_1), \mathcal{G}(I_{4f})$ and $\mathcal{H}(I_{8fs})$ as representatives of isotropic, transversely isotropic and orthotropic material and examine their convexity as a function of the right Cauchy-Green tensor $\mathbf{C}$. Indeed the sum of convex function is a polyconvex function that satisfy the hypothesis of Ball theorem. Let us start examining $\mathcal{F}(I_1)$. First we note that

$$\frac{\partial\mathcal{F}(I_1)}{\partial\mathbf{C}} = \mathcal{F}'(I_1)\mathbf{I} \qquad \text{and} \qquad \frac{\partial^2\mathcal{F}(I_1)}{\partial\mathbf{C}\partial\mathbf{C}} = \mathcal{F}''(I_1)\otimes\mathbf{I}.$$

Local convexity of $\mathcal{F}(I_1)$ as a function of $\mathbf{C}$ requires that

$$\frac{\partial^2\mathcal{F}(I_1)}{\partial\mathbf{C}\partial\mathbf{C}}[\mathbf{H},\mathbf{H}] := \mathcal{F}''(I_1)(\mathrm{tr}\mathbf{H})^2 \geq 0,$$

for all second-order tensors $\mathbf{H}$, from which we deduce that $\mathcal{F}''(I_1) \geq 0$. Note that strict convexity is not possible because $\mathbf{H}$ can be chosen so that $\mathrm{tr}\mathbf{H} = 0$. For the exponential

function in equation (2.16), i.e.

$$\mathcal{F}(I_1) = \frac{a}{2b}\exp[b(I_1 - 3)] - 1,$$

this yields $ab \geq 0$. For a non-trivial function, however, we must have $ab \geq 0$. It is also easy to see that, for the stress response (for example, in simple tension) to be exponentially increasing in the corresponding stretch, we must have $b > 0$. Thus, we have $a > 0$ and $b > 0$. For $\mathcal{G}(I_{4f})$, it follows from the definition of I_{4f} in the equation of a structurally based model for the passive myocardium, that

$$\frac{\partial \mathcal{G}}{\partial \mathbf{C}} = \mathcal{G}'(I_{4f})\mathbf{f}_0 \otimes \mathbf{f}_0 \text{ and } \qquad \frac{\partial^2 \mathcal{G}}{\partial \mathbf{C}\partial \mathbf{C}} = \mathcal{G}''(I_{4f})\mathbf{f}_0 \otimes \mathbf{f}_0 \otimes \mathbf{f}_0 \otimes \mathbf{f}_0.$$

The local convexity of $\mathcal{G}'(I_{4f})$ requires that

$$\frac{\partial^2 \mathcal{G}}{\partial \mathbf{C}\partial \mathbf{C}}[\mathbf{H}, \mathbf{H}] := \mathcal{G}''(I_{4f})[(\mathbf{H}\mathbf{f}_0) \cdot \mathbf{f}_0]^2 \geq 0$$

for all second-order tensors $\mathbf{H}$. It follows that $\mathbf{G}$ is convex in $\mathbf{C}$ provided $\mathcal{G}''(I_{4f}) \geq 0$.

For the exponential form

$$\mathcal{G}(I_{4f}) = \frac{a_f}{2b_f}\left\{\exp[b_f(I_{4f} - 1)^2] - 1\right\},$$

we obtain

$$\mathcal{G}'(I_{4f}) = a_f(I_{4f} - 1)\exp[b_f(I_{4f} - 1)^2],$$

and

$$\mathcal{G}''(I_{4f}) = a_f\exp[b_f(I_{4f} - 1)^2]\left\{1 + 2b_f(I_{4f} - 1)^2\right\}.$$

For extension in the fiber direction, we have $I_{4f} > 1$, and from the equation above indicate $\mathcal{G}'(I_{4f}) = a_f(I_{4f} - 1)\exp[b_f(I_{4f} - 1)^2]$ we deduce that for the material response associated with this term to stiffen in the fiber direction we must have $a_f > 0$ and $b_f > 0$. Moreover, these inequalities imply that $\mathcal{G}''(I_{4f}) > 0$ and hence $\mathcal{G}$ is a convex function (both in tension and in compression). Similar results hold for $\mathcal{H}(I_{8fs})$. Using the first term in definition where there are the coupling invariants associated with the pairs of directions, we calculate

$$\frac{\partial \mathcal{H}}{\partial \mathbf{C}} = \frac{1}{2}\mathcal{H}'(I_{8fs})(\mathbf{f}_0 \otimes \mathbf{s}_0 + \mathbf{s}_0 \otimes \mathbf{f}_0)$$

and

$$\frac{\partial^2 \mathcal{H}}{\partial \mathbf{C}\partial \mathbf{C}} = \frac{1}{4}\mathcal{G}''(I_{8fs})(\mathbf{f}_0 \otimes \mathbf{s}_0 + \mathbf{s}_0 \otimes \mathbf{f}_0) \otimes (\mathbf{f}_0 \otimes \mathbf{s}_0 + \mathbf{s}_0 \otimes \mathbf{f}_0).$$

For an arbitrary second-order tensor $\mathbf{A}$, we have

$$\frac{\partial^2 \mathcal{H}}{\partial \mathbf{C}\partial \mathbf{C}}[\mathbf{A}, \mathbf{A}] := \mathcal{H}''(I_{8fs})[(\mathbf{A}\mathbf{f}_0) \cdot \mathbf{s}_0]^2,$$

and for convexity this must be non-negative for all $\mathbf{A}$. Thus, $\mathcal{H}$ is convex in $\mathbf{C}$ provided $\mathcal{H}''(I_{8fs}) \geq 0$.

For the exponential form

$$\mathcal{H}(I_{8fs}) = \frac{a_{fs}}{2b_{fs}}[\exp[b_{fs}I_{8fs}^2 - 1],$$

we obtain

$$\mathcal{H}''(I_{8fs}) = a_{fs}\exp[b_{fs}(I_{8fs}-1)^2](1+2b_{fs}I_{8fs}^2),$$

so convexity is guaranteed if $a_{fs} > 0$ and $b_{fs} > 0$. In the above discussion based separately on the invariants $\mathcal{I}_1, \mathcal{I}_{4f}$ and $\mathcal{I}_{8fs}$, we have examined only the convexity of individual terms that contribute (additively) to the strain-energy function. If each term is convex, than the overall strain-energy function is convex. Note, however, that is is not necessary that each contribution be convex provided any non-convex contribution is counterbalanced by the convexity of the other terms. The analysis of convexity is relatively straightforward for a compressible material, but for an incompressible material more care is needed because not all components of $\mathbf{E}$ are independent. Strong ellipticity is one issue that arises in consideration of material stability. If it holds, then the emergence of certain types of non-smooth deformation is precluded. For three-dimensional deformations, analysis of the strong stability is difficult especially for anisotropic material. If we consider the term $\mathcal{G}(I_{4f})$ strong ellipticity requires that the inequalities

$$\mathcal{G}'(I_{4f}) + 2I_{4f}\mathcal{G}''(I_{4f}) > 0 \quad \text{and}\, \mathcal{G}'(I_{4f}) > 0$$

hold. The second term of first inequality is the component of Cauchy stress in the fiber direction. The second inequality means that strong ellipticity does not hold under fiber compression.

2.3 Comparison between active stress and active strain

The active tension due to the contraction of cardiomyocytes is included in the force balance that determines its deformation. Following the review of Pezzuto and Ambrosi [3], we describe the two possible strategies available in the literature. The most popular approach is to add an active contribution to the stress of the material. In principle, one first characterizes the passive mechanical properties of a specimen, provided that experiments are carried out in physiological conditions, and obtains a standard strain energy. Then an additive stress contribution is to be included so that the observed contraction and torsion can be reproduced. A different point of view, inspired by the theory of active materials, has been introduced by Taber and Perucchio [82] and then deeply explored by Teresi and others [71]. They adopt a multiplicative decomposition of the tensor gradient of deformation, reminiscent of the theory of plasticity and, in biology, volumetric growth. The deformation gradient rewrites then $F = F_e F_a$, where the active contribution F_a has to be constitutively provided. Notice that the factorization proposed is not to be confused with the product of deviatoric and dilational response $F = F_{vol}\tilde{F}$, where $\det(\tilde{F}) = 1$, which implies that the deformation induced by F_{vol} is influencing the change of volume in the material. The active strain F_a stores no energy, and it could be pictorially understood as a distortion of the micro-structure, that forms a kind of watermark defined in the whole body. The elastic deformation F_e must accommodate the material in order to preserve the compatibility of the deformation F, possibly undermined by the distortion F_a. We can summarize as: in active strain formulation the contraction-not-tension is regard as the direct consequence of the activation of muscle fibers; the tension arises whenever contraction is hampered by some geometrical constraint. While in active stress formulation it is take account for ionic activation of muscle fiber by adding to a standard passive stress the active stress which represent the force generated by the muscle when it is activated.

In the active formulation we take account some physiological facts, as the Frank-Starling law. While the active-passive stress-strain relations are well understood at a cellular level, to our knowledge a quantitative Frank-Starling law at a tissue scale has not been stated yet. The prototypical setup to state a force-strain relation at the macroscale is the pressure-volume curve that occurs in the heart during its cycle. The different pressure- volume loops that can be obtained in a ventricle by tuning the aortic pressure.

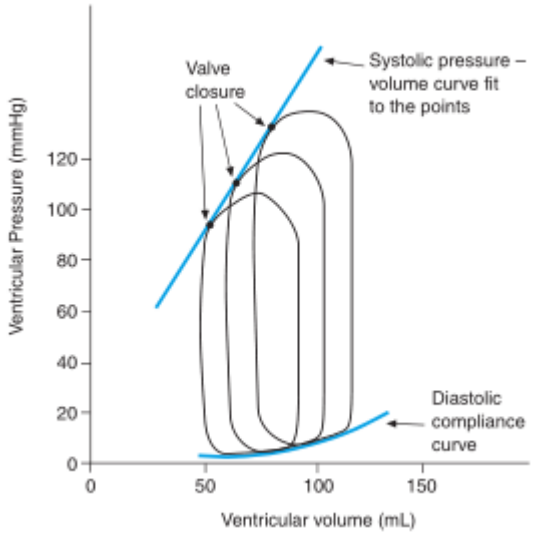

Figure 2.4: This plot provides the quantitative dependence of the active stress on the deformation: the upper and lower dashed lines denote the pressure of the fluid, i.e. the radial stress at the inner wall, both when the stress is purely passive (lower curve) and when the stress is actively produced as seen in the upper curve (from [27]).

We point out that it is not trivial to match the cellular and tissutal experiments in order to state a macroscopic constitutive equation. At the macroscale, the curves reported in the literature clearly show a strongly nonlinear dependence of the active stress (measured by the pressure of the fluid) and the strain (represented by the change in volume). The active stress grows very nonlinearly with the deformation: "Increasing end-diastolic volume actually diminishes the heart's ability to convert its fiber tension into pressure. In the physiological range, this disadvantage is greatly overshadowed by the increase in force generation that results from the longer fiber length" [27].

2.3.1 Active response based on a stress decomposition

In the active stress formulation the active forces taking place within the tissue consists of adding their contribution directly into the stress tensor. Let

$$\mathbf{P}_a = T_a \mathbf{F}\mathbf{f}_0 \otimes \mathbf{f}_0$$

represent an active stress, due to biochemical reactions inside the sarcomeres, of magnitude T_a in the direction of the fibers. We suppose that the first Piola-Kirchoff stress tensor $\mathbf{P}$

assumes the additive splitting $\mathbf{P} = \mathbf{P}_a + \mathbf{P}_p$, where

$$\mathbf{P}_p = \phi_1 \mathbf{F}_p \mathbf{F}^{-T} + \phi_{4,f} \mathbf{f} \otimes \mathbf{f}_0 + \phi_{4,s} \mathbf{s} \otimes \mathbf{s}_0 + \phi_{8,fs} (\mathbf{f} \otimes \mathbf{s}_0 + \mathbf{s} \otimes \mathbf{f}_0),$$

that is, $\mathbf{P}_p$ is the passive part of the stress given by $\frac{\partial \hat{W}}{\partial \mathbf{F}}$. Such assumption is widely used for simulations of the electromechanical activity of the heart. Since the active forces are non-conservative, no potential can be defined for them and therefore an active strain energy cannot be formulated. Nevertheless, some consistently derived variants have been proposed as active energy functions, mainly to study the overall solvability of the mechanical problem connected with strong ellipticity conditions. As for the functional form of $\mathbf{P}_a$, the active tension T_a is usually modeled considering the cross-bridge dynamics inside the sarcomeres, while for the tensorial component (which is a crucial point in the modeling of the electro-mechanical activity of cardiac tissue), several models have been proposed in the literature, but only a few of them address the correct stability conditions to guarantee the existence of solutions. For simplicity, we consider T_a to be given and we impose the force in the fibers direction using the same tensorial component as in the passive law. This choice is intended to allow the preservation of ellipticity conditions of the original passive law.

If the material is hyperelastic in its passive mechanical behavior, the condition rewrites now

$$\mathbf{H} : \frac{\partial^2 \hat{W}}{\partial \mathbf{F} \partial \mathbf{F}} : \mathbf{H} + \mathbf{H} : \frac{\partial \mathbf{P}_a}{\partial \mathbf{F}} : \mathbf{H} > 0, \qquad \forall \mathbf{F} \in \mathcal{M}^3_+, \mathbf{H} \neq \mathbf{0},$$

with the additional constraint $\mathbf{F}^{-T} : \mathbf{H} = 0$ in the case of incompressible material. Given for granted that $W = \hat{W}(\mathbf{F})$ is a rankone convex function, inequality reads as a condition on the functional form of the active stress. The ellipticity of the total stress $\mathbf{P}$ is obtain by checking the positivity of the second term at the right hand side for some specific models taken from the literature. If the active term is not positive, the inequality can still hold, depending on the specific strain energy $\hat{W}(\mathbf{F})$, but conditions can apply on the admissible strain range. Notice that possible strong mathematical properties of the active stress $\mathbf{P}_a$ (as strict monotonicity) are not to be deprecated, because the properties of the weaker one. Conversely, if $\mathbf{P}_a$ is not at least rank-one, the existence of the solution might be not ensures. Panfilov et al. proposed a form of the active tension that does not involve an active role for the fibers, in terms of second Piola-Kirchhoff active stress tensor:

$$S_a = \widetilde{S}_a C^{-1}$$

In an electromechanical model, the scalar quantity $\widetilde{S}_a$ depends on the activated state of the material, possibly thanks a delay equation, however when balance of forces applies in static form.

Here the first Piola stress reads

$$\mathbf{P} = \frac{\partial \hat{W}}{\partial \mathbf{F}} + \widetilde{S}_a \mathbf{F}^{-T},$$

where W is a strain energy of a compressible material. The ellipticity can be checked by further derivation:

$$\mathbf{H} : \frac{\partial^2 \hat{W}}{\partial \mathbf{F} \partial \mathbf{F}} : \mathbf{H} - \widetilde{S}_a \mathbf{F}^{-T} H^T \mathbf{F}^{-T} : \mathbf{H} > 0.$$

The last term at the right hand side can be negative (take, for instance, $\mathbf{H} = \mathbf{a} \otimes \mathbf{a}$) and, depending on the specific form of the strain energy, the total stress might not be

unconditionally strongly elliptic. In particular the above condition may be not satisfied for large compressions. A constitutive equation for active stress that accounts for the orientation of the fibers can be written in a general form as follows:

$$\mathbf{P}_a = S_a(I_4)\mathbf{F}\mathbf{n} \otimes \mathbf{n}$$

where S_a is a positive function of $I_4 = \mathbf{F}\mathbf{n} \cdot \mathbf{F}\mathbf{n}$ (in the range of interest). Smith et al. proposed a dependence of the following type:

$$S_a(I_4) = \widetilde{S}_a \frac{1 - \beta(\sqrt{I_4} - 1)}{I_4},$$

where β and $\widetilde{S}_a$ are constant in this context and the active stress works only when the fibers are elongated ($I_4 > 1$). The numerator of the r.h.s. term encodes the Frank-Starling effect while the denominator can be interpreted as a normalization factor accounting that S_a is a Cauchy stress per unit fiber length. Bol et al. proposed

$$S_a(I_4) = f_0 + \widetilde{S}_a(1 - e^{-\eta(\sqrt{I_4}-1)}),$$

which accounts for the Frank-Starling effect directly at a macroscopic level. Finally Pathmanathan et al. adopt a form of the active stress tensor that can be obtained deriving a scalar function:

$$\mathbf{P}_a = \widetilde{S}_a \frac{\delta}{\delta F}(log(\mathbf{F}\mathbf{n} \cdot \mathbf{F}\mathbf{n})) = 2\frac{\widetilde{S}_a}{I - 4}\mathbf{F}\mathbf{n} \otimes \mathbf{n}$$

The possibility to derive the stress from a scalar is just a technical tool that simplifies the analysis. The Piola stress above indicated is not even rank-one elliptic and therefore, for a given generic passive strain function, strong ellipticity of the total stress holds under condition. Independently of the specific form of $S_a(I_4)$, the strong ellipticity of the active stress forms illustrated above can be checked by direct derivation of the constitutive equation for active stress that accounts for the oriented of the fibers. In fact, strong ellipticity for a given deformation $\mathbf{F}_0$, with $\mathbf{H} = \mathbf{a} \otimes \mathbf{b}$ reads as follow:

$$\mathbf{H} : \frac{\partial \mathbf{P}_a}{\partial \mathbf{F}}\Big|_{\mathbf{F}_0} : \mathbf{H} = [2S'(\mathbf{F}_0\mathbf{n} \cdot \mathbf{a})^2 + S(\mathbf{a} \cdot \mathbf{a})](\mathbf{b} \cdot \mathbf{n})^2 \geq 0,$$

and here we denote

$$S = S_a|_{\mathbf{F}_0}, \qquad S' = \frac{dS_a}{dI_4}|_{\mathbf{F}_0}.$$

The condition

$$\mathbf{F}_0^{-1}\mathbf{a} \cdot \mathbf{b} = 0$$

on the admissible virtual displacements dictated by the incompressibility constraint is accomplished taking $\mathbf{a} = \mathbf{F}_0\mathbf{m}$, with $\mathbf{m}$ such that $\mathbf{m} \cdot \mathbf{b} = 0$. We start by observing that strict inequality is not satisfied if $\mathbf{b}\mathbf{n} = 0$. In the other cases the last factor can be dropped and the following condition remains:

$$2S'(\mathbf{F}_0\mathbf{n} \cdot \mathbf{a})^2 + S(\mathbf{a} \cdot \mathbf{a}) \geq 2S'(\mathbf{F}_0\mathbf{n} \cdot \mathbf{F}_0\mathbf{n})(\mathbf{a} \cdot \mathbf{a}) + S(\mathbf{a} \cdot \mathbf{a}),$$

holds the following sufficient condition for the rank-one ellipticity of active stress tensors of the form:

$$2S'(\mathbf{F}_0\mathbf{n} \cdot \mathbf{F}_0\mathbf{n}) + S \geq 0.$$

If an active stress model is not rank-one elliptic, an equilibrium solution of the force balance equation may not exist, at least for some range of the strain. In the numerical approximation of the momentum equation, the absence of equilibrium configurations might be interpreted as a numerical instability to be addressed by a more careful numerical discretization. However, no numerical strategy can cure an ellipticity loss of the differential equations. Following [3], we exploit an active stress form that satisfies rank-one ellipticity, frame indifference and, for infinitesimal strains of for homogeneous deformations along the direction of the fibers n, accommodates the Frank-Starling law in its cell-scale version. Consider

$$T = \frac{1}{J}\frac{\partial \hat{W}}{\partial \mathbf{F}}\mathbf{F}^T + \frac{S_a}{J}\frac{\mathbf{F}\mathbf{n}\otimes\mathbf{F}\mathbf{n}}{\sqrt{I_4}},$$

and, in terms of Piola stress,

$$\mathbf{P} = \frac{\partial \hat{W}}{\partial \mathbf{F}} + S_a\frac{\mathbf{F}\mathbf{n}\otimes\mathbf{n}}{\sqrt{I_4}}.$$

The active component of the Piola tensor is a strictly monotone linear operator. In fact a specific constitutive form can be obtained by derivation of scalar function

$$W_a = S_a\sqrt{I_4}.$$

As W_a is convex, the corresponding active stress tensor is monotone. In fact from holding $|Fn||Gn| \geq |Fn|\cdot|Gn|$, we have

$$\alpha W_a(F) + (1-\alpha)W_a(G) \geq W_a(\alpha F + (1-\alpha)G),$$
$$\forall\, F, G \in \mathbb{M}^3_+ \text{ and } \alpha \in (0,1) \text{ such that } \det(\alpha F + (1-\alpha)G) < 0.$$

Notice that the sum of two functions retains the regularity properties of the less regular one; in our case strict rank-one convexity of W and convexity of W_a ensure strict rank-one convexity of $W + W_a$.

2.3.2 Active strain assumption

Unlike the general approach outlined in the previous subsection, in the active strain formulation (see e.g. [3]) the deformation gradient $\mathbf{F}$ admits a factorization of the form

$$\mathbf{F} = \mathbf{F}_e\mathbf{F}_a.$$

In this relation, $\mathbf{F}_e$ is a passive elastic deformation, and $\mathbf{F}_a$ is an active factor. The latter basically represents at a macroscopic level, the dependence on the Calcium release, electrical excitation, and other phenomena taking place at a microscale. The rationale of this decomposition is the following: fibers inside the muscle contract and become shorter. Their kinematics is accounted by $\mathbf{F}_a$, a distortion that does not preserve compatibility of the body but dictates the deformation at a fiber scale. The deformation at a macroscale is measured by $\mathbf{F}_e$, that accounts both for the deformation of the material needed to ensure compatibility (possibly undetermined by $\mathbf{F}_a$) and the possible tension due to external loads. Notice that neither $\mathbf{F}_e$ nor $\mathbf{F}_a$ are gradients, so they are not integrable. In other worlds, there not exists any real motion that corresponds to fibers elongation without muscle contraction. So the multiplicative decomposition is a pure theoretical decoupling that associates the

microscale dynamics to the macroscale continuum mechanics. The direct consequence of lack of integrability of $\mathbf{F}_e$ does allow to introduce only an intermediate local configuration to such a deformation. We assume that the strain energy of cardiac muscle depend only on the deformation at the macroscale

$$W = W(\mathbf{F}_e). \tag{2.17}$$

In other words, the energy storage occurs only at macro-level.There is a micro-force that dictates the sarcomere contraction and much is known about the energy spent in such a process, but this force balance is immaterial because the kinematics is directly dictated. The force generated by sarcomere contraction is supposed to have a dissipative nature and thermodynamic issues can be properly addressed. The pathway of electric signals (bundles) cross the heart, transmitting the signal in a short time (few milliseconds). The electric propagation then travels in the whole muscle body, in a time-scale of the order of one second, this propagation occurs along preferential directions dictated by orientation of the mechanical fibers, the same ones that primarily drive the mechanical contraction. To construct the active part of the deformation, as descibed by Rossi et al. [88], we start from considerations at the cell level taking account of anisotropic behavior. Defining the variables $\gamma_f, \gamma_s, \gamma_n$ as the relative displacements in the directions $\mathbf{f}_0, \mathbf{s}_0, \mathbf{n}_0$, (fibers, sheets and sheets-normal directions) respectively, of a single cell , we write its deformation as

$$\mathbf{F}_a = I + \gamma_f \mathbf{f}_0 \otimes \mathbf{f}_0 + \gamma_s \mathbf{s}_0 \otimes \mathbf{s}_0 + \gamma_n \mathbf{n}_0 \otimes \mathbf{n}_0.$$

The variable γ_f denotes an active strain function that, in the context of the coupling of the cardiac elastostatics with the electrophysiology, carries the relevant information of the electrical propagation through the tissue (macroscopic stimuli). In previous studies, the contribution of the terms depending on γ_s and γ_n are neglected. Here we include these terms. However, for a single cell it is difficult to distinguish between the directions $\mathbf{s}_0$ and $\mathbf{n}_0$, since the collagen sheets represent a macroscopic structure that sticks together many cells. Therefore we suppose $\gamma_n = \gamma_s$, that is, we consider transverse isotropy at the microscopic level.

We emphasize that $J_a = 1$ is not considered as a constraint associated to the system to be solved, but it is rather a constitutive relation given along. Since γ_f represents the coupling between the cardiac electrophysiology and the cardiac mechanics, it should be computed via a system of ODEs activation model for physiology and by a degenerate parabolic PDEs for electric mechanisms [76], however in the following, as for T_a in the active stress case, we consider it given. The Piola stress tensor $\tilde{\mathbf{P}}$ in the locally intermediate configuration is obtained by Frechet derivative of strain energy (2.17)

$$\tilde{\mathbf{P}} = \frac{\partial W}{\partial \mathbf{F}_e}$$

and it accounts for the tension due to the deformation $\mathbf{F}_e = \mathbf{F}\mathbf{F}_a^{-1}$. The stored energy function as $\widehat{W} = W(\mathbf{F}_e)$ in intermediate configuration, which is then transformed in the reference configuration into a new strain energy function as

$$W_{new} = J_a \widehat{W} = J_a W(\mathbf{F}\mathbf{F}_a^{-1}).$$

Given the particularly simple form of $\mathbf{F}_a^{-1}$, it is possible to write is explicitly as

$$\mathbf{F}_a^{-1} = I - \frac{\gamma_f}{1+\gamma_f}\mathbf{f}_0 \otimes \mathbf{f}_0 - \frac{\gamma_s}{1+\gamma_s}\mathbf{s}_0 \otimes \mathbf{s}_0 - \frac{\gamma_n}{1+\gamma_n}\mathbf{n}_0 \otimes \mathbf{n}_0.$$

This will allow us to compute W_{new} rather straightforwardly.

Chapter 3

Mathematical analysis of some problems in cardiac electromechanics

3.1 Variational formulation

Let $B_0 \subset \mathbb{R}^d, \quad d = 2, 3$ denote a body in its reference undeformed configuration. By $\mathbf{X}$ we denote a point in B_0, while $\mathbf{x}$ denote the position of $\mathbf{X}$ in the current configuration. We call $\mathbf{u} : \bar{B}_0 \to \mathbb{R}$ the displacement field. The potential energy of a body when deformed with a deformation mapping $\varphi(\mathbf{X}) = \mathbf{x} = \mathbf{X} + \mathbf{u}(\mathbf{X})$, which gradient is $\nabla\varphi = I + \nabla\mathbf{u} = \mathbf{F}$, is computed as:

$$I[\varphi] = \int_{B_0} W(\nabla\varphi) - p(\det(\mathbf{F}) - 1)dB_0 - \int_{\partial_N B_0} \boldsymbol{t} \cdot \varphi dS - \int_{B_0} \boldsymbol{g} \cdot \varphi dB_0,$$

where $\mathbf{t}$ is a surface traction applied on part of the boundary of B_0, $\partial_N B_0 \subset \partial B_0$ and $\boldsymbol{g}$ denotes a body force applied on B_0. From the imposition of material incompressibility, a Lagrangian multiplier p interpreted as pressure [63]. Here it is assumed that $\partial_N B_0$ has positive $d-1$ Hausdorff measure and let $\partial_D B_0$ denote the part of the boundary on which Dirichlet conditions are prescribed on deformation $\varphi = \bar{\varphi}$. For our problem, Dirichlet boundary conditions are prescribed on the base of the left ventricle, while on the apex we prescribe Neumann boundary conditions. We do not consider load forces. Here W represents the strain stored energy that depends on the material chosen, on the trace of the right Cauchy-Green tensor ($\mathbf{C} = \mathbf{F}^T\mathbf{F}$) and on $\mathbf{F}$. Notice that the nonlinear elasticity problem consists in finding those deformations in which the body is in mechanical equilibrium under the imposed boundary conditions; these configurations within a space of admissible deformations defined as

$$\left\{\phi \in [H^1(B_0)]^d : \phi = \bar{\phi} \,\text{on}\, \partial_D B_0\right\},$$

where $\mathbf{N}$ is the outward unit normal vector. The admissible variations, also belonging to such space, consist of all functions of the form:

$$\delta\varphi = \frac{\partial\varphi_\epsilon}{\partial\epsilon}|_{\epsilon=0},$$

where φ_ϵ is a smooth one-parameter family of functions in $H^1_\partial(B_0)$.

An equilibrium configuration of the body is a deformation mapping $\varphi \in V$ that satisfies the stationary potential energy with respect of all admissible variations. More specifically:

$$\langle \delta I[\varphi], \delta\varphi \rangle = \frac{\partial I[\varphi_\epsilon]}{\partial \epsilon}|_{\epsilon=0} = \int_{B_0} \frac{\partial W}{\partial \mathbf{F}} : \delta\nabla\varphi \, dB_0 = 0, \, \forall \delta\varphi.$$

The corresponding Euler-Lagrange equations obtain, using derivation rule $\frac{\partial \det(\mathbf{F})}{\partial \mathbf{F}} = \det(\mathbf{F})\mathbf{F}^{-T}$ and the relation between energy and Piola-Kirchoff stress then read as follows:

$$\begin{cases} -\nabla \cdot (\frac{\partial \hat{W}(\mathbf{F})}{\partial \mathbf{F}} - pJ\mathbf{F}^{-T}) = 0 & \\ J = 1 & \text{in } B_0 \\ \boldsymbol{u} = \boldsymbol{u}_D & \text{on } \partial_D B_0 \\ \mathbf{P}(\boldsymbol{u}, p)\mathbf{N} = \mathbf{t} & \text{on } \partial_N B_0, \end{cases} \tag{3.1}$$

where $J = \det \mathbf{F}$, and $\mathbf{P}$ is the first Piola-Kirchhoff active strain tensor for Neo-Hookean material is defined as:

$$\mathbf{P} = \frac{\partial W}{\partial \mathbf{F}} = \mu J_a \mathbf{C}_a^{-1}\mathbf{F} - pJ\mathbf{F}^{-T}.$$

Here μ is a constant parameter and $\mathbf{C}_a^{-1} = \mathbf{F}_a^{-1}\mathbf{F}_a^{-T}$ represent the anisotropic behavior of the cardiac tissue at the microscale level. Let us rewrite the expression of $\mathbf{F}_a$:

$$\mathbf{F}_a = I + \gamma_f \mathbf{f}_0 \otimes \mathbf{f}_0 + \gamma_s \mathbf{s}_0 \otimes \mathbf{s}_0 + \gamma_f \mathbf{n}_0 \otimes \mathbf{n}_0$$

In order to fulfill the incompressibility condition at microscale level, we impose:

$$\gamma_s = g(\gamma_f) = \begin{cases} -\frac{\gamma_f}{1+\gamma_f} & \text{for } d = 2, \\ \frac{1}{\sqrt{1+\gamma_f}} - 1 & \text{for } d = 3. \end{cases}$$

Let us observe that the $J_a\mathbf{C}_a^{-1}$ is bounded:

$$m(\gamma_f, \mathbf{x}) = \frac{1}{\lambda_{min}(J_a\mathbf{C}_a^{-1})} \leq |J_a\mathbf{C}_a^{-1}| \leq M(\gamma_f, \mathbf{x}) = \|J_a\mathbf{C}_a^{-1}\|_\infty$$

3.2 Linearization of the finite elasticity system

Using the relations

$$D\hat{\mathbf{F}}^{-T}(\boldsymbol{u}) = -\hat{\mathbf{F}}^{-T}(\nabla \boldsymbol{u})^T\hat{\mathbf{F}}^{-T}, \quad D\hat{J}(\boldsymbol{u}) = \hat{J}\hat{\mathbf{F}}^{-T} : \nabla \boldsymbol{u}, \text{ for all } \boldsymbol{u},$$

we arrive at the following linearized nonlinear elasticity problem written in terms of deformation $\boldsymbol{u}$ and pressure p: Find $(\boldsymbol{u}, p) \in [H^1(B_0)]^d \times L^2(B_0)$ such that

$$\begin{cases} \int_{B_0} \mu J_a \mathbf{C}_a^{-1}\nabla\boldsymbol{u} : \nabla\mathbf{v} + \hat{p}\hat{J}((\nabla\hat{\boldsymbol{u}})^{-1}\nabla\boldsymbol{u})^T : (\nabla\hat{\boldsymbol{u}})^{-1}\nabla\mathbf{v}dB_0 & \\ -\int_{B_0} p\hat{J}(\nabla\hat{\boldsymbol{u}})^{-T} : \nabla\mathbf{v}dB_0 = Res(\hat{\boldsymbol{u}}, \hat{p}; \mathbf{v}) + \int_{\partial_N B_0} \boldsymbol{t}\cdot\mathbf{v}dS & \forall\, \mathbf{v} \in [H^1_\partial(B_0)]^d, \\ \int_{B_0} q\hat{J}(\nabla\hat{\mathbf{u}})^{-T} : \nabla\mathbf{u}dB_0 = \mathrm{Res}(\hat{\mathbf{u}}; q) & \forall\, q \in L^2(B_0) \end{cases} \tag{3.2}$$

where

$$Res(\hat{\mathbf{u}}, \hat{p}; \mathbf{v}) = \int_{B_0} \mu J_a \mathbf{C}_a^{-1}\nabla\hat{\boldsymbol{u}} : \nabla\mathbf{v} - \hat{p}\hat{J}(\nabla\hat{\boldsymbol{u}})^{-1} : \nabla\mathbf{v}dB_0$$

$$Res(\hat{\mathbf{u}}; q) = \int_{B_0} q(\hat{J} - 1) dB_0,$$

and $(\hat{\mathbf{u}}, \hat{p})$ is the state around which the linearization is conducted. Let us remark that the linearization of J in second term of first equation is very important in the linearization. Otherwise if we assume that $J = 1$, we increase the numerical difficulty to satisfy the exact incompressibility [6].

In [3] the authors prove the strong ellipticity and strict convexity of the strain energy function, that ensure the existence of an equilibrium point solution of the stationary potential principle associated to the nonlinear problem (3.1).

Lemma 3.2.1. *The residual of the the constraint can be explicited as*

$$q(\nabla \cdot \hat{\mathbf{u}} + \frac{1}{d} \nabla \cdot (\mathrm{Cof}\, (\nabla \hat{\mathbf{u}}) \hat{\mathbf{u}})),$$

for $d = 2$ *and as*

$$q(\nabla \cdot \hat{\mathbf{u}} + \mathrm{tr}\, (\mathrm{Cof}\, (\nabla \hat{\boldsymbol{u}})^T) + \frac{1}{d} \nabla \cdot (\mathrm{Cof}\, (\nabla \hat{\mathbf{u}}) \hat{\mathbf{u}}))$$

for $d = 3$ *where* $\hat{\mathbf{u}}$ *is the displacement calculate at previous step of Newton's algorithm.*

Proof. To achieve the explicit formula we use the expansion of Jacobian of transformation

$$\begin{aligned} &\det(I + \nabla \hat{\mathbf{u}}) = 1 + \mathrm{tr}\, (\nabla \hat{\mathbf{u}}) + \det(\nabla \hat{\mathbf{u}}) && \text{for } d = 2 \\ &\det(I + \nabla \hat{\mathbf{u}}) = 1 + \mathrm{tr}\, (\nabla \hat{\mathbf{u}}) + \mathrm{tr}\, (\mathrm{Cof}\, (\nabla \hat{\mathbf{u}})^T) + \det(\nabla \hat{\mathbf{u}}) && \text{for } \ d = 3, \end{aligned}$$

and the well known identities relating traces and determinants in term of the divergence operator (see e.g. [31, 64])

$$\begin{aligned} \mathrm{tr}\, (\nabla \hat{\mathbf{u}}) &= \nabla \cdot \hat{\mathbf{u}} \\ \det(\nabla \hat{\mathbf{u}}) &= \frac{1}{d} \nabla \cdot (\mathrm{Cof}\, (\nabla \hat{\mathbf{u}}) \hat{\mathbf{u}}) \end{aligned}$$

□

Regarding the linearized problem (3.2), notice that it can be recast in the form

$$\begin{cases} A(\mathbf{u}, \mathbf{v}) - B(\mathbf{v}, \delta p) & = F(\mathbf{v}) \\ B(\mathbf{u}, q) & = G(q) \end{cases}$$

where the involved forms are defined as

$$\begin{aligned} A(\boldsymbol{u}, \mathbf{v}) &= \int_{B_0} \mu J_a \mathbf{C}_a^{-1} \nabla \boldsymbol{u} : \nabla \mathbf{v} + \hat{p} \hat{J} ((\nabla \hat{\boldsymbol{u}})^{-1} \nabla \boldsymbol{u})^T : (\nabla \hat{\boldsymbol{u}})^{-1} \nabla \mathbf{v} dB_0, \\ B(\mathbf{v}, p) &= \int_{B_0} p \hat{J} (\nabla \hat{\boldsymbol{u}})^{-T} : \nabla \mathbf{v} dB_0, \\ G(q) &= \int_{B_0} q(\hat{J} - 1)\, dB_0, \\ F(\mathbf{v}) &= \int_{B_0} \mu J_a \mathbf{C}_a^{-1} \nabla \hat{\boldsymbol{u}} : \nabla \mathbf{v} - \hat{p} \hat{J} (\nabla \hat{\mathbf{u}})^{-1} : \nabla \mathbf{v} dB_0 + \int_{\partial_N B_0} \boldsymbol{t} \cdot \mathbf{v} dS. \end{aligned}$$

In addition, we definite the auxiliary quadrilinear form

$$\mathcal{C}((\boldsymbol{u},p),(\mathbf{v},q)) = A(\boldsymbol{u},\mathbf{v}) - B(\mathbf{v},p) - B(\boldsymbol{u},q)$$

Lemma 3.2.2. *Let Ω be a bounded connected open polyhedra domain in $\mathbb{R}^d$ ($d = 2, 3$). The classical Korn inequality (cf. [13]) states that there exists a positive constant C_B such that:*

$$|\boldsymbol{u}|_1 \leq C_\Omega(\|\epsilon(\boldsymbol{u})\|_0 + \|\boldsymbol{u}\|_0),\ \forall\, \boldsymbol{u} \in [H^1(\Omega)]^d$$

where the tensor $\epsilon(\boldsymbol{u})$ is the $d \times d$ matrix with components

$$\epsilon_{i,j}(\boldsymbol{u}) = \frac{1}{2}(\frac{\partial u_i}{\partial x_j} + \frac{\partial u_j}{\partial x_i}) \quad for\, 1 \leq i, j \leq d.$$

The Korn's first inequality is

$$|\boldsymbol{u}|_1 \leq C_{\Omega,\Gamma}\|\epsilon(\boldsymbol{u})\|_0 \qquad \forall\, \boldsymbol{u} \in [H^1(\Omega)]^d,\ \boldsymbol{u}_{|\Gamma} = \mathbf{0}$$

The Korn's second inequality [92]. Define $\tilde{H}^1(\Omega) = \left\{\boldsymbol{u} \in [H^1(\Omega)]^d : (u, r)_0 = 0\, \forall\, r \in \mathbf{R}\right\}$. Then $\tilde{H}^1(\Omega) \subset H^1(\Omega)$ is a closed, linear subspace and there exists C_Ω such that

$$|\boldsymbol{u}|_1 \leq C_{\Omega,\Gamma}\|\epsilon(\boldsymbol{u})\|_0 \qquad \forall\, \boldsymbol{u} \in \tilde{H}^1(\Omega)$$

where r is a rigid body motion.

Lemma 3.2.1. *The bilinear form A is coercive on the space $(H^1(B_0))^d \times (H^1(B_0))^d$ with coercivity constant*

$$\alpha_1 = C_{B_0}(\mu m(\gamma_f, \mathbf{x}) + C_1(|\nabla\hat{\boldsymbol{u}}|_1) \min_{X \in B_0} |\hat{p}(X)|).$$

Proof. Let us prove a more general statement, taking $\mathbf{u} \neq \mathbf{v}$. Using the boundedness of $J_a\mathbf{C}_a^{-1}$ and algebraic count we obtain:

$$\begin{aligned}\mu\, \nabla\boldsymbol{u} J_a\mathbf{C}_a^{-1} : \nabla\mathbf{v} + \hat{p}\hat{J}((\nabla\hat{\boldsymbol{u}})^{-1}\nabla\boldsymbol{u})^T : (\nabla\hat{\boldsymbol{u}})^{-1}\nabla\mathbf{v} \\ \geq 2\tilde{\epsilon}(\mu\, m(\gamma_f) + \mathrm{Cof}\,((\nabla\hat{\boldsymbol{u}})^T) \min_{X \in B_0} |\hat{p}(X)|)\end{aligned}$$

where $\tilde{\epsilon} = \frac{1}{2}(\nabla\mathbf{u} + (\nabla\mathbf{v})^T)$. Now we apply first Korn's inequality [92] for a vector field that vanishes on a part of the boundary of the domain i.e. $2\,|\tilde{\epsilon}|_{0,B_0} \geq C_{B_0}\,|\mathbf{u}|_{1,B_0}\,|\mathbf{v}|_{1,B_0}\,\forall\,\mathbf{u} \in [H^1_D(B_0)]^d$ and the second Korn's inequality for Neumann data on the remaining of the boundary (we assume that $\partial_D B_0 \cap \partial_N B_0 = \emptyset$). Notice that the constant arising from the application of Korn's inequality depends on the shape of the domain. Therefore $C_1(|\nabla\hat{\boldsymbol{u}}|_1) = \left|\mathrm{Cof}\,(\nabla\hat{\boldsymbol{u}})^T\right|_0 > 0$. Finally, taking $\mathbf{u} = \mathbf{v}$, we obtain the coercivity of the bilinear form $A(\cdot,\cdot)$. □

Lemma 3.2.2. *The bilinear form A is continuous with continuity constant explicitly given by*

$$\alpha_2 = C_{B_0}(\mu M(\gamma_f, \mathbf{x}) + C_2(|\nabla\hat{\boldsymbol{u}}|)\|\hat{p}\|_\infty).$$

Proof. The estimate is an immediate application of Cauchy-Schwarz inequality and definition of semi-norm in H^1. □

3.3 Stability of the continuous problem

The existence and uniqueness of the linearized saddle point problem is established by the following theorem [14, 62]:

Theorem 3.3.1. *Let us denote by Q,V the pair of trial and test spaces of pressure and displacement, respectively. We assume that the following proprieties of the bilinear form $A(\cdot,\cdot), B(\cdot,\cdot)$ and $B_1(\cdot,\cdot)$ are satisfied:*

- *The continuity of $A(\boldsymbol{u},\mathbf{v})$: $|A(\boldsymbol{u},\mathbf{v})| \leq a\|\delta\mathbf{u}\|_V\|\mathbf{v}\|_V$*
- *The continuity of $B(\mathbf{v},p)$: $|B(\mathbf{v},p)| \leq b_1\|\mathbf{v}\|_V\|p\|_Q$*
- *The boundedness of $F(\mathbf{v})$ and $G(q)$.*
- *The coercivity of $A(\boldsymbol{u},\mathbf{v})$: $|A(\boldsymbol{u},\mathbf{v})| \geq c\|\mathbf{u}\|_V\|\mathbf{v}\|_V$*

The inf-sup condition, i.e. it holds

$$\beta_1 := \inf_{q\in Q}\sup_{\mathbf{v}\in V}\frac{b(\mathbf{v},q)}{\|\mathbf{v}\|_V\|q\|_Q} > 0$$

Then for any $F \in V'$ and $G \in Q'$, there exists a unique solution $(\mathbf{u},p) \in V \times Q$ to the saddle point problem. Moreover it satisfies the following stability estimates:

$$\|\mathbf{u}\|_V \leq \frac{1}{c}\|F\|_{V'} + \frac{1}{\beta_1}\left(1+\frac{a}{c}\right)\|G\|_{Q'}$$
$$\|p\|_{Q/KerB^T} \leq \frac{1}{\beta_1}\left(1+\frac{a}{c}\right)\|f\|_{V'} + \frac{c}{\beta_1^2}\left(1+\frac{a}{c}\right)\|g\|_{Q'}.$$

We apply this theorem to the linearized symmetric problem (3.2). The choice of functional space in the described problem are $V = [H^1(B_0)]^d$ for displacement and $Q = L^2(B_0)$ for pressure. Let us prove the fulfillment of the hypotheses of the theorem.

Let start with the upper bound inequality. The continuity of bilinear form A is given by Lemma 1.2.4, so we replace $a = \alpha_2$. The continuity of the bilinear form B is due to application of Cauchy-Schwarz inequality and the inequality $\left|\mathrm{Cof}\left((\nabla\boldsymbol{u})^T\right)\right|_0 \leq \frac{1}{d}\left|\nabla\boldsymbol{u}\right|_0$ [64] then $b_1 = \frac{1}{\sqrt{d}}\left|(\nabla\hat{\boldsymbol{u}})\right|_1$. The term $F(\mathbf{v}) = Res(\hat{\mathbf{u}},\hat{p};\mathbf{v}) + \int_{\partial_N B_0} T\mathbf{v}dS$ is bounded by $\xi(\partial_N B_0)\left|\mathbf{v}\right|_1\|T\|_0 + C_{B_0}(\mu M(\gamma_f,\mathbf{x}) + C(|\nabla\hat{\boldsymbol{u}}|_1)\|\hat{p}\|_\infty)\left|\hat{\boldsymbol{u}}\right|_1\left|\mathbf{v}\right|_1$.Using Lemma 3.2.1, the upper bound of $\left|\mathrm{Cof}\left((\nabla\boldsymbol{u})^T\right)\right|_0$ and the Cauchy-Schwarz inequality we bound the term $G(q)$ by $(C_1(|\hat{\boldsymbol{u}}|^2) + C_2\left|\hat{\boldsymbol{u}}\right|)\|q\|_0$. The constant of coercivity of bilinear form $a(\cdot,\cdot)$ is $c = \alpha_1$, using lemma 3.2.1. The inf-sup condition on reference configuration can be expressed in the deformed configuration in the following way, using the motion map φ and the contraction operator:

$$\inf_{q\in Q}\sup_{\mathbf{v}\in V}\frac{\int_{B_t}(q(\varphi^{-1}(X))\nabla(\mathbf{v}(\varphi^{-1}(X)))dB_t}{\|q\|_Q\|\mathbf{v}\|_V} > \beta_1 > 0$$

The stability estimates for the problem (3.2) are as follows.

$$\|\mathbf{u}\|_V \leq \frac{1}{C_{B_0}(\mu m(\gamma_f,\mathbf{x}) + C_1(|\nabla\hat{\boldsymbol{u}}|_1)\min_{X\in B_0}|\hat{p}(X)|)}\left(\xi(\partial_N B_0)\left|\mathbf{v}\right|_1\|T\|_0\right.$$

$$
\begin{aligned}
&+C_{B_0}(\mu M(\gamma_f) + C(|\nabla \hat{\boldsymbol{u}}|_1)\|\hat{p}\|_\infty)\,|\hat{\boldsymbol{u}}|_1\,|\mathbf{v}|_1) \\
&+\frac{1}{\beta_1}\left(1+\frac{C_{B_0}(\mu M(\gamma_f,\mathbf{x})+C_2(|\nabla\hat{\boldsymbol{u}}|)\|\hat{p}\|_\infty)}{C_{B_0}(\mu m(\gamma_f,\mathbf{x})+C_1(|\nabla\hat{\boldsymbol{u}}|_1)\min_{X\in B_0}|\hat{p}(X)|)}\right) \\
&\cdot((C_1(|\hat{\boldsymbol{u}}|^2)+C_2\,|\hat{\boldsymbol{u}}|)\|q\|_0) \\
\|p\|_{Q/KerB^T} \leq\ &\frac{1}{\beta_1}\left(1+\frac{C_{B_0}(\mu M(\gamma_f,\mathbf{x})+C_2(|\nabla\hat{\boldsymbol{u}}|)\|\hat{p}\|_\infty)}{C_{B_0}(\mu m(\gamma_f,\mathbf{x})+C_1(|\nabla\hat{\boldsymbol{u}}|_1)\min_{X\in B_0}|\hat{p}(X)|)}\right) \\
&\cdot(\xi(\partial_N B_0)\,|\mathbf{v}|_1\,\|T\|_0 + C_{B_0}(\mu M(\gamma_f,\mathbf{x})+C(|\nabla\hat{\boldsymbol{u}}|_1)\|\hat{p}\|_\infty)\,|\hat{\boldsymbol{u}}|_1\,|\mathbf{v}|_1) \\
&+\frac{C_{B_0}(\mu m(\gamma_f,\mathbf{x})+C_1(|\nabla\hat{\boldsymbol{u}}|_1)\min_{X\in B_0}|\hat{p}(X)|)}{\beta_1^2} \\
&\cdot\left(1+\frac{C_{B_0}(\mu M(\gamma_f,\mathbf{x})+C_2(|\nabla\hat{\boldsymbol{u}}|)\|\hat{p}\|_\infty)}{C_{B_0}(\mu m(\gamma_f,\mathbf{x})+C_1(|\nabla\hat{\boldsymbol{u}}|_1)\min_{X\in B_0}|\hat{p}(X)|)}\right) \\
&\cdot(C_1(|\hat{\boldsymbol{u}}|^2)+C_2\,|\hat{\boldsymbol{u}}|)\|q\|_0.
\end{aligned}
$$

Chapter 4

Formulation and analysis of a discontinuous Galerkin method for finite elasticity

In the literature, different numerical schemes have been employed to discretize nonlinear elasticity problems, such as Taylor-Hood elements [6, 89, 12] , Mini-elements [6, 12], Petrov-Galerkin scheme [58]. The exact satisfaction of incompressibility constraint [5] is known to present numerical difficult for fully incompressible nonlinear elasticity following the ideas introduced in [97, 100, 64] for displacement-stress formulation, [91, 25] for formulations including incompressibility terms and for incompressible linearized elasticity [42].

The general discontinuous Galerkin (DG) method was originally developed in the early 70s by Reed and Hill [85] for linear hyperbolic problems where it was found that many key discretization features were advantageous by allowing for discontinuities on element boundaries. For this linear hyperbolic and for hyperbolic conservation laws, discontinuous Galerkin methods are locally conservative, stable and high-order accurate. In addition, discontinuous Galerkin methods can be enhance accuracy when the solution being approximated exhibits discontinuities, such as in gas dynamics. For a broad overview of DG methods for linear problems we refer the reader to the monograph [19]. There, DG methods are formulated not only for hyperbolic equations, but elliptic ones as well. In general, DG formulations for elliptic problems are interesting specially because the solutions to these problems are known to be smooth. Due to high computational cost of including discontinuities, there was initially little interest in using DG approximations for problems with smooth solutions, until it was found that by relaxing the continuity constraint, several benefits are realized when using low order interpolations. The benefits are of significant importance specially in solid mechanics applications, where low order elements are the prevalent choice. Although it had been known that discontinuous Galerkin methods converge with optimal order in both mesh size and polynomial order for linear elasticity problems, in the recent work [42] certain DG methods also converge with optimal order in the equally interesting incompressible limit. It was found that DG method performs well for linear elasticity problems, which are known to be prone to volumetric locking. Due to their success in linear elasticity, DG methods have recently been developed for nonlinear elasticity, e.g. in [97], where a family of schemes is

applied to a pure displacement formulation for nearly incompressible materials and in [78] a DG method is applied to compressible hyperelastic materials in the context of a formulation based on the Hu-Washizu-de Veubeke principle.

4.1 Admissible meshes

The domain B_0 is partitioned in a finite number of sets E, forming a subdivision $\mathcal{T}_h$, such that $\cup_{E\in\mathcal{T}_h} E = \bar{B}_0$. A subdivision $\mathcal{T}_h$ is called admissible if each E is closed and has nonempty interior. The interior of the sets $E \in \mathcal{T}_h$ are required to be pairwise disjoints, and the boundary, ∂E, of each E should be Lipschitz continuous. We assume that the family of admissible subdivisions $\{\mathcal{T}_h\}_h$, with $h \downarrow 0$, is quasi-uniform, so that:

$$h := \max\{\mathrm{diam}E : E \in T_h\}, \tag{4.1}$$

and

$$\exists \rho > 0 : \min\{\mathrm{diam}B_E : E \in \mathcal{T}_h\} \leq \rho h, \forall h > 0,$$

where B_E is the largest ball contained in E. Therefore, it follows that there exist positive constants c and q such that: $ch^d \leq |E| \leq qh^d$ for every element $E \in \mathcal{T}_h$ and every $h > 0$, where $|E|$ is the measure of E. In addition, we require all finite elements within the family of subdivisions to be affine equivalent to a finite number of polyhedral reference finite elements, each with a finite number of faces.

Hence the reference elements possess Lipschitz boundaries, the measure of each face of an arbitrary element in $\mathcal{T}_h$ is finite, and there exists an upper bound on the Lipschitz constant of the boundary for all elements in the family $\mathcal{T}_h$, independent of h. Moreover, form (4.1), we infer that there exists a constant $C > 0$ such that $|e|\, h \leq C\,|E|$ for all $h > 0$, and for any face e of any element $E \in \mathcal{T}_h$.

Let us define on the skeleton of the mesh the functions $\in L^\infty(\mathcal{E})$

$$h_e(\mathbf{x}) = \begin{cases} min(h_{E^+}, h_{E^-}) & \text{for } \mathbf{x} \in \partial E^+ \cup \partial E^- \in \mathcal{E}_h^I \\ h_E, & \text{for } \mathbf{x} \in \partial E \cup \partial B_0 \in \mathcal{E}_h \setminus \mathcal{E}_h^I, \end{cases}$$

and we further require a local mesh regularity condition (that is, for $e \in \partial E$, there exists $C > 0$ such that $h_e \leq h_E \leq Ch_e$).

For simplicity, we start our analysis by considering conforming meshes, so that a face e of an element is either also a face of another element or part of ∂B_0. Consider a given subdivision $\mathcal{T}_h$ of B_0. Each element $E \in \mathcal{T}_h$ has an orientable boundary, ∂E, with unit, outward normal denoted by $\mathbf{n}^E$. Define the set of internal faces

$$\mathcal{E}_h^I = \{e \subset \partial E \setminus \partial B : E \in \mathcal{T}_h\},$$

the set of Dirichlet faces

$$\mathcal{E}_h^D = \{e \subset \partial E \cap \partial_D B_0 : E \in \mathcal{T}_h\},$$

and the set of Neumann faces

$$\mathcal{E}_h^N = \{e \subset \partial E \cap \partial_N B_0 : E \in T_h\}$$

The set of all faces is denoted by $\mathcal{E}_h = \mathcal{E}_h^I \cup \mathcal{E}_h^D \cup \mathcal{E}_h^N$. Since the mesh was assumed to be conforming, each face $e \in \mathcal{E}_h^I$ is shared by precisely two elements, which we name as E^+ and E^-. In other words, $e = \bar{E^+} \cup \bar{E^-}$. Here $\mathbf{n}$ stands for the outward unit normal vector to the face $e \in \mathcal{E}_h^I$, which is chosen to be the unit normal to E^-. For faces $e \in \Gamma \setminus \mathcal{E}_h^I$, $\mathbf{n}$ simply denotes the unit outward normal to B_0.

Let V_h^E be a discrete vector space of smooth scalar functions defined on an element E. A common example is Discontinuous Galerkin (DG) finite element space the vector space of polynomials of degree at most k on E. We define $V_h = \prod_{E \in \mathcal{T}_h} V_h^E$:

$$\left\{ v \in [H^1(B_0)] : v|_E \in \mathbb{P}^k(E), \forall\, E \in \mathcal{T}_h \right\}.$$

Notice that the elements of V_h are allowed to have discontinuities across element interfaces belonging to $\mathcal{E}_h^I$. For the DG discretization of our nonlinear elasticity problem we will use two types of such spaces, V_h and W_h. The space W_h is defined to include the gradient of displacement field. We request $V_h \subset W_h$ and the compatibility condition $\nabla V_h \subset W_h^d$, which together represent a sufficient condition for the resulting method to have only displacements as unknowns. So the DG space V_h^d approximates the displacement field $\boldsymbol{u}$, whereas the space $W_h^{d\times d}$ will be used to approximate its gradient. In addition, we define the DG space $Q_h^E = \mathbb{P}^{k-1}(E)$ for the approximation of pressure. Let us denote by $\mathbb{P}^{k-1}(E)$ the space of polynomials of degree at most $k-1$ on E. The choice of degree of polynomials must respect the LBB condition [14, 75].

4.2 Jumps, averages and discontinuous gradients

Let us recall the definition of the discrete DG derivative operator [97] which will serve as an approximation to the gradient operator. For the DG method the starting equation is:

$$\int_E \mathbf{w} \cdot \mathbf{z} dV = \int_{\partial E} \hat{v} \mathbf{n}^E \cdot \mathbf{z} dS - \int_E v \nabla \cdot \boldsymbol{z} dV \tag{4.2}$$

which should hold for any $\mathbf{z} \in W_h^d$. In this equation $E \in T_h$, $v \in V_h$, and $\mathbf{w} \in W_h^d$ is an approximation to the gradient of v. The definition of the DG derivative, as well as the resulting DG methods, depend on the choice of the numerical trace $\hat{v}$, which takes a function in V_h and returns a function in $T(\mathcal{E}_h) = \prod_{E \in T_h} L^2(\partial E)$. We suppose that the functions belonging into $\mathcal{T}(\mathcal{E}_h)$ assume two values on $\mathcal{E}_h^I$.

In the literature, the most common numerical traces are linear functions of the jump $[\![\cdot]\!]$ and the average $\{\{\cdot\}\}$. We define the average and the jump as operators: $T(\mathcal{E}_h) \to (L^2(\mathcal{E}_h))^d$, for $v \in V_h$ and $\mathbf{z} \in W_h^d$ as follows. For $e \in \mathcal{E}_h^I$

$$[\![v]\!]_e = v^- - v^+, \quad [\![\mathbf{z}]\!]_e = \mathbf{z}^- - \mathbf{z}^+, \quad \{\{v\}\}_e = \frac{1}{2}(v^- + v^+), \quad \{\{\mathbf{z}\}\}_e = \frac{1}{2}(\mathbf{z}^+ + \mathbf{z}^-),$$

where $v^\pm = v|_{E^\pm}$ and $e = \bar{E^+} \cup \bar{E^-}$. For a face $e \in \mathcal{E}_h \setminus \mathcal{E}_h^I$, the trace of the functions $\mathbf{v}$ and $\mathbf{z}$ are single-valued. Moreover

$$\begin{aligned} e \in \mathcal{E}_h^N \qquad & [\![v]\!] = 0 \qquad & \{\{\mathbf{z}\}\} = \mathbf{z} \\ e \in \mathcal{E}_h^D \qquad & [\![v]\!] = v \qquad & \{\{\mathbf{z}\}\} = \mathbf{z}. \end{aligned}$$

Note that the definition of the jump depends on the chosen orientation of e, whereas the quantity $[\![\cdot]\!] \otimes \mathbf{N}$ does not. The formulation of the DG derivative starts by (4.2) and we apply it to the above definition and discretization of mesh, to obtain:

$$\begin{aligned}\sum_{E\in\mathcal{T}_h}\int_E \mathbf{w}\cdot\mathbf{z}dV &= \sum_{E\in\mathcal{T}_h}\int_{\partial E}\hat{v}\cdot\mathbf{z}\mathbf{n}^E dS - \sum_{E\in\mathcal{T}_h}\int_E v\nabla\cdot\mathbf{z}dV \\ &= \int_{\mathcal{E}_h}[\![\hat{v}]\!]\cdot\{\{\mathbf{z}\mathbf{n}\}\}dS + \int_{\mathcal{E}_h^I}\{\{\hat{v}\mathbf{n}\}\}\cdot[\![\mathbf{z}]\!]dS - \sum_{E\in\mathcal{T}_h}\int_E v\nabla\cdot\mathbf{z}dV.\end{aligned}$$

Applying integration by parts in (4.3) we get

$$\sum_{E\in\mathcal{T}_h}\int_E \nabla v\cdot\mathbf{z}dB_0 = \int_{\mathcal{E}_h}[\![v]\!]\cdot\{\{\mathbf{z}\mathbf{n}\}\}dS + \int_{\mathcal{E}_h^I}\{\{v\mathbf{n}\}\}\cdot[\![\mathbf{z}]\!]dS - \sum_{E\in\mathcal{T}_h}\int_E v\nabla\cdot\mathbf{z}dB_0,$$

which implies

$$\sum_{E\in\mathcal{T}_h}\int_E(\mathbf{w}-\nabla v)\cdot\mathbf{z}dB_0 = \int_{\mathcal{E}_h}[\![\hat{v}-v]\!]\cdot\{\{\mathbf{z}\mathbf{n}\}\}dS + \int_{\mathcal{E}_h^I}\{\{(\hat{v}-v)\mathbf{n}\}\}\cdot[\![\mathbf{z}]\!]dS. \quad (4.3)$$

Equation (4.3) holds for all $\mathbf{z}\in W_h^d$, and uniquely defines the discontinuous Galerkin derivative $\mathbf{w}$. This equation can be explicitly solved for $\mathbf{w}$ by introducing the lifting operators $\tilde{\mathbf{R}}: L^2(\mathcal{E}_h)\to W_h^d$ and $\tilde{\mathbf{L}}: L^2(\mathcal{E}_h^I)\to W_h^d$, defined to satisfy

$$\int_{B_0}\tilde{\mathbf{R}}(v)\cdot\mathbf{z}dB_0 = -\int_{\mathcal{E}_h} v\cdot\{\{\mathbf{z}\mathbf{n}\}\}dS \quad \int_{B_0}\tilde{\mathbf{L}}(v)\cdot\mathbf{z}dB_0 = -\int_{\mathcal{E}_h^I} v\mathbf{n}\cdot[\![\mathbf{z}]\!]dS \quad (4.4)$$

for all $\mathbf{z}\in W_h^d$. A simple interpretation of the lifting operators follows after noticing that both terms on the right-hand side of (4.4) are linear operators over W_h^d, for each different v. Hence, $\tilde{\mathbf{R}}(v)\in W_h^d$ and $\tilde{\mathbf{L}}(v)\in W_h^d$ are representatives of these linear operators obtained from the Riesz representation theorem under the L^2 scalar product in W_h^d. Substituting into (4.3) we obtain

$$\sum_{E\in T_h}\int_E(\mathbf{w}-\nabla v-\tilde{\mathbf{R}}([\![v-\hat{v}]\!])-\tilde{\mathbf{L}}(\{\{v-\hat{v}\}\}))\cdot\mathbf{z}dE = 0,$$

for all $\mathbf{z}\in W_h^d$. Since we assumed that $\nabla V_h\subseteq W_h^d$, it follows that

$$\mathbf{w} = D_{DG}v = \nabla v + \tilde{\mathbf{R}}([\![v-\hat{v}]\!]) + \tilde{\mathbf{L}}(\{\{v-\hat{v}\}\})\cdot\mathbf{z} \quad (4.5)$$

The latter equation defines the operator $D_{DG}: V_h\to W_h^d$, and it acts on scalar functions. For our aim, we extend it to vector fields in V_h^d, which is the space of displacements, in the following way: $D_{DG}\mathbf{v} = \mathbf{e_i}\otimes(D_{DG}v_i)$, where $\mathbf{e}_i$ is a Cartesian basis in $\mathbb{R}^d$. This definition induces the extension of the lifting operators for vector fields and the equation (4.5) holds again.

Here $\mathbf{R}: [L^2(\mathcal{E}_h\setminus\mathcal{E}_h^I)]^d\to W_h^{d\times d}$ and $\mathbf{L}: [L^2(\mathcal{E}_h^I)]^d\to W_h^{d\times d}$ are such that $\mathbf{R}(\mathbf{v}) = \mathbf{e}_i\otimes\tilde{\mathbf{R}}(v_i)$ $\mathbf{L}(\mathbf{v}) = \mathbf{e}_i\otimes\tilde{\mathbf{L}}(v_i)$ for all $\mathbf{v}\in V_h^d$. So, for all $\mathbf{v}\in[L^2(\mathcal{E}_h)]^d$ it holds

$$\int_{B_0}\mathbf{R}(\mathbf{v}):\mathbf{W}dB_0 = -\int_{\mathcal{E}_h}\mathbf{v}\cdot\{\{\mathbf{W}\cdot\mathbf{n}\}\}dS \quad \forall\,\mathbf{W}\in W_h^{d\times d}$$

Finally, we can also extend the numerical flux $\hat{v}: \hat{v}(\mathbf{v}) = \mathbf{e}_i\hat{v}(v_i)$ for any $\mathbf{v}\in V_h^d$.

4.3 Numerical traces and lifting operators

The choice of numerical flux determines the resulting DG method, for a general discussion see [4]. We choose Bassi and Rebay numerical flux [9], that is conservative, consistent and (original) unstable. As Ten Eyck and Lew articles [97], we set $\hat{v}(\mathbf{u}) = \hat{v}_0(\mathbf{u}) + \hat{v}_\partial(\mathbf{v})$, where the last term is used to impose boundary conditions.

$$\hat{v}_0(\mathbf{u}) = \begin{cases} \{\{\mathbf{u}\}\} & \text{on } \mathcal{E}_h^I \\ 0 & \text{on } \mathcal{E}_h^D \\ 0 & \text{on } \mathcal{E}_h^N \end{cases}, \quad \hat{v}_\partial(\mathbf{u}) = \begin{cases} 0 & \text{on } \mathcal{E}_h^I \\ \bar{\mathbf{u}} & \text{on } \mathcal{E}_h^D \\ \mathbf{u}_N & \text{on } \mathcal{E}_h^N \end{cases},$$

and the resulting D_{DG} operator is

$$D_{DG}\mathbf{u} = \nabla\mathbf{u} + \mathbf{R}(\llbracket\mathbf{u}\rrbracket) - \mathbf{R}(\llbracket\hat{v}_\partial(\mathbf{u})\rrbracket), \tag{4.6}$$

since $\{\{\hat{v}(\mathbf{u}) - \mathbf{u}\}\} = \{\{\{\{\mathbf{u}\}\} - \mathbf{u}\}\} = 0$ and $\llbracket\{\{\mathbf{u}\}\}\rrbracket = 0$ on $\mathcal{E}_h^I$ while $\llbracket\hat{v}_0(\mathbf{u})\rrbracket = 0$ on $\mathcal{E}_h \setminus \mathcal{E}_h^I$.

Repeating the previous argument, we define the DG operator for pressure and the numerical flux $\hat{p}_\partial$ which takes into account the boundary conditions.

Observe that from the definition of the lifting operator, multiplying both sides of (4.6) by an arbitrary $\mathbf{S}_h \in W_h^{d\times d}$ and integrating over $E^+ \cup E^-$ we have

$$\int_{B_0} D_{DG}\mathbf{v_h} : \mathbf{S}_h dB_0 = \int_{E^+\cup E^-} \nabla\mathbf{v}_h : \mathbf{S}_h dE - \int_{\mathcal{E}_h} \llbracket\mathbf{v_h} - \hat{v}_\partial(\mathbf{v}_h)\rrbracket \cdot \{\{\mathbf{S}_h \cdot \mathbf{n}\}\} dS,$$

for all $\mathbf{S}_h \in W_h^{d\times d}$. Let us decompose the lifting operators $\mathbf{L}$ and $\mathbf{R}$. Consider arbitrary fix faces $e \in \mathcal{E}_h \setminus \mathcal{E}_h^I$ and $e' \in \mathcal{E}_h^I$. We can define $\mathbf{R}^e : [L^2(e)]^d \to W_h^{d\times d}$ and $\mathbf{L}^{e'} : [L^2(e')]^d \to W_h^{d\times d}$ such that:

$$\int_{B_0} \mathbf{R}^e(\mathbf{v}) \cdot \mathbf{z} dB_0 = -\int_e \mathbf{v} \cdot \{\{\mathbf{z} \cdot \mathbf{n}\}\} dS, \quad \int_{B_0} \mathbf{L}^{e'}(\mathbf{v}) \cdot \mathbf{z} dB_0 = -\int_{e'} \mathbf{v} \cdot \llbracket\mathbf{z}\rrbracket \cdot \mathbf{n} dS,$$

for all $\mathbf{z} \in W_h^d$. We have that $\mathbf{R} = \sum_{e\in\mathcal{E}_h\setminus\mathcal{E}_h^I} \mathbf{R}^e$ and $\mathbf{L} = \sum_{e'\in\mathcal{E}_h^I} \mathbf{L}^{e'}$. Note that $\mathbf{R}^e$ and $\mathbf{L}^e$ are not null only in elements E^+ and E^- such that $E^+ \cap E^- = e$, and that

$$\mathbf{R}^e(\mathbf{v}) = \mp 2\mathbf{L}^e(\mathbf{v}) \quad \text{in } E^\pm \tag{4.7}$$

Another essential property of lifting operators is that

$$\mathbf{R}^e(\llbracket\mathbf{v}\rrbracket) = 0 \text{ in } B_0 \Leftrightarrow \llbracket\mathbf{v}\rrbracket = 0 \text{ on } e,$$

for all $\mathbf{v} \in V_h^d$ and all $e \in \mathcal{E}_h$. If $\llbracket\mathbf{v}\rrbracket = 0$ on e then $\mathbf{R}^e(\llbracket\mathbf{v}\rrbracket) = 0$. For the converse, consider a special test function $\mathbf{Z} \in W_h^{d\times d}$, such that $\{\mathbf{Z}\} \cdot \mathbf{n} = \llbracket\mathbf{v}\rrbracket$ on e. Such a function exists, given that $V_h^d \subseteq W_h^{d\times d}$, and $\|\mathbf{Z}\|_{0,B_0} \neq 0$ if $\llbracket\mathbf{v}\rrbracket \neq 0$ on e. Thus

$$\frac{1}{2}\|\llbracket\mathbf{v}\rrbracket\|_{0,e}^2 = \left|\frac{1}{2}\int_e \llbracket\mathbf{v}\rrbracket \cdot \llbracket\mathbf{v}\rrbracket dS\right| = \left|\int_{B_0} \mathbf{R}^e(\llbracket\mathbf{v}\rrbracket) \cdot \mathbf{Z} dB_0\right| \leq \|\mathbf{R}^e(\llbracket\mathbf{v}\rrbracket)\|_0 \|\mathbf{Z}\|_0,$$

so if $[\![\mathbf{v}]\!] \neq 0$ on e then $\mathbf{R}^e(\|\mathbf{v}\|) \neq 0$ or the contranominal statement. Analogously, we have that

$$\mathbf{L}^{e'}(\{\{\mathbf{v}\}\}) = 0 \Leftrightarrow \{\{\mathbf{v}\}\} = 0 \,\text{on}\, e,$$

for all $\mathbf{v} \in V_h^d$ and for all $e' \in \mathcal{E}_h^I$. This follows by (4.7) considering $\mathbf{v}' \in V_h^d$ such that $\{\{\mathbf{v}\}\} = [\![\mathbf{v}']\!]$ on e. This property of the lifting operator is a direct consequence of choosing a quasi-uniform family of admissible subdivisions, in which all elements are affine equivalent to a finite number of reference elements. Moreover, there exist two constants C^+ and C^- independent of h_e such that

$$C^- h_e^{1/2} \|\mathbf{R}^e([\![\mathbf{v}_h]\!])\|_{0,B_0} \leq \|[\![\mathbf{v}_h]\!]\|_{0,e} \leq C^+ h_e^{1/2} \|\mathbf{R}^e([\![\mathbf{v}_h]\!])\|_{0,B_0} \quad \forall\, \mathbf{v}_h \in V_h^d. \tag{4.8}$$

The chain of inequalities (4.8) is implied by the injectivity of the mapping $\mathbf{R}^e$ and it is a sufficient condition for stability of the operator. In addition, it states the equivalence between $\|\mathbf{R}^e(\cdot)\|_{0,B_0}$ and $\|\cdot\|_{0,e}$. The proof of (4.8) is based on extension of trace , trace inequality (see further details in [64], pp. 84–86).

A direct consequence of the decomposition of the right lift operator is that:

$$\|\mathbf{R}([\![\mathbf{v}_h]\!])\|_{0,E}^2 \leq \sum_{e \in \partial E} N_e \|\mathbf{R}^e([\![\mathbf{v}_h]\!])\|_{0,E}^2,$$

where N_e is a bound on the number of faces in an element. This statement and the results on boundedness of $\mathbf{R}^e$ implies the boundedness of $\mathbf{R}$.

Let us introduce some inequalities that we use in the numerical analysis of the method. In order to treat the boundary terms, we will need the following trace inequalities:

$$\|\mathbf{v}\|_{0,\partial E}^2 \leq C(h_E^{-1}\|\mathbf{v}\|_{0,E}^2 + h_E\,|\mathbf{v}|_{1,E}^2) \quad \forall\, \mathbf{v} \in H^1(E)$$
$$h_e \|\nabla \mathbf{v}_{|E}\|_{0,e}^2 \leq \tilde{C}(\|\nabla \mathbf{v}\|_K^2 + h_K^2 \|\Delta \mathbf{v}\|_K^2) \quad \forall\, \mathbf{v} \in V_h$$

with constants $C, \tilde{C} > 0$ just depending on the shape-regularity of the mesh and e is an edge of E. The standard inverse inequality yields

$$h_K^2 \|\Delta \mathbf{v}\|_K^2 \leq C \|\nabla \mathbf{v}\|_K^2 \quad \forall\, \mathbf{v} \in V_h$$

Further useful bounds for the trace operator are collected in the following results.

Lemma 4.3.1 (Trace operator bounds)**.** *Let $\Psi \in H^1(B_0)^{d\times d}$ be a tensor quantity of rank N and let $s \in L^2(e)$ be non-negative for all $e \in \mathcal{E}_h$. Then it holds*

$$\sum_{e \in \mathcal{E}_h} \|s^{1/2}\{\{\Psi\}\}\|_{0,e}^2 \leq \sum_{E \in \mathcal{T}_h} \|s^{1/2}\Psi\|_{0,\partial E}^2,$$
$$\sum_{e \in \mathcal{E}_h} \|s^{1/2}[\![\Psi]\!]\|_{0,e}^2 \leq 2 \sum_{E \in \mathcal{T}_h} \|s^{1/2}\Psi\|_{0,\partial E}^2.$$

We use often this lemma with $s = h$ or $s = h^{-1}$. For proof see ([24]).

Lemma 4.3.1. *A local inverse inequality holds for all $v_h \in V_h^k, E \in T_h$ and $0 < h \leq 1$*

$$\|v_h\|_{l,E} \leq C h_E^{m-l} \|v_h\|_{m,E},$$

where $C > 0$ depends only on the shape-regularity of the mesh.

4.4 Mixed DG formulation of the problem

Let us denote the set of external faces as $\mathcal{E}_h^{ext} := \mathcal{E}_h^D \cup \mathcal{E}_h^N$.

After the integration by parts, we add a inter-element stabilization term into the first equation, because the flux of displacement field is unstable, and into second equation in order to achieve the continuity propriety of discrete problem [19].

Lemma 4.4.1. *The stabilization term* $\beta \sum_{e\in\mathcal{E}_h} \int_e \mathbf{R}^e([\![\boldsymbol{u}]\!])\mathbf{R}^e([\![\boldsymbol{u}]\!])dS$ *can be explicited (see e.g. [78]) as*

$$\beta \sum_{e\in\mathcal{E}_h} \int_e [\![\mathbf{v}]\!] \cdot \frac{[\![\boldsymbol{u}]\!]}{h_e} \cdot dS \quad \forall\, \boldsymbol{u}, \mathbf{v} \in V.$$

Proof. This is a direct application of the definition of operator $\mathbf{R}^e$. □

The discrete functional spaces we choose, are:

$$V_{h,D}^d = \left\{ \mathbf{v}_h \in H^1(B_0) : \mathbf{v}_{h|E} \in (\mathbb{P}^{k+1}(E))^d,\, \mathbf{v}_{h|\partial_D B_0} = \boldsymbol{g},\, \forall\, E \in \mathcal{T}_h \right\}$$
$$Q_h = \left\{ q_h \in H^1(B_0) \cup L_0^2(B_0) : q_{h|E} \in (\mathbb{P}^k(E))^d, \forall\, E \in \mathcal{T}_h \right\}.$$

For both these spaces, we do not require the continuity across inter-element boundaries and $k \geq 1$ [15].

The Discontinuous Galerkin method reads as: Find $\mathbf{u}_h \in V_{h,D}^d, p_h \in Q_h$ such that:

$$\begin{cases} a_h(\mathbf{u}_h, \mathbf{v}_h) + c_h(\boldsymbol{u}_h, \mathbf{v}_h) - b_h(p_h, \mathbf{v}_h) = & F(\mathbf{v}_h) \,\forall\, \mathbf{v}_h \in W_h^d \\ -b_h(\mathbf{u}_h, q_h) + d_h(p_h, q_h) = & G(q_h) \,\forall\, q_h \in Q_h \end{cases} \tag{4.9}$$

where $W_h^d = \left\{ \mathbf{v} \in V_h^d, \mathbf{v}|_{\partial_D B} = \mathbf{0} \right\}$. The bilinear forms in (4.9) are defined as

$$a_h(\mathbf{u}_h, \mathbf{v}_h) = \sum_{E\in\mathcal{T}_h} \int_E J_a \mathbf{C}_a^{-1} \nabla \mathbf{u}_h : \nabla \mathbf{v}_h + \hat{J}\hat{p}(\hat{\mathbf{F}}^{-1}\nabla \boldsymbol{u}_h)^T : (\hat{\mathbf{F}}^{-1}\nabla \mathbf{v}) dB_0$$
$$- \sum_{e\in\mathcal{E}_h^{int}} \int_e \left\{ \left\{ \hat{J}\hat{p}(\hat{\mathbf{F}}^{-1}\nabla \boldsymbol{u}_h)^T \mathbf{n} \right\} \right\} \cdot \left[[\hat{\mathbf{F}}^{-1} \mathbf{v}_h] \right] \tag{4.10a}$$
$$- \sum_{e\in\mathcal{E}_h^{int}} \int_e \left\{ \{ J_a \mathbf{C}_a^{-1} \nabla \boldsymbol{u}_h \mathbf{n} \} \right\} [\![\mathbf{v}_h]\!] - \sum_{e\in\mathcal{E}_h^D} \int_e J_a \mathbf{C}_a^{-1} \nabla \boldsymbol{u}_h \mathbf{N} \cdot \mathbf{v}_h \tag{4.10b}$$
$$c_h(\boldsymbol{u}_h, \mathbf{v}_h) = \sum_{e\in\mathcal{E}_h^{int}} \frac{\beta}{h_e} [\![\boldsymbol{u}_h]\!][\![\mathbf{v}_h]\!] + \beta \sum_{e\in\mathcal{E}_h^D} \frac{1}{h_e} (\boldsymbol{u}_h - \mathbf{g}) \cdot \mathbf{v}_h \tag{4.10c}$$
$$b_h(\boldsymbol{u}_h, p_h) = \sum_{E\in\mathcal{T}_h} \int_E p_h \hat{J}(\hat{\mathbf{F}})^{-T} : \nabla \mathbf{v}_h - \sum_{e\in\mathcal{E}_h^{int}} \int_e \left\{ \left\{ p_h \hat{J} \nabla \hat{\boldsymbol{u}_h}^{-T} \mathbf{n} \right\} \right\} [\![\mathbf{v}_h]\!]$$
$$- \sum_{e\in\mathcal{E}_h^D} \int_e p_h \hat{J} \nabla \hat{\boldsymbol{u}_h}^{-T} \mathbf{n} \mathbf{v}_h \tag{4.10d}$$
$$d_h(p_h, q_h) = \alpha \sum_{e\in\mathcal{E}_h^I} \int_e h_e [\![p_h]\!][\![q_h]\!] + \delta \sum_{E\in\mathcal{T}_h} \int_E p_h q_h \hat{\mathbf{F}} : \mathbf{I} \tag{4.10e}$$

$$F(\mathbf{v}_h) = \int_{B_0} \hat{p}_h \hat{J}(\hat{\mathbf{F}})^{-T} : \nabla \mathbf{v}_h dB_0 + \int_{B_0} \mu J_a \mathbf{C}_a^{-1} \hat{\mathbf{F}} : \nabla \mathbf{v}_h$$
$$- \int_{B_0} \hat{p_h} \hat{J}(\hat{\mathbf{F}})^{-1} : \nabla \mathbf{v}_h dB_0 + \int_{\partial_N B_0} \boldsymbol{t} \cdot \mathbf{v}_h dS$$
$$G(q_h) = \int_{B_0} q_h(\hat{J} - 1) dB_0.$$

Let us remark that in (4.10a) and (4.10b) we use incomplete internal penalty choice since $J_a \mathbf{C}^{-1} \boldsymbol{u}_h \mathbf{N}$ is continuous across the face. The inclusion of proper term (4.10c) and (4.10e) is justified by the unstable numerical flux.The role of the last integral term of (4.10b), (4.10d) and (4.10c) and is to weakly and approximately enforce the Dirichlet boundary condition $\boldsymbol{u} = \boldsymbol{g}$ on $\partial_D B_0$ and the continuity condition $[\![\boldsymbol{u}]\!] = 0$ on the internal edges of B_0 satisfied by the analytical solution $\boldsymbol{u}$. If the problem is linear, this kind of discretization would correspond to the incomplete interior penalty of [19].
Indeed, the choice of adimensional constant β is motivated by achieving the discrete coercivity, but it cannot be choice so large in order to not increment the conditional number of stiffness matrix. Both α and β influence the decreasing of number of iterations of Newton method.

Now, in order to estimate the convergence and asymptotic consistence we introduce the mesh dependent norms :

$$|\!|\!| \mathbf{v} |\!|\!|_{DG}^2 = \sum_{E \in \mathcal{T}_h} \|\nabla \mathbf{v}\|_{0,E}^2 + \sum_{e \in \mathcal{E}_h} \frac{1}{h_e} \|[\![\mathbf{v}]\!]\|_{0,e}^2$$
$$|\!|\!| q |\!|\!|_{DG}^2 = \sum_{E \in \mathcal{T}_h} \|q\|_{0,E}^2 + \sum_{e \in \mathcal{E}_h} h_e \|[\![q]\!]\|_{0,e}^2$$

where β is positive and independent of h_e. Notice that $|\!|\!| q |\!|\!|_{DG}$ is a norm if $\alpha > 0$, while $\alpha = 0$ it is a semi-norm. Since $0 < \alpha < 1$ it is to see that:

$$|\!|\!| q |\!|\!|_{DG}^2 \leq \|q\| \quad \forall\, q \in Q_h$$

Let us define a mesh dependent norm in space $V_h^d \times Q_h$:

$$|\!|\!| (\mathbf{v}, q) |\!|\!|_{DG}^2 = \sum_{E \in \mathcal{T}_h} \|\nabla \mathbf{v}\|_{0,E}^2 + \|q\|_{0,E}^2 + \sum_{e \in \mathcal{E}_h} \frac{1}{h_e} \|[\![\mathbf{v}]\!]\|_{0,e}^2 + h_e \|[\![q]\!]\|_{0,e}^2.$$

Let us note that the discontinuous finite element space equipped with the norm $|\!|\!| \cdot |\!|\!|_{DG}$ is the so-called broken Sobolev space $W^{1,2}-$broken [15].
In the literature [4, 9, 97, 64, 24], we find different definitions of mesh dependent norms, but they are equivalent to the definitions given using inverse inequality and trace operator bounds.

Let us define the quadrilinear form:

$$\mathcal{C}_h((\mathbf{u}_h, p_h), (\mathbf{v}_h, q_h)) = a_h(\mathbf{u}_h, \mathbf{v}_h) + c_h(\boldsymbol{u}_h, \mathbf{v}_h) - b_h(p_h, \mathbf{v}_h) + b_h(\mathbf{u}_h, q_h) - d_h(p_h, q_h)$$
$$= \mathcal{F}_h(\mathbf{v}_h, q_h).$$

where $\mathcal{F}_h(\mathbf{v}_h, q_h) = F(\mathbf{v}_h) - G(q_h)$.
The proof of continuity and coercivity is based on the following lemma.

Lemma 4.4.2. *For all* $\mathbf{v}, \boldsymbol{u} \in V_h^d$ *the following inequality holds:*

$$\sum_{e\in\mathcal{E}} \int_e \{\{\nabla \boldsymbol{u}_h \mathbf{n}\}\} \cdot [\![\mathbf{v}]\!] \leq C(\|\nabla \boldsymbol{u}_h\|_E^2)^{\frac{1}{2}} (h_e^{-1} \|[\![\mathbf{v}]\!]\|_e^2)^{\frac{1}{2}} \tag{4.11}$$

Proof. Let us, without lost of generality, fix an edge $e \in \mathcal{E}_h^I$ between the elements E_1 and E_2 of $\mathcal{T}_h$, we can estimate the LHS quantity using definition of average, triangular inequality , trace inequality and standard inverse inequality:

$$\begin{aligned}
|\int_e \{\{\nabla \boldsymbol{u}_h \mathbf{n}\}\} \cdot [\![\mathbf{v}_h]\!]| &\leq C(h_e \|\nabla \boldsymbol{u}_{h|E^+}\| + h_e \|\nabla \boldsymbol{u}_{h|E^-}\|)^{\frac{1}{2}} h_e^{-\frac{1}{2}} \|[\![\mathbf{v}_h]\!]\|_e \\
&\leq C(\|\nabla \boldsymbol{u}_h\|_{E^+\cup E^-}^2 + h_e^2 \|\nabla^2 \boldsymbol{u}_h\|_{E^+\cup E^-}^2)^{\frac{1}{2}} h_e^{-\frac{1}{2}} \|[\![\mathbf{v}]\!]\|_e \\
&\leq C\|\nabla \boldsymbol{u}_h\|_{E^+\cup E^-} h_e^{-\frac{1}{2}} \|[\![\mathbf{v}_h]\!]\|_e.
\end{aligned}$$

Similarly, if $e \subset \partial_D B_0$ in and edge (face) of E then

$$\begin{aligned}
|\int_e \{\{\nabla \boldsymbol{u}_h \mathbf{n}\}\} [\![\mathbf{v}_h]\!]| &\leq C(h_e \|\nabla \boldsymbol{u}_{h|E}\|_e^2)^{\frac{1}{2}} h_e^{-\frac{1}{2}} \|[\![\mathbf{v}_h]\!]\|_e \\
&\leq C\|\nabla \boldsymbol{u}_h\|_E h_e^{-\frac{1}{2}} \|[\![\mathbf{v}_h]\!]\|_e
\end{aligned}$$

After summing over $E \in \mathcal{T}_h$, taking into account the above inequality we obtain the RHS of (4.11). □

Lemma 4.4.3. *The bilinear form* $a_h(\boldsymbol{u}_h, \mathbf{v}_h)$ *is continuous, that is,*

$$\begin{aligned}
|a_h(\boldsymbol{u}_h, \mathbf{v}_h)| \leq \max \Big\{ & C_B(\mu M(\gamma_f, \mathbf{x}) + C_2(|\nabla \hat{\boldsymbol{u}}|)\|\hat{p}\|_0), \mu^2 M(\gamma_f, \mathbf{x}) \tilde{M}(\gamma_f), \\
& \|\hat{J}\hat{p}(\nabla \hat{\boldsymbol{u}}^T)^2\|_0, C\beta \Big\} |\!|\!| \boldsymbol{u} |\!|\!|_{DG} |\!|\!| \mathbf{v}_h |\!|\!|_{DG},
\end{aligned}$$

where $\tilde{M}(\gamma_f) = \|\{\{J_a \mathbf{C}_a^{-1}\}\}\|$.

Proof. Using Cauchy-Schwarz inequality, the continuity of $a_h(\boldsymbol{u}_h, \mathbf{v}_h)$ of the continuous problem, triangular inequality and (4.4.2), we obtain:

$$\begin{aligned}
|a_h(\boldsymbol{u}_h, \mathbf{v}_h)| \leq & C_{B_0}(M(\gamma_f, \mathbf{x}) + C_2(|\nabla \hat{\boldsymbol{u}}|)\|\hat{p}\|_0)\|\nabla \boldsymbol{u}\|_{E,0} \|\nabla \mathbf{v}_h\|_{E,0} \\
& + \mu^2 M(\gamma_f, \mathbf{x}) \tilde{M}(\gamma_f)((\|\nabla \boldsymbol{u}\|_{E,0}^2)^{\frac{1}{2}} (\sum_{e\in\mathcal{E}} h_e^{-1} |\!|\!| [\![\mathbf{v}_h]\!] \|_e |^2)^{\frac{1}{2}}) \\
& + C\beta (\sum_{e\in\mathcal{E}_h} h_e^{-1} |\!|\!| [\![\mathbf{v}_h]\!] \|_e |^2)^{\frac{1}{2}} (\sum_{e\in\mathcal{E}} h_e^{-1} |\!|\!| [\![\mathbf{v}_h]\!] \|_e |^2)^{\frac{1}{2}} \\
& + \|\hat{J}\hat{p_h}(\nabla \hat{\boldsymbol{u}}^T)^2\|_0 (\|\nabla \boldsymbol{u}\|_{E,0}^2)^{\frac{1}{2}} (\sum_{e\in\mathcal{E}} h_e^{-1} |[\![\mathbf{v}_h]\!]|_e^2)^{\frac{1}{2}}.
\end{aligned}$$

□

Lemma 4.4.4. *The bilinear form* $a_h(\boldsymbol{u}_h, \mathbf{v}_h) + c_h(\boldsymbol{u}_h, \mathbf{v}_h)$ *is coercive, i.e., the following relation holds*

$$|a_h(\boldsymbol{u}_h, \boldsymbol{u}_h) + c_h(\boldsymbol{u}_h, \boldsymbol{u}_h)|$$

$$\geq C(\hat{U},\hat{p},\gamma_f)\min\left\{(1-\epsilon),\beta+m(\gamma_f,\mathbf{x})-\frac{\tilde{m}(\gamma_f,\mathbf{x})}{\epsilon}\right\}\|\!|\boldsymbol{u}_h|\!\|_{DG}{}^2,$$

where β is independent of h and $\epsilon\in(1,\frac{\tilde{m}(\gamma_f,\mathbf{x})}{\beta+m(\gamma_f,\mathbf{x})})$.

Proof. Applying triangular inequality, tensor Young's inequality, boundedness of the lifting operators, mesh regularity, standard inverse inequality and the arithmetic-geometric inequality to (4.11), we have:

$$\begin{aligned}
&|a_h(\boldsymbol{u}_h,\boldsymbol{u}_h)+c_h(\boldsymbol{u}_h,\boldsymbol{u}_h)|\\
&\quad\geq C_B(1-\epsilon)(m(\gamma_f,\mathbf{x})+C(\hat{\boldsymbol{u}})\|\hat{p}\|_0)\|\nabla\boldsymbol{u}_h\|_0^2\\
&\qquad-\sum_{e\in\mathcal{E}_h}\frac{1}{\epsilon}(\tilde{m}(\gamma_f,\mathbf{x})+\tilde{C}(\hat{\boldsymbol{u}})\|\hat{p}\|_0)h_e^{-1}\|[\![\boldsymbol{u}_h]\!]\|_0^2+\sum_{e\in\mathcal{E}_h}\beta h_e^{-1}\|[\![\boldsymbol{u}_h]\!]\|_0^2\\
&\quad\geq C(\hat{\boldsymbol{u}},\hat{p},\gamma_f)\min\left\{(1-\epsilon),\beta+m(\gamma_f,\mathbf{x})-\frac{\tilde{m}(\gamma_f,\mathbf{x})}{\epsilon}\right\}\|\!|\boldsymbol{u}_h|\!\|_{DG}{}^2,
\end{aligned}$$

where $\tilde{m}(\gamma_f,\mathbf{x})=\|\{\{m(\gamma_f,\mathbf{x})\}\}\|$ □

Lemma 4.4.5. *The bilinear form $b(\mathbf{v}_h,q_h)$ is continuous, i.e.*

$$|b_h(\boldsymbol{u}_h,q_h)|\leq C(\hat{\boldsymbol{u}})\|\!|\boldsymbol{u}|\!\|_{DG}\|\!|q|\!\|_{DG}.$$

Proof.

$$\begin{aligned}
|b_h(\boldsymbol{u}_h,q_h)|&\leq\|\hat{J}\nabla\hat{\boldsymbol{u}}^{-T}\|_\infty(\|\nabla\boldsymbol{u}_h\|^2)^{\frac{1}{2}}\|q_h\|\\
&\quad+\|\left\{\left\{\hat{J}\nabla\hat{\boldsymbol{u}}^{-T}\right\}\right\}\|_\infty\sum_{e\in\mathcal{E}}(h_e\|q_h\|_e^2)(h_e^{-1}\|[\![\boldsymbol{u}_h]\!]\|_e^2)^{\frac{1}{2}},
\end{aligned}$$

and the result follows directly from the definition of the mesh dependent norm for the pressure. □

Let us notice that the coercivity of $-d(p_h,q_h)$ follows by Cauchy-Schwarz inequality, regularity of the mesh and norm mesh dependent:

$$-d_h(q_h,q_h)\geq h_e^{-1}\alpha\|\!|q|\!\|_{DG}{}^2$$

Theorem 4.4.6. *The following relations hold, implying the continuity and coercivity of the form $\mathcal{C}_h((\boldsymbol{u}_h,p_h),(\mathbf{v}_h,q_h))$.*

$$\begin{aligned}
&|\mathcal{C}_h((\boldsymbol{u}_h,p_h),(\mathbf{v}_h,q_h))|\\
&\quad\leq\max\Big\{C_B(\mu M(\gamma_f,\mathbf{x})+C_2(|\nabla\hat{\boldsymbol{u}}|)\|\hat{p}\|_0),\mu^2M(\gamma_f,\mathbf{x})\tilde{M}(\gamma_f,\mathbf{x}),\\
&\quad\|\hat{J}\hat{p}(\nabla\hat{\boldsymbol{u}}^T)^2\|_0,C\beta,C(\hat{\boldsymbol{u}}),\alpha\Big\}(\|\!|\boldsymbol{u}|\!\|_{DG}+\|\!|p|\!\|_{DG})\cdot(\|\!|\mathbf{v}_h|\!\|_{DG}+\|\!|q_h|\!\|_{DG}),
\end{aligned}$$

and

$$\begin{aligned}
&\mathcal{C}_h((\boldsymbol{u}_h,p_h),(\boldsymbol{u}_h,p_h))\\
&\quad\geq C(\hat{\boldsymbol{u}},\hat{p},\gamma_f)\min\left\{(1-\epsilon),m(\gamma_f,\mathbf{x})+\beta-\frac{\tilde{m}(\gamma_f,\mathbf{x})}{\epsilon}\right\}\|\!|\boldsymbol{u}_h|\!\|_{DG}{}^2+\frac{\alpha}{h_e}\|\!|p_h|\!\|_{DG}{}^2\\
&\quad=C(\hat{\boldsymbol{u}},\hat{p},\gamma_f,\alpha,\beta)(\|\!|\boldsymbol{u}_h|\!\|_{DG}{}^2+\|\!|p_h|\!\|_{DG}{}^2).
\end{aligned}$$

Proof. Using Cauchy-Schwarz inequality and previous lemmas about continuity of the bilinear forms $a(\cdot,\cdot), b(\cdot,\cdot), d(\cdot,\cdot)$ we obtain the continuity upper bound. Next, the symmetry of the saddle-point problem and the coercivity of $a(\cdot,\cdot)$ along with triangular inequality eventually yield the coercivity of $\mathcal{C}_h((\boldsymbol{u}_h, p_h), (\mathbf{v}_h, q_h))$. □

Notice that the continuity and coercivity constants depend on the fixed state around which the linearization is performed, and the activation function γ_f, but they are independent on the meshsize and of the solution itself.

Let us introduce the following lemma regarding the interpolation operators [84, 28], that we use it in convergence analysis. By $\mathbf{I}_h : C^0(B_0) \to V_{h,D}^d$ and $\mathbf{\Pi}_h : L_0^2(B_0) \to Q_h$ we will denote a discontinuous interpolation (such as e.g. Brezzi-Douglas- Marini interpolant) and the Clément interpolant, respectively.

Lemma 4.4.7 (Interpolate local operators)**.** *Let $\mathbf{v} \in H^s(B_0)^d$ and $q \in H^{s-1}(B_0) \cap L_0^2(B_0)$, for $1 \leq s \leq k+1$ and $E \in \mathcal{T}_h$. Then, the following inequalities hold:*

$$
\begin{aligned}
|\mathbf{v} - \mathbf{I}_h^E \mathbf{v}|_{m,E} &\leq C h_E^{s-m} |\mathbf{v}|_{s,E} \\
|\mathbf{v} - \mathbf{I}_h^E \mathbf{v}|_{0,\partial E} &\leq C h_E^{s+\frac{1}{2}} |\mathbf{v}|_{s,E} \\
|I_h^E \mathbf{v}|_{1,B_0} &\leq C |\mathbf{v}|_{1,B_0} \\
|q - \mathbf{\Pi}_h^E q|_{s,E} &\leq C h_E^{s-1-m} |\mathbf{v}|_{s,E} \\
|q - \mathbf{\Pi}_h^E q|_{0,\partial E} &\leq C h_E^{s-\frac{1}{2}} |q|_{s-1,E} \\
|\mathbf{\Pi}_h^E q|_{0,B_0} &\leq C |q|_{0,B_0}.
\end{aligned}
$$

where $0 \leq m \leq 1$ and $C > 0$.
When dealing with the fully DG space, we can define the global interpolator:

$$
\begin{aligned}
\mathbf{I}_h \mathbf{v}(\mathbf{x}) &= I_h^E \mathbf{v}(\mathbf{x}) \\
\mathbf{\Pi}_h q(\mathbf{x}) &= \mathbf{\Pi}_h^E q(\mathbf{x}), \quad \forall\, \mathbf{x} \in E \,\forall E \in \mathcal{T}_h
\end{aligned}
$$

Using the previous lemma, we can estimate the interpolation error in the mesh dependent norm:

Theorem 4.4.8. *Let $\mathbf{v} \in H^s(B_0)^d$ and $q \in H^{s-1}(B_0) \cap L_0^2(B_0)$, for $1 \leq s \leq k+1$ and $E \in \mathcal{T}_h$. Then, the following inequalities hold:*

$$
\begin{aligned}
\|\!|\mathbf{v} - \mathbf{I}_h^E \mathbf{v}|\!\|_{DG} &\leq C h^{s-1} |\mathbf{v}|_s && \text{(4.12a)} \\
\|\!|\mathbf{I}_h^E \mathbf{v}|\!\|_{DG} &\leq C |\mathbf{v}|_s \\
\|\!|q - \mathbf{\Pi}_h^E q|\!\|_{DG} &\leq C h^{s-1} |q|_{s-1} && \text{(4.12b)} \\
\|\!|(\mathbf{v} - \mathbf{I}_h^E \mathbf{v}, q - \mathbf{\Pi}_h^E q)|\!\|_{DG} &\leq C h^{s-1} (|\mathbf{v}|_s + |q|_{s-1}) && \text{(4.12c)}
\end{aligned}
$$

Proof. Using the definition of norms, triangular inequality, the estimate of the previous lemma and trace inequality, we have:

$$
\begin{aligned}
\|\!|\mathbf{v} - \mathbf{I}_h^E \mathbf{v}|\!\|_{DG}^2 &= \|\nabla(\mathbf{v} - \mathbf{I}_h^E \mathbf{v})\|_0^2 + \sum_{e \in \mathcal{E}} h_e^{-1} \| [\![\mathbf{v} - \mathbf{I}_h^E \mathbf{v}]\!] \|_e^2 \\
&\leq C h^{2s-2} |\mathbf{v}|_{k+1}^2 + C \sum_{E \in \mathcal{T}_h} (|\mathbf{v} - \mathbf{I}_h^E \mathbf{v}|_{1,E}^2 + h_E^2 |\mathbf{v} - \mathbf{I}_h^E \mathbf{v}|_{2,E}^2)
\end{aligned}
$$

$$\leq Ch^{2s-2} |\mathbf{v}|_s^2 .$$

Similarly, for the second upper bound inequality, we have:

$$\begin{aligned} \|\mathbf{I}_h^E \mathbf{v}\|_{DG}{}^2 &= \|\nabla(\mathbf{I}_h^E \mathbf{v})\|_0^2 + \sum_{e\in\mathcal{E}} h_e^{-1} \| [\![\mathbf{I}_h^E \mathbf{v}]\!] \|_e^2 \\ &\leq C |\mathbf{v}|_s^2 \end{aligned}$$

Using the definition of norm, triangular inequality, the estimate of previous lemma and trace inequality, we have:

$$\begin{aligned} \|q - \mathbf{\Pi}_h^E q\|_{DG}{}^2 &= \|q - \mathbf{\Pi}_h^E q)\|_0^2 + \sum_{e\in\mathcal{E}} h_e \| [\![q - \mathbf{\Pi}_h^E q]\!] \|_e^2 \\ &\leq Ch^{2s-2} |q|_k^2 + C \sum_{e\in\mathcal{E}} \|h_e^{\frac{1}{2}} (q - \mathbf{\Pi}_h^E q)\|_e^2 \\ &\leq Ch^{2s-2} |q|_{s-1}^2 . \end{aligned}$$

The inequality (4.12c) is obtained combining the definition of mesh dependent norm, triangular inequality, (4.12a) and (4.12b). □

Theorem 4.4.9. *Let $(\boldsymbol{u}, p)$ be the unique solution of the linearized problem. Then, the discontinuous Galerkin formulation is asymptotically consistent, that is:*

$$\begin{aligned} \mathcal{C}_h((\boldsymbol{u} - \boldsymbol{u}_h, p - p_h), (\mathbf{v}_h, q_h)) &\leq Ch \|v_h\|_{DG_h} \\ \mathcal{C}_h((\boldsymbol{u} - \boldsymbol{u}_h, 0), (\mathbf{v}_h, q_h)) &\leq Ch \|v_h\|_{DG_h} \\ \mathcal{C}_h((0, p - p_h), \mathbf{v}, q_h) &= 0 \end{aligned}$$

where $C = C(\mu M(\gamma_f, \mathbf{x}), \hat{\boldsymbol{u}}, \hat{p}, \mathbf{g}, \mathbf{t}) > 0$. In particular, if V_h and P_h are continuous spaces, then the Galerkin orthogonality condition is recovered

$$\mathcal{C}_h((\boldsymbol{u} - \boldsymbol{u}_h, p - p_h), (\mathbf{v}_h, q_h)) = 0.$$

Proof. Let us observe that, for regularity assumption on the pressure and the displacement, we have $[\![p]\!] = 0$, $[\![\boldsymbol{u}]\!] = 0$ and $\{\{p\}\} = p$. In addition, using the definition of continuous and discrete form we obtain:

$$\begin{aligned} &\mathcal{C}_h((\boldsymbol{u} - \boldsymbol{u}_h, p - p_h), (\mathbf{v}_h, q_h)) \\ &\quad = a_h(\boldsymbol{u}, \mathbf{v}_h) - b_h(p, \mathbf{v}_h) + b_h(\boldsymbol{u}, q_h) - d_h(p, q_h) - \mathcal{F}_h(\mathbf{v}_h, q_h) \\ &\quad a(\boldsymbol{u}, \mathbf{v}_h) + \sum_{e\in\mathcal{E}_h^{int}} \int_e \nabla\boldsymbol{u}\mu J_a \mathbf{C}_a^{-1}\mathbf{n} \cdot [\![\mathbf{v}_h]\!] ds + \sum_{e\in\mathcal{E}_h^{int}} \hat{J}\hat{p}(\hat{\mathbf{F}}\nabla\boldsymbol{u})^T \mathbf{n} \cdot \hat{\mathbf{F}} [\![\mathbf{v}_h]\!] \\ &\quad + b(p, \mathbf{v}_h) - \sum_{e\in\mathcal{E}_h^{int}} \int_e p\hat{J}\hat{\mathbf{F}}^{-T}\mathbf{n} \cdot [\![\mathbf{v}_h]\!] ds - b(q_h, \boldsymbol{u}) - \mathcal{F}_h(\mathbf{v}_h, q_h) \\ &\quad \sum_{e\in\mathcal{E}_h^{int}} \int_e \nabla\boldsymbol{u}\mu J_a \mathbf{C}_a^{-1}\mathbf{n} \cdot [\![\mathbf{v}_h]\!] ds + \sum_{e\in\mathcal{E}_h^{int}} \hat{J}\hat{p}(\hat{\mathbf{F}}\nabla\boldsymbol{u})^T \mathbf{n} \cdot \hat{\mathbf{F}} [\![\mathbf{v}_h]\!] \\ &\quad - \sum_{e\in\mathcal{E}_h^{int}} \int_e p\hat{J}\hat{\mathbf{F}}^{-T}\mathbf{n} \cdot [\![\mathbf{v}_h]\!] ds =: S_1. \end{aligned}$$

Using Hölder inequality we have:

$$S_1 \leq C(\mu M(\gamma_f, \mathbf{x}), \hat{\boldsymbol{u}}, \hat{p})h \sum_{e \in \mathcal{E}_h^{int}} (h_e^{-1} \|\nabla \boldsymbol{u}\|_{0,e}^2)^{\frac{1}{2}} (h_e^{-1} \|[\![\mathbf{v}_h]\!]\|_{0,e}^2)^{\frac{1}{2}}$$
$$+ C(\hat{\boldsymbol{u}})h \sum_{e \in \mathcal{E}_h^{int}} (h_e^{-1} \|p\|_{0,e}^2)^{\frac{1}{2}} (h_e^{-1} \|[\![\mathbf{v}_h]\!]\|_{0,e}^2)^{\frac{1}{2}} =: S_2.$$

Using the continuous dependence on the Dirichlet and Neumann data $\mathbf{g}$ and $\mathbf{t}$ and the mesh-dependent norm we obtain:

$$\begin{aligned} S_2 &\leq C(\mu M(\gamma_f, \mathbf{x}), \hat{\boldsymbol{u}}, \hat{p})(\|\mathbf{g}\|_{1/2,\partial_D B_0}^2 + \|\mathbf{t}\|_{1/2,\partial_N B_0}^2)^{1/2} h |\!|\!| \mathbf{v}_h |\!|\!|_{DG} \\ &\leq C(\mu M(\gamma_f, \mathbf{x}), \hat{\boldsymbol{u}}, \hat{p}, \mathbf{g}, \mathbf{t})h |\!|\!| \mathbf{v}_h |\!|\!|_{DG}, \end{aligned}$$

which concludes the proof.

□

4.5 Convergence analysis

Theorem 4.5.1. *Let $(\boldsymbol{u}_h, p_h) \in V_{h,D} \times Q_h$ be the unique solution of 4.9 and $(\boldsymbol{u}, p) \in H^{k+1}(B_0)^d \times H^k(B_0)$ the unique solution of 3.2. Then, there exists $C > 0$ such that*

$$|\!|\!| \boldsymbol{u} - \boldsymbol{u}_h |\!|\!|_{DG} + |\!|\!| p - p_h |\!|\!|_{DG} \leq C h^k (|\boldsymbol{u}|_{k+1} + |p|_k)$$

where $C = C(M(\gamma_f)/m(\gamma_f), \hat{\boldsymbol{u}}_h, \hat{p}_h, \boldsymbol{g}, \boldsymbol{t})$.

Proof. Applying the consistency result, we obtain the lower bound. Moreover, the coercivity and continuity results together with Cauchy-Schwarz inequality imply that

$$\begin{aligned} &C_{coerc}(|\!|\!| \mathbf{I}_h \boldsymbol{u} - \boldsymbol{u}_h |\!|\!|_{DG} + |\!|\!| \boldsymbol{\Pi}_h p - p_h |\!|\!|_{DG}) \\ &\quad \leq C_h((\mathbf{I}_h \boldsymbol{u} - \boldsymbol{u}_h, \boldsymbol{\Pi}_h p - p_h), (\mathbf{I}_h \boldsymbol{u} - \boldsymbol{u}_h, \boldsymbol{\Pi}_h p - p_h)), \end{aligned}$$

where $C_{coerc} = \min\left\{(1-\epsilon), m(\gamma_f, \mathbf{x}) + \beta, \alpha h_e^{-1}\right\}$. Next, the consistency result imply that

$$\begin{aligned} &C_h((\mathbf{I}_h \boldsymbol{u} - \boldsymbol{u}_h, \boldsymbol{\Pi}_h p - p_h), (\mathbf{I}_h \boldsymbol{u} - \boldsymbol{u}_h, \boldsymbol{\Pi}_h p - p_h)) \\ &\quad \leq C_h((\mathbf{I}_h \boldsymbol{u} - \boldsymbol{u}_h, \boldsymbol{\Pi}_h p - p_h), (\mathbf{I}_h \boldsymbol{u} - \boldsymbol{u}_h, \boldsymbol{\Pi}_h p - p_h)) \\ &\qquad + C_{cons} h |\!|\!| \mathbf{I}_h \boldsymbol{u} - \boldsymbol{u}_h |\!|\!|_{DG} \\ &\quad =: M_1, \end{aligned}$$

where $C_{cons} = C(M(\gamma_f, \mathbf{x}), \hat{\boldsymbol{u}}_h, \hat{p}_h, \boldsymbol{g}, \boldsymbol{t})$.

Combining the Cauchy-Schwarz inequality and continuity of the form $C((\boldsymbol{u}_h, p_h), (\mathbf{v}_h, q_h))$, we have:

$$\begin{aligned} M_1 \leq (\, &C(\hat{\boldsymbol{u}}_h, \hat{p}_h, M(\gamma_f, \mathbf{x}))(|\mathbf{I}_h \boldsymbol{u} - \boldsymbol{u}_h|_1^2 + \sum_{e \in \mathcal{E}_h} |\{\{\mathbf{I}_h \boldsymbol{u} - \boldsymbol{u}_h\}\}\mathbf{n}|_{1,e}^2) \\ &+ C(\hat{\boldsymbol{u}}_h, \hat{p})(\|\boldsymbol{\Pi}_h p - p_h\|_0^2 + \sum_{e \in \mathcal{E}_h} \|\{\{\boldsymbol{\Pi}_h p - p_h\}\}\mathbf{n}\|_{0,e}^2) \end{aligned}$$

$$
\begin{aligned}
&+ \sum_{e\in\mathcal{E}_h} \alpha h_e \left|[\![\boldsymbol{\Pi}_h p - p_h]\!]\right|_{1,e}^2 + \sum_{e\in\mathcal{E}_h} \beta h_e^{-1} \left|[\![\mathbf{I}_h \boldsymbol{u} - \boldsymbol{u}_h]\!]\mathbf{n}\right|_{1,e}^2)^{1/2} \\
&\times (\left|\mathbf{I}_h \boldsymbol{u} - \boldsymbol{u}_h\right|_1^2 + \sum_{e\in\mathcal{E}_h} (1+\beta h_e) \left|[\![\mathbf{I}_h \boldsymbol{u} - \boldsymbol{u}_h]\!]\mathbf{n}\right|_{1,e}^2 + \|\boldsymbol{\Pi}_h p - p_h\|_0^2 \\
&+ \sum_{e\in\mathcal{E}_h} \|\{\{\boldsymbol{\Pi}_h p - p_h\}\}\mathbf{n}\|_{0,e}^2 + \sum_{e\in\mathcal{E}_h} \alpha h_e \|[\![\boldsymbol{\Pi}_h p - p_h]\!]\mathbf{n}\|_{0,e}^2 + h^2 [\![\mathbf{I}_h \boldsymbol{u} - \boldsymbol{u}_h]\!]_{DG}{}^2)^{1/2} .
\end{aligned}
$$

Using the interpolation error in the mesh dependent norm 4.12a and 4.12b, we obtain:

$$
\begin{aligned}
&C_{coerc}([\![\mathbf{I}_h \boldsymbol{u} - \boldsymbol{u}_h]\!]_{DG} + [\![\boldsymbol{\Pi}_h p - p_h]\!]_{DG}) \\
&\quad \leq Ch^k (C(\hat{\boldsymbol{u}}_h, \hat{p}_h, M(\gamma_f, \mathbf{x})) \left|\boldsymbol{u}\right|_{k+1}^2 \\
&\qquad + C(\hat{\boldsymbol{u}}_h, \hat{p}_h) \left|p\right|_k^2)([\![\mathbf{I}_h \boldsymbol{u} - \boldsymbol{u}_h]\!]_{DG} + [\![\boldsymbol{\Pi}_h p - p_h]\!]_{DG})^{1/2}.
\end{aligned}
$$

The proof is complete after applying triangular inequality and the interpolation error in the mesh dependent norm once again. □

Notice that if we only assume $p \in H^{k-1}(B_0)$, then the convergence result from Theorem 4.5.1 reads

$$
[\![\boldsymbol{u} - \boldsymbol{u}_h]\!]_{DG} + [\![p - p_h]\!]_{DG} \leq C(\frac{M(\gamma_f, \mathbf{x})}{m(\gamma_f, \mathbf{x})}, \hat{\boldsymbol{u}}_h, \hat{p}_h, \boldsymbol{g}, \boldsymbol{t})(h^k \left|\boldsymbol{u}\right|_{k+1} + h^{k-1} \left|p\right|_k)
$$

Theorem 4.5.2. *Let $(\boldsymbol{u}_h, p_h) \in V_{h,D} \times Q_h$ be the unique solution of 4.9 and $(\boldsymbol{u}, p) \in H^{k+1}(B_0)^d \times H^k(B_0)$ the unique solution of 3.2. Then, there exists $C > 0$ such that*

$$
\|\boldsymbol{u} - \boldsymbol{u}_h\|_{0,B_0} + \|p - p_h\|_{0,B_0} \leq Ch^{k+1}(|\boldsymbol{u}|_{k+1,B_0} + |p|_{k,B_0})
$$

where $C = C(M(\gamma_f, \mathbf{x})/m(\gamma_f, \mathbf{x}), \hat{\boldsymbol{u}}_h, \hat{p}_h, \boldsymbol{g}, \boldsymbol{t})$ and k is the polynomial degree.

Proof. The proof is based on duality argument. Let $(\boldsymbol{w}, \xi) \in H^k(B_0) \times H^{k-1}(B_0) \cap L_0^2(B_0)$ be the unique solution of adjoint problem which strong formulation is given by

$$
\begin{aligned}
-\nabla \cdot (J_a \mathbf{C}_a^{-1} \nabla \boldsymbol{w} + \hat{p} \hat{J} \nabla(\hat{\boldsymbol{u}})^{-T} \nabla \boldsymbol{w} \nabla(\hat{\boldsymbol{u}})^{-T}) - \nabla(\xi \hat{J} \nabla \hat{\boldsymbol{u}}^{-T}) &= \boldsymbol{u} - \boldsymbol{u}_h, \\
\nabla \cdot (\hat{J} \nabla(\hat{\boldsymbol{u}})^{-T} \boldsymbol{w}) &= p - p_h.
\end{aligned} \tag{4.13}
$$

The existence of $(\boldsymbol{w}, \xi)$ is guaranteed by the continuous inf-sup condition satisfied by the spaces pair $H^k(B_0)^d \times H^{k-1}(B_0)$ and by the assumed regularity of the domain B_0(convex and bounded polygon or polyhedron) [37]. In addition, the following continuous dependency on datum holds:

$$
\begin{aligned}
|\mathbf{w}|_{k+1} + |\xi|_k &\leq C\|\mathbf{u} - \mathbf{u}_h\|_{0,B_0}, \\
|\mathbf{w}|_{k+1} &\leq C\|p - p_h\|_{0,B_0}.
\end{aligned}
$$

Let us write the weak form of system (4.13), using the quadrilinear form $C((\cdot,\cdot),(\cdot,\cdot))$: find $(\boldsymbol{w}, \xi)$ such that

$$
\mathcal{C}((\boldsymbol{w}, \xi), (\boldsymbol{u} - \boldsymbol{u}_h, 0)) := \int_{B_0} J_a \mathbf{C}_a^{-1} \nabla \mathbf{v} : \nabla \boldsymbol{w} + \hat{p} \hat{J} \nabla(\hat{\boldsymbol{u}} \nabla \mathbf{v})^T : (\nabla(\hat{\boldsymbol{u}}) \nabla \boldsymbol{w})^T
$$

$$-\xi\hat{J}\nabla\hat{\boldsymbol{u}}^{-T} : \nabla\mathbf{v}dB_0 = \int_{B_0}(\boldsymbol{u}-\boldsymbol{u}_h)\mathbf{v}$$
$$\mathcal{C}((\boldsymbol{w},0),(0,q)) := \int_{B_0} q\hat{J}\nabla\hat{\boldsymbol{u}}^{-T} : \nabla\boldsymbol{w} = \int_{B_0}(p-p_h)q$$

for all $(\mathbf{v},q)$. Choosing in particular $(\mathbf{v},q)=(\boldsymbol{u}-\boldsymbol{u}_h, p-p_h)$, the asymptotic consistency implies that

$$\left|C((\boldsymbol{w},\xi),(\boldsymbol{u}-\boldsymbol{u}_h,0)) - \|\boldsymbol{u}-\boldsymbol{u}_h\|_0^2\right| \leq Ch(|\boldsymbol{w}|_{k+1}+|\xi|_k)\|\!|\boldsymbol{u}-\boldsymbol{u}_h|\!\|_{DG}$$
$$\left|C((\boldsymbol{w},0),(0,p-p_h)) - \|p-p_h\|_0^2\right| \leq Ch\,|\boldsymbol{w}|_{k+1}\,\|\!|p-p_h|\!\|_{DG}.$$

Then we write $\boldsymbol{w}=\boldsymbol{w}-\mathbf{I}_h\boldsymbol{w}+\mathbf{I}_h\boldsymbol{w}$ and $\xi=\xi-\boldsymbol{\Pi}_h\xi+\boldsymbol{\Pi}_h\xi$, and after applying the continuity of the bilinear forms C and C_h and consistency result, we arrive at

$$\begin{aligned}\|\boldsymbol{u}-\boldsymbol{u}_h\|_{0,B_0}^2 &\leq Ch(|\boldsymbol{w}|_{k+1,B_0}+h\,|\xi|_{k,B_0})\|\!|\boldsymbol{u}-\boldsymbol{u}_h|\!\|_{DG}\\ &\quad + C(\|\!|\boldsymbol{w}-\mathbf{I}_h\boldsymbol{w}|\!\|_{DG}+\|\!|\xi-\boldsymbol{\Pi}\xi|\!\|_{DG})\|\!|\boldsymbol{u}-\boldsymbol{u}_h|\!\|_{DG}\\ \|p-p_h\|_{0,B_0}^2 &\leq Ch\,|\boldsymbol{w}|_{k+1,B_0}\,\|\!|p-p_h|\!\|_{DG}\\ &\quad + C(\|\!|\boldsymbol{w}-\mathbf{I}_h\boldsymbol{w}|\!\|_{DG})\|\!|p-p_h|\!\|_{DG}.\end{aligned}$$

Applying the continuous dependency on the datum and classical interpolant estimates yields

$$\|\boldsymbol{u}-\boldsymbol{u}_h\|_{0,B_0} \leq Ch\|\!|\boldsymbol{u}-\boldsymbol{u}_h|\!\|_{DG}$$
$$\|p-p_h\|_{0,B_0} \leq Ch\|\!|p-p_h|\!\|_{DG},$$

and by virtue of Theorem 4.4.8 once again, the proof is finished. □

Let us define the constraint space $D_h(\mathbf{v}) = \{\mathbf{v}\in V_h : b(\mathbf{v},q)=g(q),\ \forall q\in P_h\}$.

Theorem 4.5.3. *The discontinuous Galerkin finite element method, for linearized fully incompressible case, is locking-free, that is [33, 7]:*

$$\inf_{\mathbf{v}_h\in D_h}\|\boldsymbol{u}-\mathbf{v}_h\| \leq C\inf_{\mathbf{v}_h\in V_h}\|\boldsymbol{u}-\mathbf{v}_h\|,$$

where C is a constant independent of h.

Proof. If the solution $\boldsymbol{u}_h$ of (4.9) lies in D_h then it satisfies:

$$a(\boldsymbol{u}_h,\mathbf{v}) = f(\mathbf{v}) - g(p). \tag{4.14}$$

Subtracting (4.14) from $a(\boldsymbol{u},\mathbf{v})-b(\mathbf{v},p)=f(\mathbf{v})$ gives

$$a(\boldsymbol{u}-\boldsymbol{u}_h,\mathbf{v}) = b(\mathbf{v},p)-g(p) = b(\mathbf{v},p-\boldsymbol{\Pi}p)-g(p-\boldsymbol{\Pi}p)-g(\boldsymbol{\Pi}p).$$

Then, for any $\mathbf{v}\in D_h$, using coercivity of bilinear form $a(\cdot,\cdot)$, continuity of $a(\cdot,\cdot)$ and $b(\cdot,\cdot)$, we have:

$$\|\!|\boldsymbol{u}_h-\mathbf{v}|\!\|_{DG}^2 \leq \frac{1}{Coer(a)}a(\boldsymbol{u}_h-\mathbf{v},U_h-\mathbf{v})$$

$$
\begin{aligned}
&= \frac{1}{Coer(a)}(a(\boldsymbol{u}_h - \boldsymbol{u}, U_h - \mathbf{v}) + a(\boldsymbol{u} - \mathbf{v}, U_h - \mathbf{v})) \\
&= \left| Coer(a)^{-1}(b(\boldsymbol{u}_h - \mathbf{v}, \boldsymbol{\Pi}_h p - p) + a(\boldsymbol{u} - \mathbf{v}, \boldsymbol{u}_h - \mathbf{v}) - g(p)) \right| \\
&\leq \frac{Cont(b)}{Coer(a)} |\!|\!| \boldsymbol{u}_h - \mathbf{v} |\!|\!|_{DG} |\!|\!| \boldsymbol{\Pi}_h p - p |\!|\!|_{DG} \\
&\quad + \frac{Cont(a)}{Coer(a)} |\!|\!| \boldsymbol{u} - \mathbf{v} |\!|\!|_{DG} |\!|\!| \boldsymbol{u}_h - \mathbf{v} |\!|\!|_{DG},
\end{aligned}
$$

where $Cont(b) = C_1(\hat{\boldsymbol{u}}), Coerc(a) = C_2(\gamma_f, \hat{\boldsymbol{u}}, \beta, \alpha, \hat{p}), Cont(a) = C_3(\gamma_f, \hat{\boldsymbol{u}}, \beta, \alpha, \hat{p})$, and then all constants employed are independent of h.

Finally, taking the limit $h \to 0^+$ gives:

$$
\inf_{\mathbf{v} \in D_h} |\!|\!| \boldsymbol{u}_h - \mathbf{v} |\!|\!|_{DG} \leq C(\gamma_f, \hat{\boldsymbol{u}}, \hat{p}, \beta, \alpha) \inf_{\mathbf{v} \in \mathbf{v}_h} |\!|\!| \boldsymbol{u} - \mathbf{v} |\!|\!|_{DG}.
$$

□

Let us consider a particular choice of space, the intersection between the continuous space $H_0^k(B_0) \times H^{k-1}(B_0) \cap L_0^2(B_0)$ with the discontinuous space $V_{h,D}^d \times Q_h$. As in [89] we employ piecewise $d-$quadratic elements for deformations and piecewise $d-$linear elements for the pressure field:

$$
\hat{V}_h := V_h^d \cap C^0(E) \quad \hat{P}_h := P_h^d \cap C^0(E) \quad \text{for } E \in \mathcal{T}_h
$$

This finite element pair is know to satisfy the discrete inf-sup condition [14]. The finite element method reads: Find $\boldsymbol{u}_h \in \hat{V}_h, p_h \in \hat{P}_h$ such that:

$$
\begin{cases}
a(\mathbf{u}_h, \mathbf{v}_h) - b(p_h, \mathbf{v}_h) & = f(\mathbf{v}_h) \, \forall \, \mathbf{v}_h \in \hat{V}_h \\
-b(\mathbf{u}_h, q_h) & = g(q_h) \, \forall \, q_h \in \hat{P}_h
\end{cases}
$$

Let $\left\{\phi^l\right\}_{l=1}^{N_h}$ and $\left\{\xi^l\right\}_{l=1}^{M_h}$ denote the basis for the spaces $\hat{V}_h$ and $\hat{Q}_h$. Then the Galerkin scheme reads:

$$
\begin{cases}
\boldsymbol{u}_{k+1}^m a_k(\phi^m, \phi^l) + p_{k+1}^n b_k(\phi^l, \xi^n) = F_k(\phi^l) & m = 1, \ldots, N_h \\
\boldsymbol{u}_{k+1}^m b_k(\phi^m, \xi^n) = G_k(\xi^n) & n = 1, \ldots, M_h
\end{cases}
$$

This scheme exhibits the optimal convergence results, as well known [84].

Chapter 5

Numerical results

This chapter contains five tests assessing the accuracy and robustness of the discontinuous Galerkin formulation proposed in previous chapter. For sake of comparison, we will also present convergence results for classical Taylor-Hood finite element. We use an iterative Newton method to solve nonlinear elastostatic problem. This procedure requires as consistent linearization of the original weak formulation, as proposed in Chapter 2. Moreover in each iteration the linearized has to fulfill, at least for sufficiently small deformations, solvability and stability in the sense of the classical Babuska-Brezzi thoery for saddle-point problems.

5.1 Test problem 1: Contraction of a 2D Neo-Hookean slab

As a sample of our results, we present a test problem for 2D neo-Hookean contraction. In the first test case, we consider a square domain $B_0 = [0,1]^2$, where the fiber are aligned with a fixed angle of $\pi/2$, that is, $\mathbf{f}_0 = (0,-1)^T$ and sheet are in the orthogonal direction $\mathbf{s}_0 = (1,0)^T$. On the bottom side $\Gamma_D = (0,1) \times \{0\}$, we impose nonhomogeneous Dirichlet boundary condition $\boldsymbol{u} = (x,y)$ and Neumann traction $\boldsymbol{t}$ on other side, in such a way that the problem have the analytical solution in the closed form. In particular the exact position and pressure depend on the direction of fiber and sheet:

$$\boldsymbol{u} = \left(bx + \frac{a}{2}\mathbf{f}_0^y y^2, \frac{y}{b}\right)^T,\ p = \mu ab(1+\gamma_f \mathbf{f}_0^{y,2})^2 \left(x + \frac{ay^2}{2b}\right).$$

This solution satisfies the incompressibility constraint $\det \nabla \boldsymbol{u} = 1$. The chosen parameters are $\mu = 400$, $a = 0.5$, $b = 1$. The mechanical activation is assumed constant $\gamma_f = -0.3$. The stabilization factors take the values $\alpha = 0.1$, $\beta = 10^{11}$, $\delta = 10^{-5}$.

5.2 Newton method and implementation details

The non-linear system of equations resulting from the discretization of the static mechanic problem is solved using an incremental iterative Newton-Raphson solution procedure. We denote the solution at the (sub) iteration step k by $(\boldsymbol{u}^k, p^k)$ and the incremental growth of the discrete position by $\delta\boldsymbol{u}^{k+1}$ and that of pressure by δp^{k+1}. Since the speed of convergence

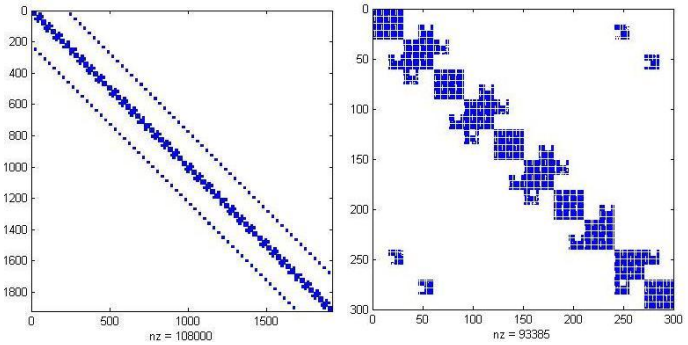

Figure 5.1: Using a stabilized $\mathbb{P}^2_{\text{disc}} - \mathbb{P}^1_{disc}$ on uniform mesh of 64 elements, the picture display the sparsity of complete matrix of the system (left) and a zoom on first block of (300×300) show the nonsymmetry of the system (right).

of Newton's iterations is known to depend on its proper initialization, as initial guess for the iteration process we use $\boldsymbol{u}^0 = \mathbf{0}$ (the null vector), that is, we start from the reference (undeformed $\mathbf{F}^0 = \mathbf{I}$) configuration. The problem in its weak form reads:

$$
\begin{aligned}
&\sum_{E\in T_h}\int_E J_a\mathbf{C}_a^{-1}\nabla\boldsymbol{u}_h^{k+1} : \nabla\mathbf{v}_h + J^k p^k((\mathbf{F}^k)^{-1}\nabla\boldsymbol{u}_h^{k+1})^T : ({\mathbf{F}^{-1}}^k\nabla\mathbf{v}_h)dB_0\\
&\quad - \sum_{e\in\mathcal{E}_h^{int}}\int_e \left\{\left\{ J^k p^k((\mathbf{F}^{-1})^k\nabla\boldsymbol{u}_h^{k+1})^T\mathbf{n}\right\}\right\}\cdot\left[\left[(\mathbf{F}^{-1})^k\mathbf{v}_h\right]\right]\\
&\quad - \sum_{e\in\mathcal{E}_h^{int}}\int_e \left\{\left\{ J_a\mathbf{C}_a^{-1}\nabla\boldsymbol{u}_h^{k+1}\mathbf{n}\right\}\right\}[\![\mathbf{v}_h]\!] - \sum_{e\in\mathcal{E}_h^{D}}\int_e J_a\mathbf{C}_a^{-1}\nabla\boldsymbol{u}_h^{k+1}\mathbf{N}\cdot\mathbf{v}_h\\
&\quad + \sum_{e\in\mathcal{E}_h^{int}}\frac{\beta}{h_e}\left[\left[\boldsymbol{u}_h^{k+1}\right]\right][\![\mathbf{v}_h]\!] + \beta\sum_{e\in\mathcal{E}_h^{D}}\frac{1}{h_e}(\boldsymbol{u}_h^{k+1}-\mathbf{g})\cdot\mathbf{v}_h\\
&\quad - \sum_{E\in T_h}\int_E p_h^{k+1}J^k(\mathbf{F}^k)^{-T} : \nabla\mathbf{v}_h + \sum_{e\in\mathcal{E}_h^{int}}\int_e\left\{\left\{ p_h^{k+1}J^k(\nabla\boldsymbol{u}_h^{k+1})^{-T}\mathbf{n}\right\}\right\}[\![\mathbf{v}_h]\!]\\
&\quad - \sum_{e\in\mathcal{E}_h^{D}}\int_e p_h^{k+1}J^k(\nabla{\boldsymbol{u}_h}^k)^{-T}\mathbf{n}\mathbf{v}_h\\
&= \int_{B_0} p_h^k J^k(\mathbf{F}^k)^{-T} : \nabla\mathbf{v}_h dB_0 + \int_{B_0}\mu J_a\mathbf{C}_a^{-1}\mathbf{F}^k : \nabla\mathbf{v}_h - {p_h}^k J^k(\mathbf{F}^k)^{-1} : \nabla\mathbf{v}_h dB_0\\
&\quad + \int_{\partial_N B_0}\boldsymbol{t}\cdot\mathbf{v}_h dS,
\end{aligned}
$$

for all $\mathbf{v}_h$, and

$$
\begin{aligned}
&- \sum_{E\in T_h}\int_E q_h J^k(\mathbf{F}^k)^{-T} : \nabla\boldsymbol{u}_h^{k+1} + \sum_{e\in\mathcal{E}_h^{int}}\int_e\left\{\left\{ q_h J^k\nabla(\boldsymbol{u}_h^k)^{-T}\mathbf{n}\right\}\right\}\left[\left[\boldsymbol{u}_h^{k+1}\right]\right]\\
&\quad - \sum_{e\in\mathcal{E}_h^{D}}\int_e q_h J^k(\nabla\boldsymbol{u}_h^k)^{-T}\mathbf{n} + \alpha\sum_{e\in\mathcal{E}_h^{I}}\int_e h_e\left[\left[p_h^{k+1}\right]\right][\![q_h]\!]
\end{aligned}
$$

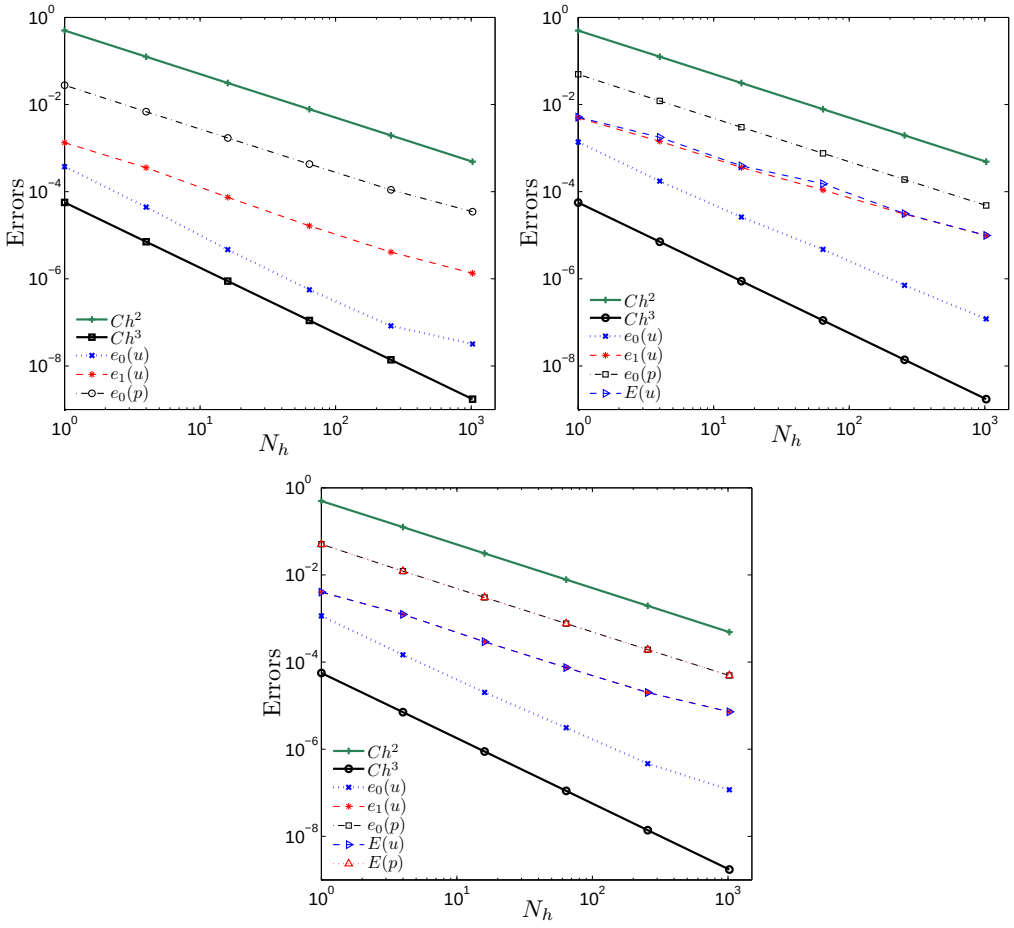

Figure 5.2: Test 1: Convergence behavior of a Taylor-Hood method (top left) and stabilized DG methods of type $\mathbb{P}^2_{\text{disc}} - \mathbb{P}^1$ and $\mathbb{P}^2_{\text{disc}} - \mathbb{P}^1_{\text{disc}}$ (top right and bottom, respectively). The displayed quantities correspond to relative errors as defined in previous chapter.

$$+ \delta \sum_{E \in \mathcal{T}_h} \int_E p_h^{k+1} q_h \mathbf{F}^k : \mathbf{I} = \int_{B_0} q_h (J^k - 1) dB_0,$$

for all q_h. The stopping criterion for the algorithm corresponds to

$$\epsilon_k = \frac{\|\boldsymbol{u}_h^{k+1} - \boldsymbol{u}_h^k\|_{DG}}{\|\boldsymbol{u}_h^k\|_{DG}} + \frac{\|p_h^{k+1} - p_h^k\|_{DG}}{\|p_h^k\|_{DG}} < \epsilon,$$

with ϵ being a given tolerance ($\epsilon = 10^{-7}$). Even though the nonlinear weak formulation of the problem admits a unique solution, the previous Newton scheme may not converge for any arbitrary value of the activation function $\gamma_{\mathbf{f}_0}$. As we will present in the next section, for some large deformation problems it is required to employ an incremental step method, which consists essentially in moving smoothly from $(\mathbf{0}, 0)$ to the desired final state.

To assess the convergence of the stabilized method, we make use of relative errors and experimental rates of convergence defined by

$$e_m(\boldsymbol{u}) := \frac{|\boldsymbol{u} - \boldsymbol{u}_h|_{H^k}}{|\boldsymbol{u}|_{H^k}}, \; e_0(p) := \frac{\|p - p_h\|_{L^2}}{\|p\|_{L^2}}, E(\boldsymbol{u}) := \frac{\|\boldsymbol{u} - \boldsymbol{u}_h\|_{DG}}{\|\boldsymbol{u}\|_{DG}},$$

N_h	$e_0(\boldsymbol{u})$	$r_0(\boldsymbol{u})$	$e_1(\boldsymbol{u})$	$r_1(\boldsymbol{u})$	$e_0(p)$	$r_0(p)$	$E(\boldsymbol{u})$	$R(\boldsymbol{u})$	$E(p)$	$R(p)$
CG Method, Taylor-Hood elements										
4	4.4234e−5	–	3.5506e−4	–	6.8512e−3	–				
16	4.6937e−6	3.0817	7.4418e−5	1.9092	1.7119e−3	2.0229				
64	5.5959e−7	3.2364	1.6423e−5	2.2543	4.2949e−4	2.0013				
256	8.3036e−8	3.0683	4.1159e−6	2.1799	1.0997e−4	1.9944				
1024	1.0554e−8	2.0193	1.3363e−6	1.9965	3.4756e−5	1.9655				
Stabilized DG Method, $\mathbb{P}^2_{\text{disc}} - \mathbb{P}^1$ elements										
4	1.7530e−4	–	1.4313e−3	–	6.8499e−3	–	1.7647e−3	–		
16	2.6164e−5	2.9743	3.5913e−4	1.8904	1.7122e−3	2.0314	3.9184e−4	1.5355		
64	4.7416e−6	2.7442	1.0931e−4	1.9948	4.2967e−4	2.0013	1.5201e−4	2.1711		
256	7.0650e−7	2.5641	3.0571e−5	1.8161	1.0995e−4	1.9943	3.1277e−5	1.6631		
1024	1.2019e−7	2.7546	9.8542e−6	1.8382	3.4740e−5	1.9937	9.9213e−6	2.2810		
Stabilized DG Method, $\mathbb{P}^2_{\text{disc}} - \mathbb{P}^1_{\text{disc}}$ elements										
4	1.4654e−4	–	1.2483e−3	–	1.2228e−2	–	1.3559e−3	–	1.4167e−2	–
16	2.0092e−5	2.9683	2.9221e−4	1.7963	3.0457e−3	2.0502	2.9431e−4	1.6869	3.1578e−3	1.9812
64	3.1150e−6	2.8666	7.4835e−5	2.0949	7.6494e−4	2.0055	7.6494e−5	1.9467	7.8095e−4	2.0049
256	4.6556e−7	2.6993	2.0044e−5	1.9652	1.9254e−4	1.9933	2.1091e−5	1.9114	1.9618e−4	1.9752
1024	1.1715e−7	2.7422	7.2251e−6	1.9005	4.9198e−5	1.9201	7.4252e−6	1.9671	4.9324e−5	1.9230

Table 5.1: Test 1: Convergence histories for a $\mathbb{P}^2 - \mathbb{P}^1$ method (Taylor-Hood), a stabilized $\mathbb{P}^2_{\text{disc}} - \mathbb{P}^1$ and a stabilized $\mathbb{P}^2_{\text{disc}} - \mathbb{P}^1_{\text{disc}}$ method. The displayed quantities correspond to relative errors and rates as defined in the previous chapter.

$$E(p) := \frac{\|p - p_h\|_{DG}}{\|p\|_{DG}},\ r_m(\boldsymbol{u}) := \frac{\log(e_m(\boldsymbol{u})/\hat{e}_m(\boldsymbol{u}))}{\log(h/\hat{h})},\ r_0(p) := \frac{\log(e_0(p)/\hat{e}_0(p))}{\log(h/\hat{h})},$$
$$R(\boldsymbol{u}) := \frac{\log(E(\boldsymbol{u})/\hat{E}(\boldsymbol{u}))}{\log(h/\hat{h})},\ R(p) := \frac{\log(E(p)/\hat{E}(p))}{\log(h/\hat{h})},$$

$m \in \{0, 1\}$, where e_m and $\hat{e}_m$ are errors obtained for two consecutive meshes of sizes h and $\hat{h}$. We consider a sequence of successively uniformly refined triangular meshes of $1, 9, 49, 225$ and 961 interior nodes. On each iteration, the (nonsymmetric) linear systems are solved with the UMFPACK method. The sparse pattern of stiffness matrix is represent in Figure 5.1.

For the first test problem, Figure 5.2 displays the convergence behavior and Table 5.1 reports the comparison of relative errors between Taylor-Hood and stabilized discontinuous methods of type $\mathbb{P}^2_{\text{disc}} - \mathbb{P}^1$ and $\mathbb{P}^2_{\text{disc}} - \mathbb{P}^1_{\text{disc}}$.

A convergence rate of h^3 is observed for L^2-norm of deformations and of h^2 for the L^2-norm of the pressure and H^1-seminorm of the deformation, in accordance with theoretical results of chapter 4.

The approximate solution (deformation represented on the reference body and pressure field on the deformed configuration) is plotted in Figures 5.3 and 5.4.

According with theoretical estimates on convergence of displacement in L^2-norm, there is a linear dependence on activation fiber parameter γ_f. The Figures 5.5, 5.6, 5.7 and 5.8 display this relation between $e_0(\boldsymbol{u})$ and the linear variation of γ_f (as constant value) in the interval $[-0.3, 0)$, using the stabilized DG methods $\mathbb{P}^2_{\text{disc}} - \mathbb{P}^1_{disc}$ and $\mathbb{P}^2_{\text{disc}} - \mathbb{P}^1$.

As we have claimed in the chapter 4, the optimal choices of penalty parameters α and β influence the convergence rate's of displacement and pressure. The choice of large β is dictated for ensure the coercivity of the scheme. The Figure 5.9 and 5.10 display the optimal choice that is for β is 10^{11} and for $\alpha = 10^{-1}$. Moreover, β has only influence on

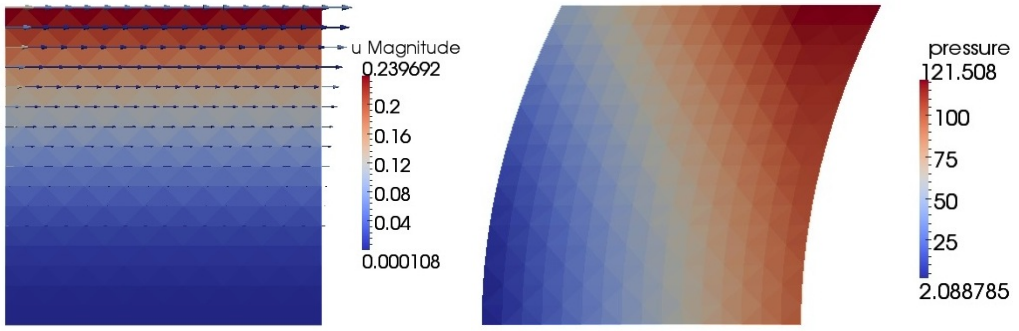

Figure 5.3: Deformation field on reference configuration (left) and pressure distribution on the corresponding deformed domain (right). Solution obtained on a uniform mesh of 512 elements, using a stabilized $\mathbb{P}^2_{\text{disc}} - \mathbb{P}^1$ method.

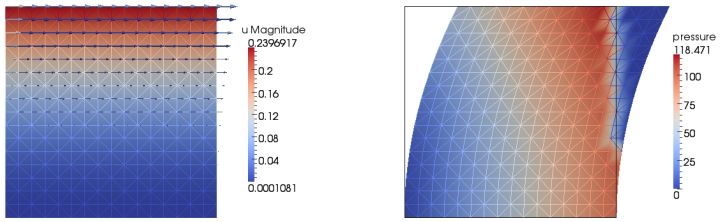

Figure 5.4: Deformation field on reference configuration (left) and pressure distribution on the corresponding deformed domain (right). Solution obtained on a uniform mesh of 512 elements , using a stabilized $\mathbb{P}^2_{\text{disc}} - \mathbb{P}^1_{disc}$ scheme.

displacement's rate instead α has influence on both variables: displacement and pressure.

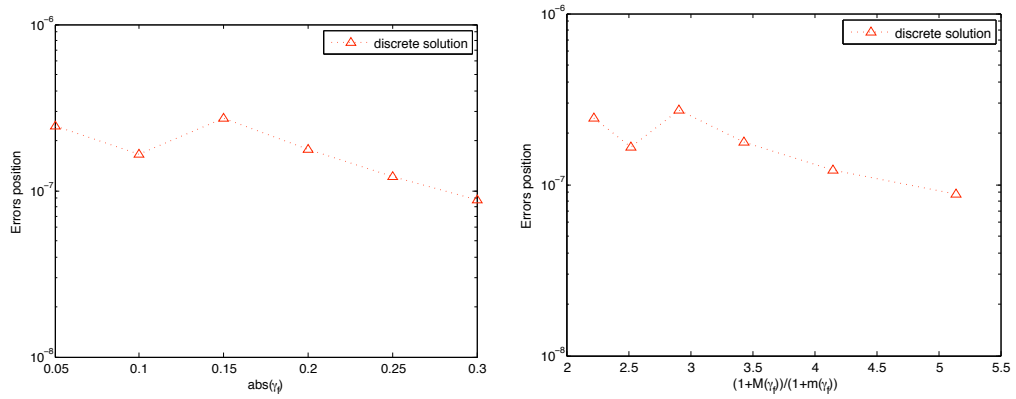

Figure 5.5: Dependence on the active parameter γ_f, using a stabilized $\mathbb{P}^2_{\text{disc}} - \mathbb{P}^1_{disc}$ method on a uniform mesh of 512 elements.

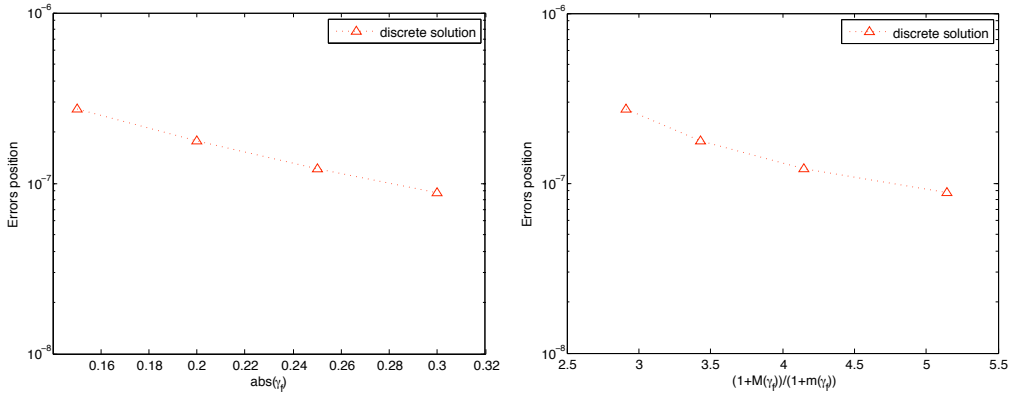

Figure 5.6: Zoom of dependence on the active parameter $\gamma_f \in [-0.3, -0.15]$, belong in the physiological activation range, using a stabilized $\mathbb{P}^2_{\text{disc}} - \mathbb{P}^1_{disc}$ scheme on a uniform mesh of 512 elements.

5.3 Test Problem 2: smooth active response of 2D neo-Hooeakean slab

In the second example we consider the simulation of the active contraction of a Neo-Hookean material with elastic modulus $\mu = 400$ and fibers and sheets aligned with $\mathbf{f}_0 = (0,1)^T$ and $\mathbf{s}_0 = (-1,0)^T$, respectively. The activation function is no longer constant, but we choose $\gamma_f = 0.3\exp(4[y-0.25]^2)$ to take account of smooth active response. The choice of gaussian function is justify by the clinical test on concentration of Calcium in the cardiac tissue. On the base of the square we impose $\boldsymbol{u} = \mathbf{0}$. With a mesh of 225 interior nodes, Taylor-Hood elements exhibit reverse triangle deformation, and volumetric locking. With $\mathbb{P}^2_{\text{disc}} - \mathbb{P}^1$ elements we obtained correct deformations, but the pressure presented spurious oscillations near the lines $x = 0$ and $x = 1$ 5.11. The best results were obtained with a stabilized $\mathbb{P}^2_{\text{disc}} - \mathbb{P}^1_{\text{disc}}$ method, for which the numerical solution is depicted in Figure 5.12; we observed no oscillations in the pressure field, and preservation of the material's volume.

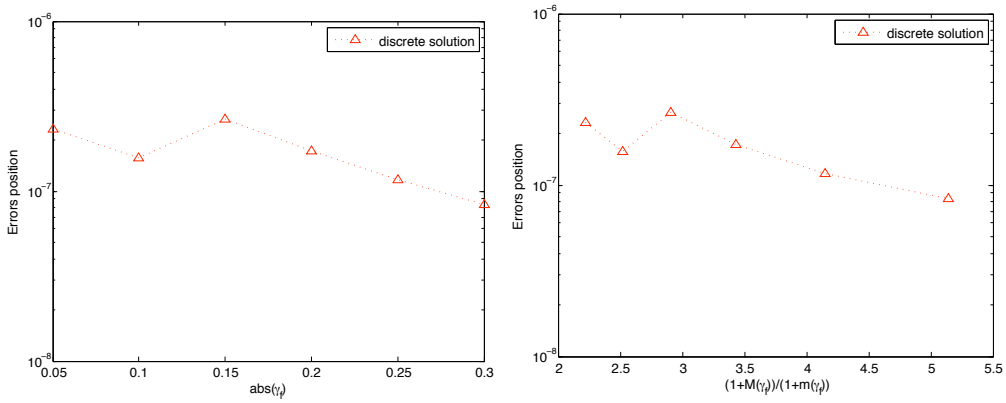

Figure 5.7: Dependence on the active parameter γ_f, using a stabilized $\mathbb{P}^2_{\text{disc}} - \mathbb{P}^1$ method on a uniform mesh of 512 elements.

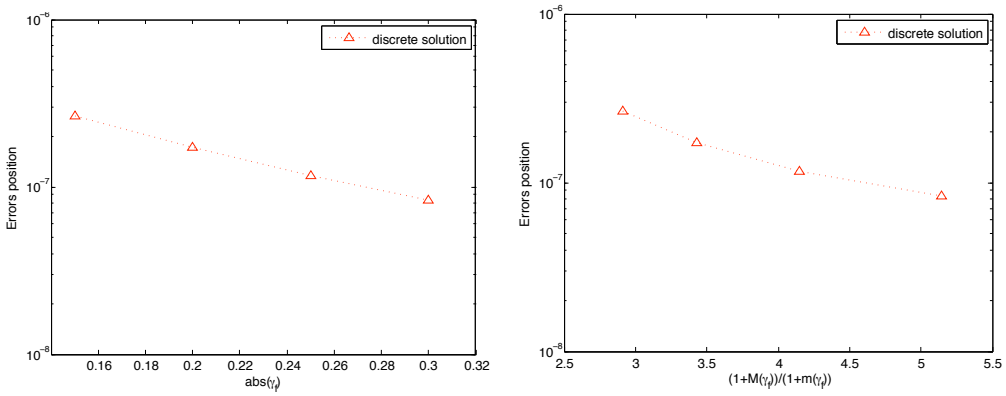

Figure 5.8: Zoom of dependence on the active parameter $\gamma_f \in [-0.3, -0.15]$ belong in the physiological activation range, using a stabilized $\mathbb{P}^2_{\text{disc}} - \mathbb{P}^1$ method on a uniform mesh of 512 elements.

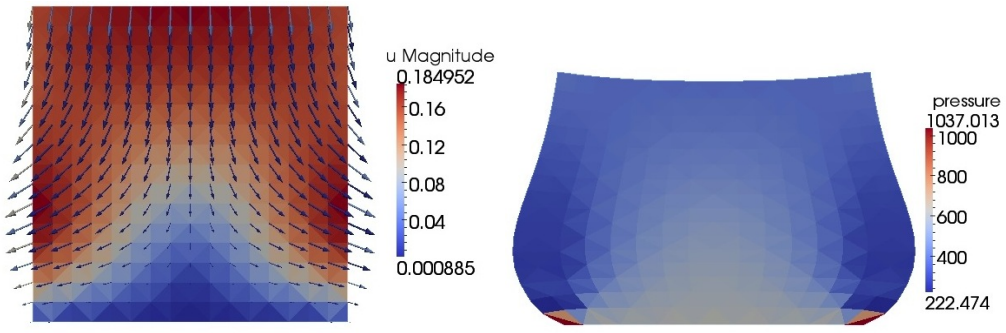

Figure 5.11: Test 2: Deformation field on reference configuration (left) and pressure distribution on the corresponding deformed domain (right). Solution obtained on a uniform mesh of 512 elements, using a stabilized $\mathbb{P}^2_{\text{disc}} - \mathbb{P}^1$ formulation.

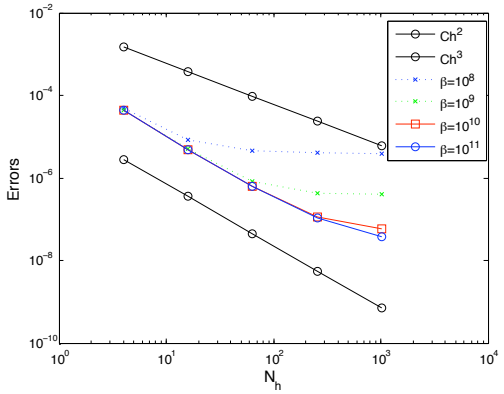

Figure 5.9: Influence of penalty parameter $\beta = 10^8, 10^9, 10^{10}, 10^{11}$ on displacement's history of error, using the stabilized $\mathbb{P}^2_{\text{disc}} - \mathbb{P}^1_{disc}$ method with $\delta = 10^{-5}$ and $\alpha = 10^{-1}$.

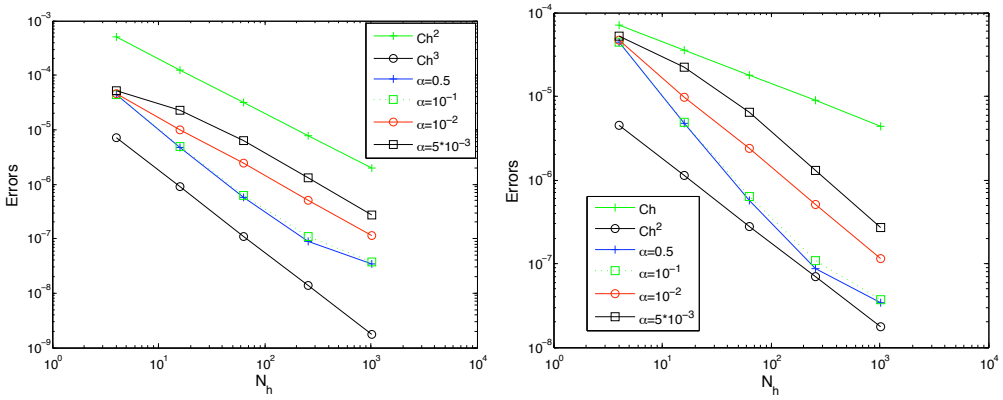

Figure 5.10: Influence of penalty parameter $\alpha = 0.5, 0.1, 0.01, 0.05$ on displacement's (left) and pressure's(right) history of error, using the stabilized $\mathbb{P}^2_{\text{disc}} - \mathbb{P}^1_{disc}$ method with $\delta = 10^{-5}$ and $\beta = 10^{11}$.

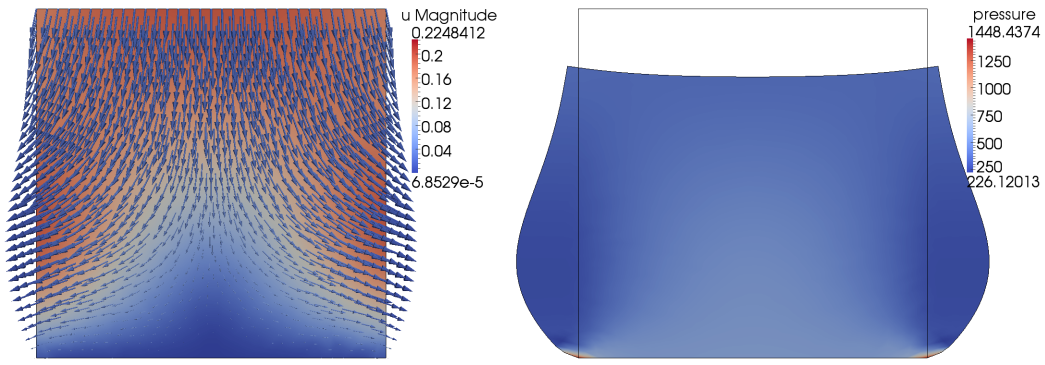

Figure 5.12: Test 2: Deformation field on the reference configuration (left) and pressure distribution on the corresponding deformed domain (right). Solution obtained using a stabilized $\mathbb{P}^2_{\text{disc}} - \mathbb{P}^1_{\text{disc}}$ method.

5.4 Test Problem 3: discontinuous active response of 2D neo-Hooeakean slab

We can also take account of discontinuous active response, that is, we image to divide the myocardium tissue with two part in which the behavior at the microscale is different: $\gamma_f = -0.3$ for $y > 0.5$ and $\gamma_f = -0.15$ otherwise. Let us notice that the discontinuity is take along fiber direction. With a mesh of 225 interior nodes, Taylor-Hood elements exhibit volumetric locking. The Figures 5.13 and 5.14 exhibit the performance of stabilized DG method proposed.

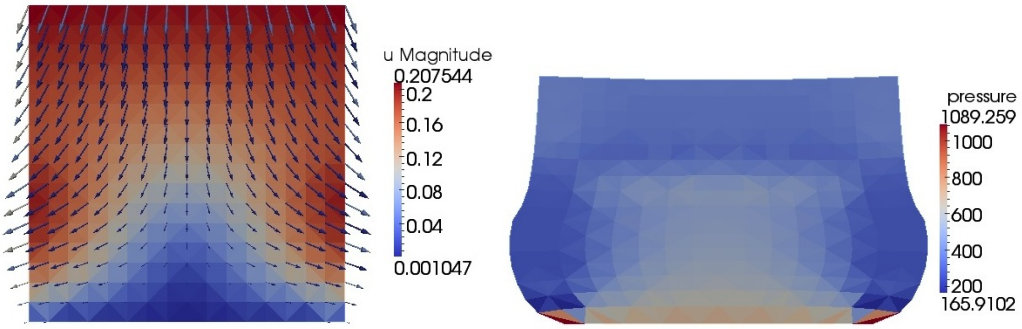

Figure 5.13: Deformation field on reference configuration (left) and pressure distribution on the corresponding deformed domain (right). Solution obtained on a uniform mesh of 512 elements, using a stabilized $\mathbb{P}^2_{\text{disc}} - \mathbb{P}^1$ method.

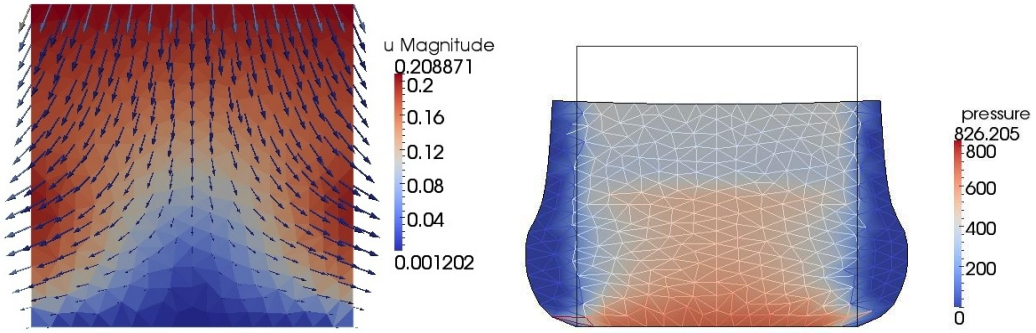

Figure 5.14: Deformation field on reference configuration (left) and pressure distribution on the corresponding deformed domain (right). Solution obtained on a uniform mesh of 512 elements, using a stabilized $\mathbb{P}^2_{\text{disc}} - \mathbb{P}^1_{disc}$ method.

5.5 Test Problem 4: discontinuous active parameter with smooth active response of 2D Neo-Hookean slab

Test 4 takes account of discontinuous active parameter with a smooth active response in the two regions $\gamma_f = -0.3 \exp -4(y - \frac{1}{2})$ for $y > 0.5$ and $\gamma_f = -0.15 \exp -4(y - \frac{1}{2})$ otherwise. Also in this test problem, with a mesh of 225 interior nodes, Taylor-Hood elements exhibit volumetric locking. The Figures 5.15 and 5.16 exhibit the "locking-free" propriety of the proposed stabilized DG method.

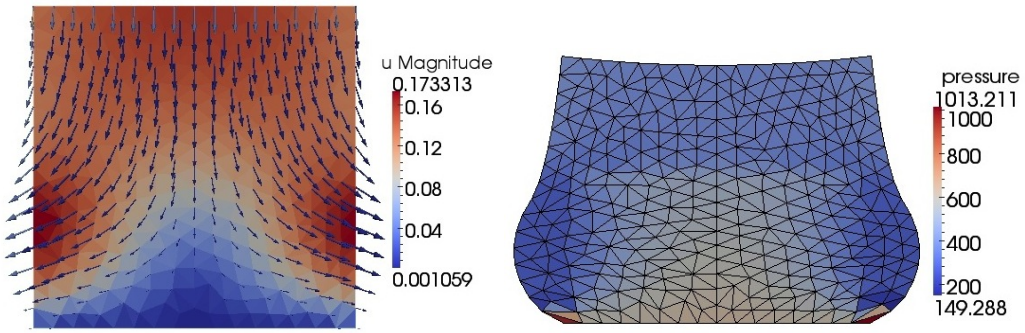

Figure 5.15: Deformation field on reference configuration (left) and pressure distribution on the corresponding deformed domain (right). Solution obtained on a uniform mesh of 512 elements, using a stabilized $\mathbb{P}^2_{\text{disc}} - \mathbb{P}^1$ method.

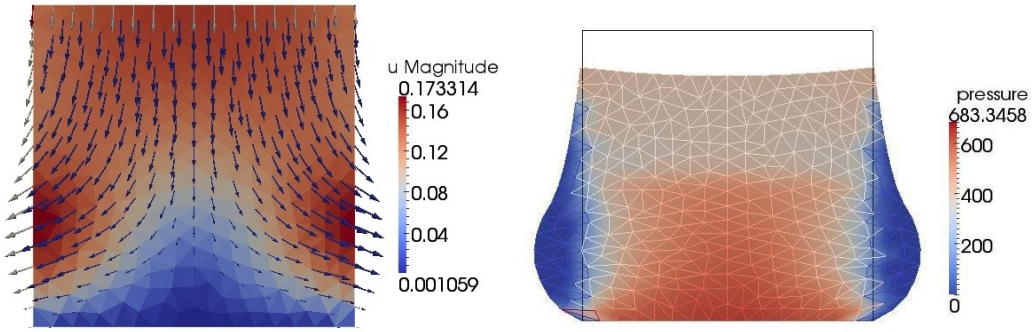

Figure 5.16: Deformation field on reference configuration (left) and pressure distribution on the corresponding deformed domain (right). Solution obtained on a uniform mesh of 512 elements, using a stabilized $\mathbb{P}^2_{\text{disc}} - \mathbb{P}^1_{disc}$ method.

5.6 Test problem 5: changing continuously of fiber and sheet direction at microscale

Next we consider the situation where sheets and fibers can change they direction continuously in the slab of tissue. The fibers and sheets are parametrized by:

$$\mathbf{f}_0^x = \begin{cases} \cos((1-y)\theta_{\max} + y\theta_{\min}) & x > 0 \\ -\cos((1-y)\theta_{\max} + y\theta_{\min}) & x \leq 0 \end{cases}$$

$$\mathbf{f}_0^y = \begin{cases} \sin((1-y)\theta_{\max} + y\theta_{\min}) & x > 0 \\ -\sin((1-y)\theta_{\max} + y\theta_{\min}) & x \leq 0 \end{cases}$$

$$\mathbf{s}_0^x = \begin{cases} -\sin((1-y)\theta_{\max} + y\theta_{\min}) & x > 0 \\ \sin((1-y)\theta_{\max} + y\theta_{\min}) & x \leq 0 \end{cases}$$

$$\mathbf{s}_0^y = \begin{cases} \cos((1-y)\theta_{\max} + y\theta_{\min}) & x > 0 \\ -\cos((1-y)\theta_{\max} + y\theta_{\min}) & x \leq 0 \end{cases}$$

In Figures 5.6 and 5.6 the values of parameters are $\theta_{max} = -\pi/2$ and $\theta_{min} = 0$. Let us notice again that with a mesh of 225 interior nodes, Taylor-Hood elements exhibit volumetric locking, instead the discontinuous stabilized Galerkin are locking-free as predicted in chapter 4.

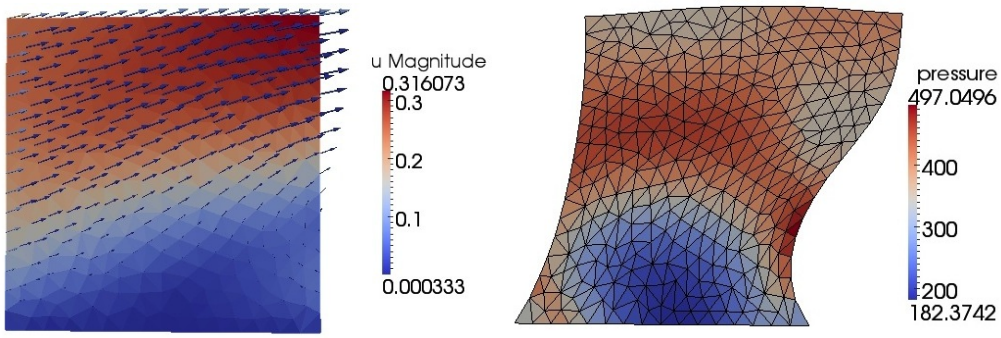

Figure 5.17: Test 5: Deformation field on reference configuration (left) and pressure distribution on the corresponding deformed domain (right). Solution obtained on a uniform mesh of 512 elements , using a stabilized $\mathbb{P}^2_{\text{disc}} - \mathbb{P}^1$

In the Figures 5.6 and 5.20 the values of parameters are $\theta_{max} = -\pi$ and $\theta_{min} = \pi/2$.

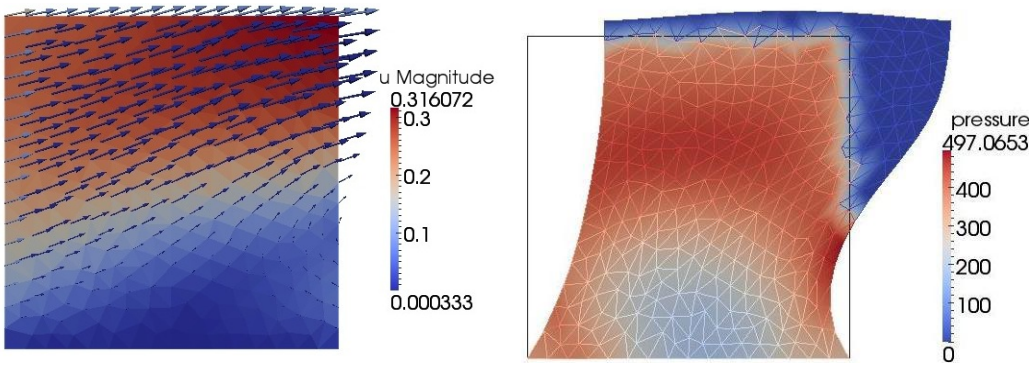

Figure 5.18: Test 5: Deformation field on reference configuration (left) and pressure distribution on the corresponding deformed domain (right). Solution obtained on a uniform mesh of 512 elements, using a stabilized $\mathbb{P}^2_{\text{disc}} - \mathbb{P}^1_{disc}$ method.

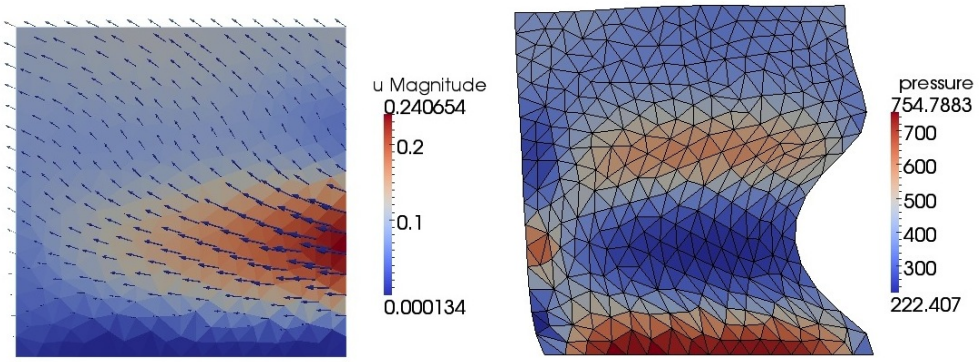

Figure 5.19: Deformation field on reference configuration (left) and pressure distribution on the corresponding deformed domain (right). Solution obtained on a uniform mesh of 512 elements, using a stabilized $\mathbb{P}^2_{\text{disc}} - \mathbb{P}^1$ method.

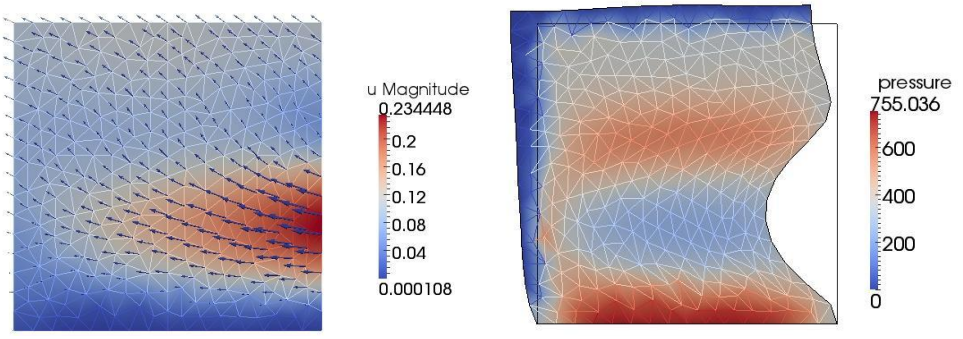

Figure 5.20: Deformation field on reference configuration (left) and pressure distribution on the corresponding deformed domain (right). Solution obtained on a uniform mesh of 512 elements, using a stabilized $\mathbb{P}^2_{\text{disc}} - \mathbb{P}^1_{disc}$ method.

5.7 Test problem 6: Active contraction in a cube

Finally we perform a 3D test involving an active Neo-Hookean 3D domain with elastic modulus $\mu = 400$ and fibers, sheets and transversal directions $\mathbf{f}_0 = (0, 0, 1)^T$, $\mathbf{s}_0 = (0, 1, 0)^T$, and $\mathbf{n}_0 = (-1, 0, 0)^T$, respectively. The mechanical activation is $\gamma_f = 0.3 \exp(-4[z - 0.35]^2)$. On the bottom of the unitary cube we assume $\boldsymbol{u} = \mathbf{0}$. The solution, corresponding to a volume-preserving contraction in the direction of $\mathbf{f}_0$, is plotted in Figure 5.21. Using continuous finite elements, we were not able to achieve convergence of the Newton method without using a homothopy (or incremental load) method, that is, starting with a small magnitude of γ_f (namely, $\gamma_f = -0.005 \exp(-4[z - 0.35]^2)$) and increasing it progressively until the desired value was achieved. With discontinuous formulations, we found that such strategy was no longer needed.

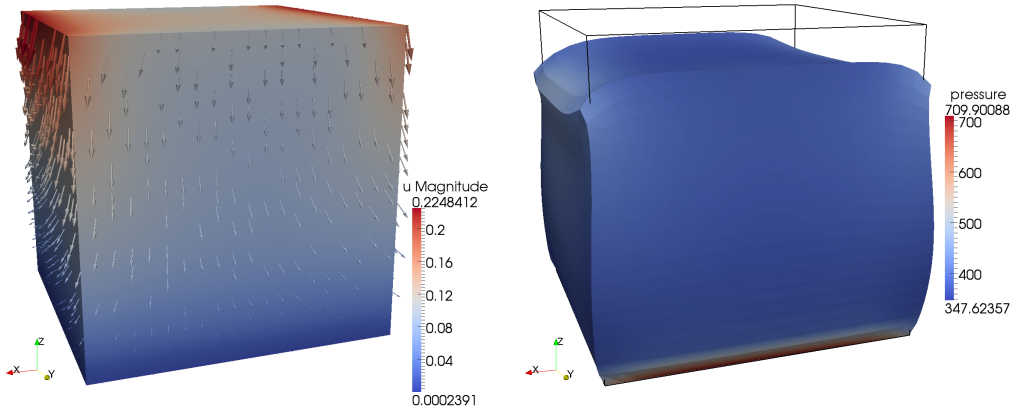

Figure 5.21: Test 6: Deformation field on the reference configuration (left) and pressure distribution on the corresponding deformed domain (right). Solution obtained using a stabilized $\mathbb{P}^2 - \mathbb{P}^1_{\text{disc}}$ method.

5.8 Details of implementation

In this section we give details on the implementation of numerical scheme proposed performed in the object-oriented open-source software FreeFem++ [43]. It is a high level integrated development environment for numerical solving differential equations. It is develop by F. Hecht and J. Morice in INRIA . The main characteristic of FreeFem++ are: writing the variational formulation of the problem in a friendly mathematical language, easy geometric input by analytic description of boundary pieces; automatic mesh generator, based Delaunay-Voronoi algorithm, inner point density is proportional to the density of points on the boundary, an integrated environment with medit for design 3D mesh; a large variety of triangular finite elements: linear and quadratic Lagrangian, discontinuous P1 and Raviart-Thomas elements, mini-elements; tool to define discontinuous Galerkin formulation via finite elements P0, P1dc, P2dc and keywords:jump,mean,intalledges; a large variety of linear direct and iterative solvers (LU, Cholesky, Crout, CG, GMRES, UMFPACK) and eigenvalue and eigenvector solvers. Moreover it offers a near optimal execution speed, online graphics, generation of .vtk, .dat,.txt,.eps, .mesh file for further manipulation of input and output data; a parallel version using mpi.

The postprocessing of results is carried out in Paraview and Matlab. Paraview [81] is an open-source, multi-platform data analysis and visualization application. We use the visualization capabilities of Paraview to inspect vectors fields, applying glyphs (arrows, cones, lines, spheres, and various 2D glyphs) to the points in a dataset. The glyphs can be scaled by scalars, vector component or vector magnitude and can be oriented using a vector field. Using Matlab, we display results of rate of convergence and pattern of sparsity of matrix.

5.8.1 FreeFem++ codes

At first, we load the package UMFPACK64, in order to solve the non-symmetric linearized system at each iteration in parallel version. The package iovtk is used to export deformation field, pressure, fiber and sheet alignment on the reference and on the deformed configuration in .vtk format for post-processing elaboration.

```
load "UMFPACK64";
load "iovtk";
```

The variational formulation of linearized nonlinear elasticity is implement using"macro" tool. A macro is like in ccp preprocessor of C++, but the syntax of macro in FreeFem++ begin by

```
macro
```

and the end of the macro definition is

```
//
```

for instance, we have the following definitions

```
// Active deformation tensor, depending on
// f0x,f0y (alignment of the fibers) and gam (activation function)
```

```
macro Fo11(gam1,gam2) (1+gam1*f0x^2+gam2*s0x^2) //
macro Fo12(gam1,gam2) (gam1*(f0x*f0y)+gam2*(s0x*s0y)) //
macro Fo21(gam1,gam2) (gam1*(f0y*f0x)+gam2*(s0y*s0x)) //
macro Fo22(gam1,gam2) (1+gam1*f0y^2+gam2*s0y^2) //

//  Determinant of the active deformation tensor
macro Jo(gam1,gam2) ((1+gam1)*(1+gam2))//

// Diffusion weight
macro JoCoinv11(gam1,gam2) Jo(gam1,gam2)
*(Fo22(gam1,gam2)^2+Fo12(gam1,gam2)^2)//
macro JoCoinv12(gam1,gam2) Jo(gam1,gam2)
*(-Fo22(gam1,gam2)*Fo21(gam1,gam2)-
Fo12(gam1,gam2)*Fo11(gam1,gam2)) //
macro JoCoinv21(gam1,gam2) Jo(gam1,gam2)
*(-Fo21(gam1,gam2)*Fo22(gam1,gam2)-
Fo12(gam1,gam2)*Fo11(gam1,gam2)) //
macro JoCoinv22(gam1,gam2) Jo(gam1,gam2)
*(Fo21(gam1,gam2)^2+Fo11(gam1,gam2)^2)//
```

Let us assign the physical parameter: elastic coefficient μ, fiber and sheet alignment, declaring the type of variables and applying assignements.

```
real mu = 400;//Elastic coefficient
real f0x = 0, f0y = 1, s0x=-1, s0y=0;
// Alignment of the fibers and sheets
real aminf=-pi/2, amaxf=0;
func f0x=cos((1-y)*amaxf+y*aminf)*(x>0)-cos((1-y)*amaxf+y*aminf)*(x<=0) ;
func f0y=sin((1-y)*amaxf+y*aminf)*(x>0)-sin((1-y)*amaxf+y*aminf)*(x<=0) ;
func s0x=-sin((1-y)*amaxf+y*aminf)*(x>0)+sin((1-y)*amaxf+y*aminf)*(x<=0);
func s0y=cos((1-y)*amaxf+y*aminf)*(x>0)-cos((1-y)*amaxf+y*aminf)*(x<=0);
```

For tests 1,2,3,4,5 we need to generate a square domain. FreeFem++ defines a domain as being on the left of its segments of a paramemetrized boundary, that only intersect at their end points. The `buildmesh` command joins the border. The variable `nps` indicate the number of point of each boundary. The mesh generate by $buildmesh$ is unstructured,instead the mesh generate by square with flag type 1 is a Union Jack flag type of mesh.

```
//Initial mesh
real doma=0, domb=1;
border Gamma1(t=doma,domb) {x=t; y=doma; label=1;}
border Gamma2(t=doma,domb) {x=domb; y=t; }
border Gamma3(t=doma,domb) {x=domb-t; y=domb; label=3;}
border Gamma4(t=doma,domb) {x=doma; y=domb-t; }
int nps=16;
mesh Th = square(nps,nps,flags=1);
```

For example 6 we generate a cube using medit and msh3 packages. Cube mesh function is defined in cube.ipd code:

```
load "medit"
load "msh3"
func mesh3 Cube(int[int] & NN,real[int,int] &BB ,int[int,int] & L)
{
// first build the 6 faces of the hex.
real x0=BB(0,0),x1=BB(0,1);
real y0=BB(1,0),y1=BB(1,1);
real z0=BB(2,0),z1=BB(2,1);
int nx=NN[0],ny=NN[1],nz=NN[2];
mesh Thx = square(nx,ny,[x0+(x1-x0)*x,y0+(y1-y0)*y],flags=3);
int[int] rup=[0,L(2,1)], rdown=[0,L(2,0)],
```

```
rmid=[1,L(1,0), 2,L(0,1), 3, L(1,1), 4, L(0,0) ];
mesh3 Th=buildlayers(Thx,nz, zbound=[z0,z1],
labelmid=rmid, labelup = rup,
labeldown = rdown);
return Th;
}
```

Let us generate the 3d mesh for test 6:

```
load "medit"
include "cube.idp"
int nps=8;
    int[int]  Nxyz=[8,8,8];
    real [int,int]  Bxyz=[[0,1],[0,1],[0,1]];
    int [int,int]  Lxyz=[[1,1],[1,1],[1,1]];
mesh3 Th=Cube(Nxyz,Bxyz,Lxyz);
```

We fix the parameter $dparm[0]$ of tolerance for the convergence of UMFPACK64, that is an unsymmetric-pattern multifrontal method for sparse LU factorization.

```
real[int] dparm(6);
dparm[0]=1e-20;
```

Let define the finite element space for position and pressure: P2dc piecewise P2 discontinuous finite element (2d, the 3d version is P2dc3d), P1dc piecewise linear discontinuous finite element and P1 piecewise linear continuous finite element(2d,3d):

```
fespace Vh(Th,P2dc);
fespace Ph(Th,P1dc);
Vh  phi, xc1=x, xc2=y, phi1, phi2, xc1k, xc2k, varxc1, varxc2;
Ph  p, pk, varp, q;
```

Let us define the activation parameter functions γ_f and γ_s for tests proposed in previuous sections:

```
func salto= 1.0*(y<0.5)+0.5*(y>=0.5) ;
Vh gam1=-0.3*salto;
Vh gam2=-gam1/(1.0+gam1);
```

Let us fixing the stabilization parameters and analytical solution for first test:

```
real beta=1e+12; alpha=1e-1; b=1.0; a=0.5;
func solex=b*x+a*y^2/2; dxsolex=b; dysolex=a*y; solex2=y/b;
func dxsolex2=0; dysolex2=1/b; pressure=mu*b*a*(1+gam1*f0y^2+gam2*s0y^2)^2
/Jo(gam1,gam2)*(x+a/b*0.5*y^2);
```

Let us initialize the Th2 mesh.

```
mesh Th2 = movemesh(Th, [solex, solex2]);
```

Now using macro tool define above, we define variational formualtion and impose sparse solver .

```
problem pureMechanic([varxc1, varxc2, varp],[phi1, phi2, q]
,solver=sparsesolver) =

int2d(Th)(
    mu * (
  (Grad11(varxc1,varxc2)*JoCoinv11(gam1,gam2)
   +Grad12(varxc1,varxc2)*JoCoinv21(gam1,gam2))*Grad11(phi1,phi2) +
  (Grad11(varxc1,varxc2)*JoCoinv12(gam1,gam2)
   +Grad12(varxc1,varxc2)*JoCoinv22(gam1,gam2))*Grad12(phi1,phi2) +
```

```
   (Grad21(varxc1,varxc2)*JoCoinv11(gam1,gam2)
    +Grad22(varxc1,varxc2)*JoCoinv21(gam1,gam2))*Grad21(phi1,phi2) +
   (Grad21(varxc1,varxc2)*JoCoinv12(gam1,gam2)
    +Grad22(varxc1,varxc2)*JoCoinv22(gam1,gam2))*Grad22(phi1,phi2))
     )

+int2d(Th)(pk*J(xc1k,xc2k)*(GradinvGrad11(xc1k,xc2k,varxc1,varxc2)
\ *GradinvGrad11(xc1k,xc2k,phi1,phi2)
    +GradinvGrad21(xc1k,xc2k,varxc1,varxc2)
*GradinvGrad12(xc1k,xc2k,phi1,phi2)
    +GradinvGrad12(xc1k,xc2k,varxc1,varxc2)
*GradinvGrad21(xc1k,xc2k,phi1,phi2)
   +GradinvGrad22(xc1k,xc2k,varxc1,varxc2)
*GradinvGrad22(xc1k,xc2k,phi1,phi2))
      )

-int2d(Th)(varp * J(xc1k,xc2k)*(
     GradinvT11(xc1k,xc2k)*Grad11(phi1,phi2)
     +GradinvT12(xc1k,xc2k)*Grad12(phi1,phi2)
     +GradinvT21(xc1k,xc2k)*Grad21(phi1,phi2)
     +GradinvT22(xc1k,xc2k)*Grad22(phi1,phi2)))

-int2d(Th)(q * (J(xc1k,xc2k) +(1-J(xc1k,xc2k))/J(xc1k,xc2k))
      *(GradinvT11(xc1k,xc2k)*Grad11(varxc1,varxc2)
       +GradinvT12(xc1k,xc2k)*Grad12(varxc1,varxc2)
       +GradinvT21(xc1k,xc2k)*Grad21(varxc1,varxc2)
       +GradinvT22(xc1k,xc2k)*Grad22(varxc1,varxc2)))

// internal residual
+int2d(Th)(mu *((Grad11(xc1k,xc2k)*JoCoinv11(gam1,gam2)
+Grad12(xc1k,xc2k)*JoCoinv21(gam1,gam2))
*Grad11(phi1,phi2) +
    (Grad11(xc1k,xc2k)*JoCoinv12(gam1,gam2)
+Grad12(xc1k,xc2k)*JoCoinv22(gam1,gam2))
*Grad12(phi1,phi2) +
    (Grad21(xc1k,xc2k)*JoCoinv11(gam1,gam2)
+Grad22(xc1k,xc2k)*JoCoinv21(gam1,gam2))
*Grad21(phi1,phi2) +
    (Grad21(xc1k,xc2k)*JoCoinv12(gam1,gam2)
+Grad22(xc1k,xc2k)*JoCoinv22(gam1,gam2))
*Grad22(phi1,phi2)))

-int2d(Th)(pk * J(xc1k,xc2k)*(
GradinvT11(xc1k,xc2k)*Grad11(phi1,phi2)
+GradinvT12(xc1k,xc2k)*Grad12(phi1,phi2)+
GradinvT21(xc1k,xc2k)*Grad21(phi1,phi2)
+GradinvT22(xc1k,xc2k)*Grad22(phi1,phi2)))

+int2d(Th)((1-J(xc1k,xc2k))*q)

-intalledges(Th)((nTonEdge-1)* mu * (
mean((Grad11(varxc1,varxc2)*JoCoinv11(gam1,gam2)
+Grad12(varxc1,varxc2)*JoCoinv21(gam1,gam2))*N.x  +
(Grad11(varxc1,varxc2)*JoCoinv12(gam1,gam2)
+Grad12(varxc1,varxc2)*JoCoinv22(gam1,gam2))*N.y)*jump(phi1) +
 mean((Grad21(varxc1,varxc2)*JoCoinv11(gam1,gam2)
+Grad22(varxc1,varxc2)*JoCoinv21(gam1,gam2))*N.x +
   (Grad21(varxc1,varxc2)*JoCoinv12(gam1,gam2)
  +Grad22(varxc1,varxc2)*JoCoinv22(gam1,gam2))*N.y)*jump(phi2)))

-intalledges(Th)(s*(nTonEdge-1)*
jump(varxc1)*mean( (JoCoinv11(gam1,gam2)*Grad11(phi1,phi2)
+ JoCoinv21(gam1,gam2)*Grad21(phi1,phi2))*N.x+
(JoCoinv11(gam1,gam2)*Grad12(phi1,phi2)
+ JoCoinv21(gam1,gam2)*Grad22(phi1,phi2))*N.y)
   +jump(varxc2)*mean( (JoCoinv12(gam1,gam2)*Grad11(phi1,phi2)
+ JoCoinv22(gam1,gam2)*Grad21(phi1,phi2))*N.x+
  (JoCoinv12(gam1,gam2)*Grad12(phi1,phi2)+
```

```
 JoCoinv22(gam1,gam2)*Grad22(phi1,phi2))*N.y) )

+intalledges(Th)((nTonEdge-1)*
(mean( varp * J(xc1k,xc2k)*(GradinvT11(xc1k,xc2k)*N.x+
    +GradinvT12(xc1k,xc2k)*N.y))*jump(phi1)+
 mean(  varp * J(xc1k,xc2k)*(GradinvT21(xc1k,xc2k)*N.x+
    +GradinvT22(xc1k,xc2k)*N.y))*jump(phi2)))

+intalledges(Th)((nTonEdge-1)*(mean
        ( q * (J(xc1k,xc2k)+(1-J(xc1k,xc2k))/J(xc1k,xc2k))
*(GradinvT11(xc1k,xc2k)*N.x+
    +GradinvT12(xc1k,xc2k)*N.y))*jump(varxc1)+
    mean(q * (J(xc1k,xc2k)+(1-J(xc1k,xc2k))/J(xc1k,xc2k))
*(GradinvT21(xc1k,xc2k)*N.x+
    +GradinvT22(xc1k,xc2k)*N.y))*jump(varxc2)))

+intalledges(Th)((nTonEdge-1)*((alpha*lenEdge)*jump(varp) * jump(q) ))

-intalledges(Th)((nTonEdge-1)* (
 mean(J(xc1k,xc2k)*pk*( GradinvGrad11(xc1k,xc2k,varxc1,varxc2)
+ GradinvGrad21(xc1k,xc2k,varxc1,varxc2) ))
  *(jump(Gradinv11(xc1k,xc2k)*phi1)+jump(Gradinv12(xc1k,xc2k)*phi2))
+mean(J(xc1k,xc2k)*pk*( GradinvGrad12(xc1k,xc2k,varxc1,varxc2)*N.x
+ GradinvGrad22(xc1k,xc2k,varxc1,varxc2)*N.y ))
*jump(Gradinv21(xc1k,xc2k)*phi1+Gradinv22(xc1k,xc2k)*phi2) ))

-int1d(Th,1)(mu * (
  ((Grad11(varxc1,varxc2)*JoCoinv11(gam1,gam2)
   +Grad12(varxc1,varxc2)*JoCoinv21(gam1,gam2))*N.x +
  (Grad11(varxc1,varxc2)*JoCoinv12(gam1,gam2)
   +Grad12(varxc1,varxc2)*JoCoinv22(gam1,gam2))*N.y)*phi1 +
   ((Grad21(varxc1,varxc2)*JoCoinv11(gam1,gam2)
    +Grad22(varxc1,varxc2)*JoCoinv21(gam1,gam2))*N.x +
   (Grad21(varxc1,varxc2)*JoCoinv12(gam1,gam2)
    +Grad22(varxc1,varxc2)*JoCoinv22(gam1,gam2))*N.y)*phi2))

-  int1d(Th,1)(s*varxc1*( (JoCoinv11(gam1,gam2)*Grad11(phi1,phi2)
+ JoCoinv21(gam1,gam2)*Grad21(phi1,phi2))*N.x+
    (JoCoinv11(gam1,gam2)*Grad12(phi1,phi2)
+ JoCoinv21(gam1,gam2)*Grad22(phi1,phi2))*N.y)
    +varxc2*( (JoCoinv12(gam1,gam2)*Grad11(phi1,phi2)
+ JoCoinv22(gam1,gam2)*Grad21(phi1,phi2))*N.x+
   (JoCoinv12(gam1,gam2)*Grad12(phi1,phi2)+
  JoCoinv22(gam1,gam2)*Grad22(phi1,phi2))*N.y))

 -int1d(Th,1)((4*beta/lenEdge)*((JoCoinv11(gam1,gam2)
+JoCoinv21(gam1,gam2))*(varxc1)*(phi1)
 +(JoCoinv12(gam1,gam2)+JoCoinv22(gam1,gam2))*(varxc2)*(phi2)))

-int1d(Th,2,3,4)(((mu/Jo(gam1,gam2)*b
*(1+gam1*f0y^2+gam2*s0y^2)^2-pressure/b)*N.x
+mu/Jo(gam1,gam2)*a*y*(1+gam1*f0y^2+gam2*s0y^2)^2*N.y)*phi1)
  -int1d(Th,2,3,4)((pressure*a*y*N.x
+(mu/Jo(gam1,gam2)/b*(1+gam1*f0x^2+gam2*s0x^2)^2-pressure*b)*N.y)*phi2);
```

We define the tollerance, loopmax, loopcount, residual and initial step of position and pressure for Newton's algorithm:

```
//------ Newton step
// Tolerance for Newton
real tol = 1.e-7; int loopmax = 40; xc1k = x; xc2k = y; pk=0.0;
real res = 2.0 * tol; int loopcount = 0;

while (loopcount <= loopmax && res > tol)
{
loopcount ++;
```

```
pureMechanic;
xc1 = xc1k + varxc1; xc2 = xc2k + varxc2;
p = pk + varp;
res=Energynormpressure+errorenerpos;
mesh Th2 = movemesh(Th, [xc1, xc2]);
real volum=Th2.area;
fespace Kh(Th,P0); Kh h = hTriangle;
real minarea=checkmovemesh(Th,[xc1, xc2]);
if(minarea>0 && res<tol) {
  mesh Th1 = movemesh(Th, [xc1, xc2]);
  plot(Th2,Th1,fill=1,value=0,wait=1);
  savevtk("P2dcP1c_vtk/"+ save+".vtk", Th, p,
          [f0x,f0y],[s0x,s0y], [xc1-x, xc2-y,0], dataname="pressure fiber sheet u");
  savevtk("P2dcP1c_vtk/"+ save+"deformedconfiguration.vtk", Th1, p
,[f0x,f0y],[s0x,s0y], [xc1-x, xc2-y,0], dataname="pressure fiber sheet u");}
if(minarea<=0 && res<tol){
  break;}
xc1k=xc1; xc2k=xc2; pk=p;
}
```

Using savevtk we export data on reference and deformed configuration in .vtk format:

```
 savevtk("disc_cont.vtk", Th, p,[f0x,f0y],[s0x,s0y],
 [xc1-x, xc2-y,0], dataname="pressure fiber sheet u");
 savevtk("disc_cont_deformed.vtk", Th2, p,[f0x,f0y],
[s0x,s0y], [xc1-x, xc2-y,0], dataname="pressure fiber sheet u");
```

In order to elaborate the sparsity of pattern, we define with `varf` the variational form associated to the matrix of the system, then define the matrix associated and export it in `.dat` format in order to postprocess with Matlab.

```
fespace Rh(Th,[P2dc,P2dc,P1dc]);
 matrix cx=Complete(Rh,Rh);
 {
  ofstream file("test_complete.dat");
  file << cx <<endl;
  }
```

With Matlab, we import .dat format, using the command `spconvert` we create sparse matrices from a simple sparse format easily produced by other sparse programs. Finally using spy command we visualize sparsity pattern of matrix.

Chapter 6

Conclusion and perspectives

In this Chapter, we critically analyze the novel results presented and describe a few possible perspectives.

In the second Chapter of this thesis, we have focused in the biophysical modeling of active deformations in soft biological tissues, which under some assumptions, can be considered as hyperelastic materials. We have exposed the state of art of the passive modeling of living materials and the study of anisotropic living materials such as heart tissue, which presents the ability of actively deform without need of external loads. In a simplified model, we have assumed that the passive behavior of the living tissue can be described by a Neo-Hookean constitutive law, whereas the active contribution is encoded in some additional terms appearing after applying a so-called active strain decomposition.

In the third Chapter, we have derived the linearization of elastostatic system and analyzed of its solvability and its stability to ensure the convergence of numerical scheme to solution of nonlinear elasticity problem.

In the fourth Chapter, we have presented the novel contributiionn of the thesis, which lies in convergence study of interior penalty DG formulation for nonlinear incompressible elastic materials, in particular for Neo-Hookean material. The deformation and pressure field are discretized with piecewise polynomials of maximal degree k and $k-1$, respectively. The error analysis we have carried out shows that the approximate deformations in the energy norm, and pressure in the L^2-norm, converge with optimal order $\mathcal{O}(h^k)$ and $\mathcal{O}(h^{k+1})$, respectively. Moreover we have proved the locking-free property of the scheme and estimated the dependence on active parameter of the model in the displacement error.

In the fifth Chapter we have validated the convergence estimate of chapter 4. Moreover we have set different tests on active contraction in a 2D slab and in a cube to evaluate the robustness of numerical scheme. In particular in test problems 2,3,4 and 5 the stabilized discontinuous Galerkin method exhibits a locking-free behavior, as expected from the discussion in Chapter 4. Instead, the Taylor-Hood discretization shows volumetric locking, in which the displacement decreases severely in a non-physical fashion. In test 6 we have stressed that using continuous finite element we were not able to achieve convergence of the Newton method without using an homotopy argument (incremental load method), whereas discontinuous formulations do not need any kind of incremental load technique and the deformations are well resolved at a reasonable computational cost.

As possible extensions of the work here presented we envisage the study of cardiac fluid structure interaction phenomena from both the modelling and numerical viewpoints. The emphasis in this topic is to understand which physical factors are affected in pathological situations, such as ischaemic events. Here a special interest is also the use of sophisticated time advancing techniques that would allow certain reduction in computational effort while still capturing the main features of the phenomenon. Moreover, we plan to extend the treatment for simulating the electro-mechanical interaction in cardiac tissue. While the underlying coupling mechanisms are straightforward, it is much more difficult to translate this energy exchange to cardiac output, a source of major physiological and clinical interest. Answering questions on the functional behavior of the heart requires a detailed knowledge of cardiac mechanics. In this sense, coupled mathematical models of fluid/solid mechanics provide an important foundation for in silico investigation.

In addition we plan to include a convergence analysis for a discontinuous Galerkin formulation applied to the Holzapfel-Ogden passive model, which we have described in second chapter. We are also interested in the design of robust preconditioners to speed-up the solution of the involved nonsymmetric mixed formulations. A second goal in this respect would be to use different constitutive laws for different layers of the cardiac muscle (endocardium, myocardium and epicardium), which calls for appropriate coupling techniques to ”glue together” models with variable mechanical properties (thickness, conductivities, elastic moduli) across the muscle wall.

Finally we are interested in the implementation of the stabilized discontinuous Galerkin schemes described in Chapter 4 in a parallel code to optimize the computational cost required. We need to be able to benefit from the growing computer power and the development of efficient and scalable algorithms, in order to perform real-time simulations with multiscale models of cardiac mechanics and electromechanics. In this regard, a very important aspect consists in the development of efficient parallel algorithms and we plan to carry out this task using LifeV, a parallel finite element library which was originally initiated by the CMCS group at the EPFL, the MOX Laboratory at the Politecnico di Milano, and INRIA (REO project) in 1999/2000 (see http://www.lifev.org).

Acknowledgments

It is a great pleasure to thank my supervisor, Prof. Alfio Quarteroni, for having offered me the opportunity of coming to the EPFL (CSCM), working on an exciting master's thesis project and giving me the possibility to take part to seminars and workshops, that enrich my scientific knowledge.

A very special thanks goes out to Prof. Giorgio Mantica, who motivates and encourages me to consider a master project.
I truly appreciated the amount of time and energy that Dr.Ric. Ricardo Ruiz-Baier invested in guiding me throughout this work, his support in the most critical moments, the many enriching scientific discussions and the patience he showed while I am writing this thesis.
In addition, I would like to extend my gratitude to all the member of Prof. Quarteroni's team who contribute in making the CSCM such a stimulating, lively and friendly place.

I am especially grateful to all Professors and students of department of physics and mathematics of Insubria for making the interesting life in Insubria University.
I wish to thank my friend Antoine for stimulating conversations and I hope that his dream will be realized.

I am indebted to both Prof. Giorgio Mantica and Prof. Vincenzo Pennati that provided me with direction, scientific riflections and became more of mentors and friends, than professors.

Thank friends Filippo, Davide and Cristina for continuous encouragement and good episode of life passed together.

Lastly, my family without whose support none of this would have been possible.

Bibliography

[1] B. Alberts, D. Bray, J. Lewis, M. Raff, K. Roberts and J.D. Watson, *Molecular Biology of the Cell*, 3rd ed. 1994; Garland Publishing, New York.

[2] D. Ambrosi, G. Arioli, F. Nobile and A. Quarteroni, Electromechanical coupling in cardiac dynamics: The active strain approach. *SIAM Journal of Applied Mathematics*, 2011; **71**:605–621.

[3] D. Ambrosi and S. Pezzuto, Active stress vs. active strain in mechanobiology: Constitutive issues. *Journal of Elasticity*, to appear.

[4] D. N. Arnold, F. Brezzi, B. Cockburn and L. D. Marini, Unified analysis of discontinuous Galerkin methods for elliptic problems. *SIAM Journal of Numerical Analysis*, 2002; **39**:1749–1779.

[5] F. Auricchio, L. Beirão da Veiga, C. Lovadina and A. Reali, A stability study of some mixed finite element for large deformation elasticity problem. *Computer Methods in Applied Mechanics and Engineering*, 2005; **194**:1075–1092.

[6] F. Auricchio, L. Beirão da Veiga, C. Lovadina and A. Reali, The importance of the exact satisfaction of the incompressibility constraint in nonlinear elasticity: mixed FEMs versus NURBS-based approximations. *Computer Methods in Applied Mechanics and Engineering*, 2010; **199**:314-323.

[7] I. Babuška and M. Suri, Locking effects in the finite element approximation of elasticity problems. *Numerische Mathematik*, 1992; **62**:439–463.

[8] J.M. Ball, Convexity conditions and existence theorems in nonlinear elasticity. *Archive for rational mechanics and analysis*, 1977; **63**(4):337–403.

[9] F. Bassi and S. Rebay, A higher order accurate discontinuous Galerkin finite element method for the numerical solution of the compressible Navier-Stokes equations. *Journal of Computational Physics*, 1997; **131**:267–279.

[10] J.E. Bischoff, E.M. Arruda and K. Grosh, A microstructurally based orthotropic hyperelastic constitutive law. *Journal of Applied Mechanics*, 2002; **69**:570–579.

[11] J. Botsis and M. Deville, *Mécanique des milieux continus: Une introduction*. Presses Polytechniques et Universitaires Romandes, 2006.

[12] D. Braess and P. Ming, A finite element method for nearly incompressible elasticity problems. *Mathematics of Computation*, 2005; **74**:25–52.

[13] S.C. Brenner, Korn's inequalities for piecewise H^1 vector fields. *Mathematics of Computation*, 2004; **73**(247):1067–1087.

[14] F. Brezzi and M. Fortin, *Mixed and Hybrid Finite Element Methods*. Springer-Verlag, New York, 1991.

[15] A. Buffa and C. Ortner, Compact embeddings of broken Sobolev spaces and applications. *IMA Journal of Numerical Analysis*, 2009; **29**:827–855.

[16] P.G. Ciarlet, *Mathematical Elasticity, Vol. I : Three-Dimensional Elasticity*, Series Studies in Mathematics and its Applications, North-Holland, Amsterdam, 1988.

[17] P.G. Ciarlet and C. Mardare, An introduction to shell theory. In Differential Geometry: Theory and Applications (P.G. CIARLET and Ta-Tsien LI, Editors), pp. 94–184, Series in Contemporary Mathematics, Vol.9, World Scientific, Singapore, 2008.

[18] C. Cherubini, S. Filippi, P. Nardinocchi and L. Teresi, An electromechanical model of cardiac tissue: Constitutive issues and electrophysiological effects. *Progresses in Biophysics and Molecular Biology*, 2008; **97**:562–573.

[19] B. Cockburn, G.E. Karniadakis, C.W. Shu, eds. *Discontinuous Galerkin Methods. Theory, Computation and Applications*, vol. 11 Springer-Verlag, 2000.

[20] K.D. Costa. The structural basis of three-dimensional ventricular mechanics. Ph.D. thesis, University of California, La Jolla, California, 1996.

[21] K.D. Costa, J.W. Holmes and A. McCulloch, Modelling cardiac mechanical properties in three dimensions. *Philosophical Transactions of the Royal Society of London. Series A*, 2001; **359**:1233–1250.

[22] H. Demiray, Stresses in ventricular wall. *Journal of Applied Mechanics*, 1976; **98**:194–197.

[23] A. Di Carlo, S. Quiligotti, Growth and balance. *Mech. Res. Comm.*, 2002; **29**:449–456.

[24] D.A. Di Pietro, Analysis of a discontinuous Galerkin approximation of the stokes problem based on an article compressibility flux. *International Journal for Numerical Methods in Fluids*, 2007; **55**:793–813.

[25] D.A. Di Pietro and A. Ern, Discrete functional analysis tools for discontinuous Galerkin methods with application to the incompressible Navier-stokes equation. *Mathematics of Computation*, 2010; **79**(271):1303–1330.

[26] S. Dokos, B.H. Smaill, A.A. Young and I.J. LeGrice, Shear proprieties of passive myocardium. *American Journal of Physiology. Heart and Circulatory Physiology*, 2002; **283**:H2650–H2659.

[27] J.M. Dowey, *The Mechanical Activity of the Heart, Essential Medical Physiology*, 3rd edition by L. Johnson, 2004; Chapter 13, Elsevier Science.

[28] A. Ern and J.-L. Guermond, *Theory and Practice of Finite Elements*. Appl. Math. Ser. 159, Springer-Verlag, 2004.

[29] S. Federico, A. Grillo, G. Giaquinta and W. Herzog, Convex Fung-type potentials for biological tissues. *Meccanica*, 2008; **43**(3):279–288.

[30] M.R. Franz, R. Cima, R. Wang, D. Profitt and R. Kurz, Electrophysiological effects of myocardial stretch and mechanical determinants of stretch-activated arrythmia. *Circulation Research*, 1992; **86**:968–978.

[31] I. Fonseca and J. Maly, Remarks on the determinant in nonlinear elasticity and fracture mechanics. *Applied Nonlinear Analysis*, 2002; **26**(49):117–132.

[32] R. FitzHugh, Impulses and physiological states in theoretical models of nerve membrane. *Biophysical Journal*, 1961; **1**:445–466.

[33] J.F. Gerbeau and C. Farhat, *The finite element method for fluid mechanics*, Springer-Verlag 2009.

[34] Y.C. Fung, Biorheology of soft tissue. *Biorheology*, 1973; **10**:139–155.

[35] Y.C. Fung, K. Fronek and P. Paticucci, Pseudoelasticity of arteries and the choice of its mathematical expression. *American Journal of Physiology*, 1979; **237**:H620–631.

[36] Y.C. Fung, *Biomechanics: mechanical properties of living tissue*, 2nd Edition, Springer-Verlag, New York, 1993.

[37] V. Girault and P.A. Raviart, *Finite element methods for Navier-Stokes equations*, Springer-Verlag, Paris, 1986.

[38] S. Göktepe, S.N.S. Acharya, J. Wong and E. Kuhl, Computational modeling of passive myocardium. *International Journal for Numerical Methods in Biomedical Engineering*, 2011; **27**:1–12.

[39] S. Göktepe and E. Kuhl, Computational modelling of cardiac electrophysiology: A novel finite element approach *International Journal for Numerical Methods in Biomedical Engineering*, 2009; **79**:156–178.

[40] J.M. Guccione, A.D. McCulloch and L.K. Waldman, Passive material proprieties of intact ventricular myocardium determined from cylindrical model, *Journal of Biomechanical Engineering*, 1991; **113**:42–55.

[41] V. Gurev, T. Lee, J. Constantino, H. Arevalo and N.A. Trayanova, Models of cardiac electromechanics based on individual hearts imaging data. *Biomechanics and Modeling in Mechanobiology*, 2011; **10**:295–306.

[42] P. Hansbo and M.G. Larson, Discontinuous Galerkin methods for incompressible and nearly incompressible elasticity by Nitsche's method. *Computer Methods in Applied Mechanics and Engineering*, 2002; **191**:3669–3750.

[43] F. Hecht, O.Pironneau, Freefem++: Manual.*http://www.freefem.org*, Paris,2002.

[44] G. Holzapfel and R.W. Ogden, Constitutive modelling of passive myocardium: a structurally based framework for material characterization. *Philosophical Transactions of the Royal Society of London. Series A*, 2009; **367**:3445–3475.

[45] A.L. Hodgkin and A.F. Huxley, A quantitative description of membrane current and its application to conduction and excitation in nerve. *Journal of Physiology*, 1952; **117**:500-544.

[46] J.D. Humphrey and F.C. Yin, On constitutive relations and finite deformations of passive cardiac tissue. Part I. A pseudo-strain energy function. *Journal of Biomechanical Engineering*, 1987; **109**:298–304.

[47] J.D. Humphrey, R.K. Strumpf and F.C. Yin, Determination of constitutive relation for passive myocardium. I. A new functional form. *Journal of Biomechanical Engineering*, 1990; **112**:333-339.

[48] J.D. Humphrey, *Cardiovascular Solid Mechanics*, Springer-Verlag, Berlin, 2002.

[49] P.J. Hunter, M.P. Nash and G.B. Sands, Computational electromechanics of the heart. *Computational biology of the heart*, 1996; eds A.V. Panfilov and A.V. Holden, pp 345–401. Chichester, UK; Wiley.

[50] J.M.R.J. Huyghe, D.H. van Campen, T. Arts and R.M. Heethaar, The constitutive behaviour of passive heart muscle tissue: a quasi-linear viscoelastic formulation. *Journal of Biomechanics*, 1991; **24**(9):841–849.

[51] M. Itskov, A.E. Ehret and D. Mavrilas, A polyconvex anisotropic strain-energy function for soft collagenous tissues. *Biomechanics and Modeling in Mechanobiology*, 2006; **5**:17–26.

[52] R.C.P. Kerckhoffs, P.H.M. Bovendeerd, J.C.S Kotte, K. Smith and T. Arts, Homogeneity of cardiac contraction despite physiological asynchrony of depolarization: a model study. *Annals of Biomedical Engineering*, 2003; **31**:536–547.

[53] R.C.P. Kerckhoffs, S.N. Healy, T.P. Usyk, A.D. McCulloch, Computational methods for cardiac electromechanics. *Proceedings of the IEEE*, 2006; **94**:769–783.

[54] P. Kohl and U. Ravens, Cardiac mechano-electric feedback: past, present, and prospect. *Progresses in Biophysics and Molecular Biology*, 2003; **82**:3–9.

[55] P. Kohl and F. Sachs, Mechanoelectric feedback in cardiac cells. *Philosophical Transactions of the Royal Society of London. Series A*, 2001; **359**:1173–1185.

[56] E. Kröner, Allgemeine Kontinuumstheorie der Versetzungen und Eigenspannungen, *Archive for Rational Mechanics and Analysis*, 1959; **4**(1):273–334.

[57] M.J. Lab, Contraction-excitation feedback in myocardium, physiological basis and clinical relevance. *Circulation Research*, 1982; **50**:757–766.

[58] B.P. Lamichhane, A mixed finite element method for non-linear and nearly incompressible elasticity based on biorthogonal systems. *International Journal for Numerical Methods in Engineering*, 2009; **79**:870–886.

[59] E.H. Lee, Elastic and plastic deformation at finite strain. *ASME Journal of Applied Mechanics*, 1969; **36**:1956–1969.

[60] I.J. LeGrice, B.H. Smaill, L.Z. Chai, S.G. Edgar, J.B. Gavin and P.J. Hunter. Laminar structure of heart: ventricular myocytes arrangement and constitutive tissue architecture in the dog.*American Journal of Physiology. Heart and Circulatory Physiology*, 2003; **269**:H571–H582.

[61] I.J. LeGrice, P. Hunter, A. Young and B.H. Smaill, The architecture of the heart: a data-based model. *Philosophical Transactions of the Royal Society of London. Series A*, 2001; **359**:1217–1232.

[62] P. LeTallec, Existence and approximation results for nonlinear mixed problems: Application to incompressible finite elasticity. *Numerische Mathematik*, 1982; **38**:365–382.

[63] P. LeTallec and J.T. Oden, Existence and characterization of hydrostatic pressure in finite deformations of incompressible elastic bodies. *Journal of Elasticity*, 1981; **11**:341–357.

[64] A. Lew, P. Neff, D. Sulsky and M. Ortiz, Optimal BV estimate for a discontinuous Galerkin method for linear elasticity. *Applied Mathematics Research eXpress*, 2004; **3**:73–104.

[65] D.A. MacKenna, J.H. Omens and J.W. Covell, Left ventricular perimysial collagen fibers uncoil rather than stretch during diastolic filling. *Basic Research in Cardiology*, 1994; **91**:111–122.

[66] J.E. Marsden and T.J.R. Hughes, *Mathematical foundations of elasticity*. Courier Dover Publications, 1994.

[67] A.D. McCulloch, *Cardiac Biomechanics*. Chapter 31: 418–439, Section III in: The Biomedical Engineering Handbook, Bronzino JD (Ed.) CRC Press, Boca Raton, FL, 1995.

[68] J. Merodio and R.W. Ogden, The influence of the invariant I_8 on the stress-deformation and ellipticity characteristics of doubly fiber-reinforced non-linearly elastic solids. *International Journal of Nonlinear Mechanics*, 2006; **41**(4):556–563.

[69] C.B. Morrey, Quasi-convexity and the semi-continuity of multiple integrals. *Pacific J. Math.*, 1952; **2**:25–53.

[70] J.S. Nagumo, S. Arimoto and S. Yoshizawa, An active pulse transmission lien simulating nerve axon. *Proc. I.R.E.*, 1962; **50**:2061-2071.

[71] P. Nardinocchi and L. Teresi, On the active response of soft living tissues. *Journal of Elasticity*, 2007; **88**:27–39.

[72] M.P. Nash, Mechanical and material proprieties of the heart using an anatomically accurate mathematical model. PhD thesis, University of Auckland, New Zealand, 1998.

[73] M.P. Nash and P.J. Hunter, Computational mechanics of the heart: from tissue structure to ventricular function. *Journal of Elasticity*, 2000; **61**:113–141.

[74] M.P. Nash and A.V. Panfilov, Electromechanical model of excitable tissue to study reentrant cardiac arrhythmias. *Progresses in Biophysics and Molecular Biology*, 2004; **85**:501–522.

[75] R. Nicolaides, Existence, uniqueness and approximation for generalized saddle point problems: Remarks on the determinant in nonlinear elasticity and fracture mechanics. *SIAM Journal on Numerical Analysis*, 1982; **19**:349–357.

[76] F. Nobile, A. Quarteroni and R. Ruiz-Baier, An active strain electromechanical model for cardiac tissue. *International Journal for Numerical Methods in Biomedical Engineering*, 2012; **28**:52–71.

[77] D. Noble, A modification of the Hodgkin-Huxley equations applicable to Purkinje fiber action and pacemaker potentials. *Journal of Physiology*, 1962; **160**:317-352.

[78] L. Noels and R. Radovitzky, A general discontinuous Galerkin method for finite hyperelasticity. Formulation and numerical applications. *International Journal for Numerical Methods in Engineering*, 2006; **68**:64-97.

[79] R.W. Ogden, Nonlinear elasticity, anisotropy, material stability and residual stresses in soft tissue. In: *Biomechanics of Soft Tissue in Cardiovascular systems*, CISM Courses and Lectures Series, eds G.A. Holzapfel and R.W. Ogden, **441**:65–108. Springer-Verlag, Wien, 2003.

[80] A.V. Panfilov and R.H. Keldermann, Self-organized pacemakers in a coupled reaction-diffusion-mechanics system. *Physical Review Letters*, 2005; **95**(25):258104/1–258104/4.

[81] A. Henderson,The ParaView Guide: A Parallel Visualization Application. Kitware, Inc., 2004

[82] R. Perucchio and L. A. Taber, Modeling heart development. *Journal of Elasticity*,2000;**61**: 165-197. Reprinted in S. C. Cowin and J. D. Humphrey, Eds., Cardiovascular Soft Tissue Mechanics, Dordrecht, The Netherlands : Kluvier, pp. 165-197, 2002.

[83] R. Plonsey and J. Malmivuo, *Bioelectromagnetism*, Oxford University Press, 1995.

[84] A. Quarteroni and A. Valli, *Numerical Approximation of Partial Differential Equations*, Springer-Verlag, 1997.

[85] W. H. Reed, and T. R. Hill, Technical Report LA-UR-73-479, Los Alamos Scientific Laboratory, 1973.

[86] A.M. Robertson, *Nonlinear elasticity*, Springer, 2009.

[87] E.K. Rodriguez, A. Hoger and A.D. McCulloch, Stress-dependent finite growth in soft elastic tissues. *Journal of Biomechanics*, 1994; **27**(4):455-467.

[88] S. Rossi, R. Ruiz-Baier, L. Pavarino and A. Quarteroni, Active strain and activation models in cardiac electromechanics. *Proceedings in Applied Mathematics and Mechanics*, 2011; **11**:119–120.

[89] S. Rossi, R. Ruiz-Baier, L. Pavarino and A. Quarteroni, An orthotropic active strain model for the numerical simulation of cardiac biomechanics. *International Journal for Numerical Methods in Biomedical Engineering*, to appear.

[90] H. Schmid, M.P. Nash, A.A. Young and P.J. Hunter, Myocardial material parameter estimation- a comparative study for simple shear. *Journal of Biomechanical Engineering*, 2006; **128**:742–750.

[91] D. Schotzau, C. Schwab and A. Toselli. Mixed hp-DGFEM for incompressible flows,*SIAM Journal of Numerical Analysis*, 2003; **40**:2179–2194.

[92] C. Schwab, *$p-$ and $hp-$ Finite Element Methods: Theory and Applications in Solid and Fluid Mechanics*, Oxford Science Publication, 1998.

[93] W.J. Sigurdson, A. Ruknudin and F. Sachs, Calcium imaging of mechanically induced fluxes in tissue-cultured chick heart: role of stretch-activated ion channels. *American Journal of Physiology*, 1992; **262**:H1110–H1115.

[94] B.H. Smaill and P.J. Hunter, Structure and function of the diastolic heart: material properties of passive myocardium. In: *Theory of heart: biomechanics, biophysics, and nonlinear dynamics of cardiac function* eds L.Glass, P.J. Hunter and A.D. McCulloch, 1–29, Springer-Verlag, New York, 1984.

[95] W. Sun and M.S. Sacks, Finite element implementation of a generalized Fung-elastic constitutive model for a planar soft tissue, *Biomechanics and Modeling in Mechanobiology*, 2005; **4**:190–199.

[96] L.A. Taber, Biomechanics of growth, remodeling, and morphogenesis. *ASME Appl. Mech. Rev.*, 1995; **48**(8):487–545.

[97] A. Ten Eyck and A. Lew, Discontinuous Galerkin methods for nonlinear elasticity. *International Journal for Numerical Methods in Engineering*, 2006; **67**:1204–1243.

[98] C.A. Walker and F.G. Spinale, The structure and function of the cardiac myocyte: a review of fundamental concepts. *The Journal of Thoracic and Cardiovascular Surgery*, 1999; **118**:375–382.

[99] J.R. Walton and J.P. Wilber, Sufficient conditions for strong ellipticity for a class of anisotropic materials *International Journal of Non-Linear Mechanics*, 2003; **38**:441–455.

[100] J.P. Whiteley, Discontinuous Galerkin finite element methods for incompressible non-linear elasticity. *Computer Methods in Applied Mechanics and Engineering*, 2009; **198**:3464–3478.

[101] F.C.P. Yin, C.C.H. Chan and R.M. Judd, Compressibility of perfused passive myocardium. *American Journal of Physiology. Heart and Circulatory Physiology*, 1996; **271**:H1864–H1870.

Riassunto

Questo elaborato di tesi propone di analizzare un problema di elastiticità non lineare ed incomprimibile in fomulazione Lagrangiana, di sviluppare il metodo di approssimazione Discontinuous Galerkin (DG) stabilizzato mediante interior penalty e di studiare l'analisi della convergenza del metodo DG proposto.
Questo tipo di problema trova un gran numero di applicazioni nell'analisi strutturale, in bio-meccanica e nel design industriale. Questa classe di equazioni alle derivate parziali viene utilizzata per modellizzare il comportamento anisotropico del tessuto cardiaco, che ha l'abilità di deformarsi attivamente senza che vengano esercitate forze esterne. I problemi di elastiticità finita richiedono una risoluzione non banale di equazioni alle derivate parziali di tipo quasi-lineare ellittico, tengono conto del principio di conservazione del momento e delle leggi constitutive del modello. In particolare, il sistema di equazioni del modello è costituito dall'equazione del momento e da un vincolo non lineare che rappresenta la richiesta di conservazione del volume. Questa seconda equazione non lineare viene espressa imponendo che il determinante del gradiente di deformazione sia unitario ed è dovuta all'assunzione di incoprimibilità del materiale modellizzato e all'utilizzo della formulazione Lagrangiana. Mentre nella meccanica dei fluidi, nella elasticità lineare e nelle formulazioni euleriane il vincolo di incomprimibità viene espresso tramite la condizione di divergenza.
Per risolvere i problemi di nonlineare elasticità, abbiamo utilizzato la procedura iterattiva, detta metodo di Newton, che richiede una consistente linearizzazione del problema iniziale in forma variazionale. Inoltre, per il generico passo dell'algoritmo, abbiamo provato la buona positura del problema linearizzato (almeno per le deformazioni sufficientemente piccole), l'esistenza di una soluzione e la stabilità in senso classico della teoria di Babuska-Brezzi, per un problema di punto-sella.
Per approssimare i problemi di elasticità, la strategia pi comune per la risoluzione del sistema di equazioni statiche è il metodo di Galerkin classico, il cui utilizzo è motivato dalla sua flessibilità e dalla sua robustezza computazionale. Per i problemi di iper-elasticità, oggetto dell'elaborato, bisogna tenere conto delle diverse difficoltà numeriche. Nello stato dell'arte anche metodi leggermente diversi possono avere differenze sostanziali dipendenti dalla scelta degli spazi degli elementi finiti, dal tipo di elementi di riferimento della griglia quali tetraedri o esaedri , dagli spazi di approssimazione conformi o non conformi e dai sistemi lineari simmetrici o nonsimmetrici ottenuti, eccetera.
Inoltre, è ben noto che la principale difficoltà numerica nei metodi di approssimazione con elementi finiti di basso ordine, per problemi di elasticità soggetti a vincolo che preserva il volume, è il fenomeno di locking volumetrico che consiste nella diminuzione del campo

di spostamento in modo non fisico. Per questo motivo, nel lavoro di tesi si è proposto una formulazione del metodo Discontinuous Galerkin con la variante interior penalty che ci permette di imporre la continuità tra elementi adiacenti. L'inclusione dei termini di penalty nel funzionale dell'energia è una strategia classica che riduce le instabilità numeriche spurie generate dalla formulazione con elementi finiti discontinui. I vantaggi riscontrati dall'utilizzo del metodo DG sono: abilità di approssimare in domini complessi, con griglie anisotrope e nonconformi; di discretizzare equazioni alle derivate parziali con coefficienti discontinui, di utilizzare tecniche di raffinamento p- e hp- adattivo, di migliorare l' accuratezza rispetto al metodo classico agli elementi finiti a parità di gradi di libertà.
L' introduzione presentata nel capitolo 1 motiva l'interesse nella modellizzazione fisica del comportamento meccanico del tessuto cardiaco tramite la teoria della meccanica solida. In questo capitolo, si è data una breve esposizione della struttura morfologica del tessuto cardiaco e del suo comportamento elettrico-fisiologico a livello di micro-scala per far conoscere al lettore il comportamento attivo e passivo delle pareti del miocardio.
Nel secondo capitolo, sono state introdotte le nozioni di base della meccanica del continuo. Vengono presentati alcuni recenti risultati nella modellistica del comportamento passivo del muscolo cardiaco, dovuto ad eccitazione e a forze esterne, e del suo comportamento attivo dovuto alle forze interne, principalmente alla contrazione delle fibre del miocardio. Nell'ultima sezione di questo capitolo viene presentata la formulazione active strain, che si basa sulla decomposizione moltiplicativa. In questo modello, l'accoppiamento tra la meccanica cardiaca e l' elettro-fisiologia cardiaca è rappresentato dalla funzione di attivazione γ_f, che è inclusa come parametro nell'equazione nonlineare elastica alle derivate parziali. Il modello proposto viene confrontato con la formulazione classica, active stress, che si basa sulla decomposizione additiva. In particolare, la nuova formulazione è capace di catturare la variazione dei dettagli a livello microscopico riguardante la contrazione della fibra.
Nel terzo capitolo, viene analizzato il modello fisico dal punto di vista matematico. L'equazione alle derivate parziali del problema iperelastico, che descrive la deformazione del tessuto cardiaco e contemporamente la contrazione della lunghezza del sarcomero a livello di micro-scala durante il ciclo cardiaco, è accoppiata con un vincolo nonlineare che rappresenta la conservazione del volume. Utilizzando il principio di Hamilton-Lagrange e la derivata di Gataux, si è linearizzato il problema rispetto ad una arbitraria configurazione e si è studiato la buona positura.
Il capitolo 4 è dedicato al contributo originale di questo lavoro di tesi, introducendo la formulazione di una famiglia di metodi Discontinuous Galerkin tramite gli operatori di lifting per approssimare il problema di nonlineare elasticità incomprimibile con condizioni al bordo miste. Inoltre si è dimostrato la convergenza ottimale del metodo e la sua proprietà di locking-free.
Nel capitolo 5, viene simulato numericamente lo schema proposto in 2D per convalidare l'ottima convergenza stimata. Per mostrare la robustezza e la proprietà di locking free, vengono proposti alcuni test significativi con parametri attivi discontinui, che simulano la variazione dell'input elettro-fisiologico prendendo una continua parametrizzazione della direzione delle fibre. In questa tesi viene messo in evidenza il fenomeno di locking volumetrico che si incontra utilizzando il metodo classico degli elementi finiti ed inoltre si osserva che non è necessario utilizzare la tecnica di incremental loading durante le iterazioni del metodo di Newton per ottenere la sua convergenza, come è richiesto nell'utilizzo del metodo agli elementi finiti. Il capitolo viene concluso con alcune simulazioni sulla contrazione attiva di un cubo utilizzando sia elementi continui che discontinui per la pressione e discontinui per la variabile spostamento. In questo test si è nuovamente osservata la robustezza del metodo

presentato.
Infine, nel capitolo 6 vengono presentate sia un'analisi critica che le conclusioni significative del lavoro di tesi con alcune linee future di ricerca.